

# Microwave Tubes

G. Faillon, G. Kornfeld, E. Bosch, and M.K. Thumm

## 1.1 Introduction

### 1.1.1 Review of State-of-the-Art and Present Situation

For more than 60 years, microwave tubes are used in many applications as oscillators and, in particular, as powerful amplifiers of electromagnetic waves at frequencies ranging from about 300 MHz to several hundreds of GHz, with some even reaching the 1 to 2 THz range.

A number of microwave tube types exist, classified on the basis of their operating frequency and output power. At the same time, they may be divided into two general categories: pulse wave tubes and continuous wave (CW) tubes. The power/frequency relationships of the most commonly used microwave tubes are shown in Fig. 1.1.

Microwave tubes may be broadly used in three main areas of applications:

- radio, TV and telecommunications;
- radars and military systems (especially airborne);
- industrial, scientific, medical (ISM).

Even though microwave tube performance is generally described in terms of power, efficiency and gain, other factors of specific and professional interests to each user should also be taken into consideration: bandwidth, linearity, signal/noise ratio, mode of propagation, tube and transmitter weight, reliability, etc.

### 1.1.2 Historical Development

One century ago, in 1904, Sir J.A. Fleming discovered the valve, or the diode, immediately used to detect the electromagnetic waves recently demonstrated by H.R. Hertz. In fact, the diode was the first vacuum tube, with a poor vacuum, although vacuum. A few months later, in 1906, Lee de Forest has been inspired to

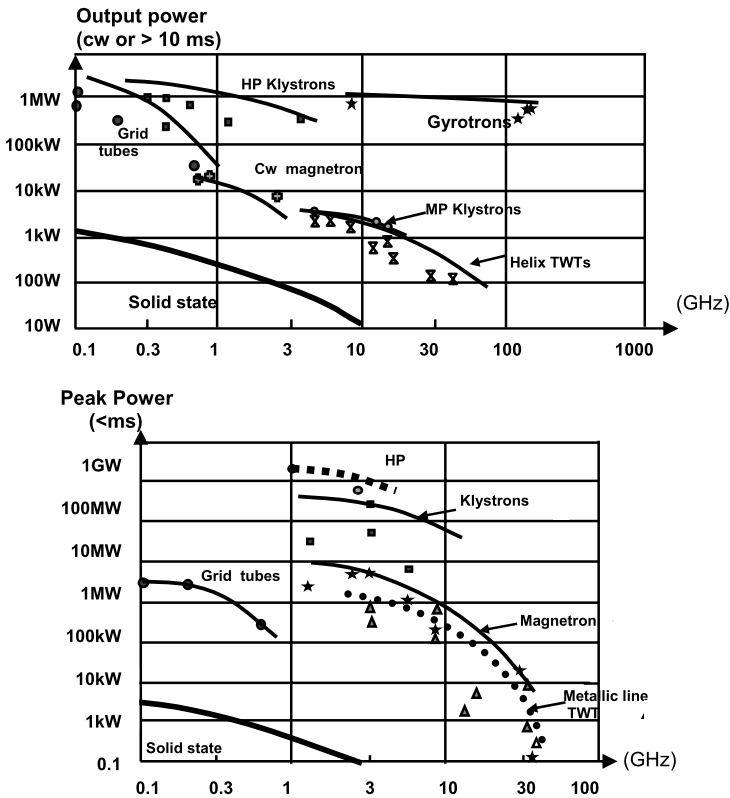


Fig. 1.1. Peak and CW power of various microwave tubes vs frequency

add a 3rd electrode, and in that way the triode was born. After about 10 years of tests and discussions, this new vacuum tube has been used as a very attractive amplifier, which gave rise, in the 1920s, to a rapid expansion of the broadcasting and the radio-links.

At the same time, research was carried not only to improve the triodes, but also to consider other vacuum devices at higher frequencies. In 1920, H. Barkhausen invented the retarding-field tube (or reflex triode), which can be regarded as the first transit time tube. The magnetron has been discovered by A.W. Hull in 1921, followed by E. Habann and A. Zacek. Twelve years later, K. Posthumous understood the operating principles of such an oscillator, and in 1939 H.A.H. Boot and J.T. Randall used “klystron” type resonators for confining the RF fields. The introduction of the oxide cathode with a high secondary emission coefficient was also a major improvement. During World War II, the urgent need for high power microwave generators for radar transmitters led to the development of the magnetron to its present state.

In 1953 W.C. Brown introduced the crossed-field amplifier (CFA), a magnetron with an interrupted RF circuit to provide input and output connections. At the same

time the backward oscillator (MBWO), or “carcinotron”, derived from the CFA but with an injected beam and a specific delay line came into light on both sides of the Atlantic Ocean. This oscillator offered the advantage to be electrically frequency tunable over a very large band.

Nevertheless, neither the triodes nor the magnetrons were high frequency and large gain amplifiers. In 1934–35, A. & O. Heil were the first scientists to imagine the use of a periodic and localized electron velocity variation in order to get bunches. After the registration of patents in 1937, Hahn & Metclaff and especially R. & H. Varian gave the exact description of the multicavity klystron. The first prototype delivered  $\approx 50$  W at 3 GHz with a gain of 30 dB, and very soon 30 to 50 dB gain 1 to 10 GHz klystrons have been widely used, for instance, on radars and particle accelerators. Born from the principles of this klystron and from previous studies on electron reflectors free of microwave fields, the “reflex klystrons” made great strides as local oscillators in radars.

The possibility of traveling wave interaction has been described in 1942 by R. Kompfner, who developed the first TWT, one year later, using a helix as the delay line. But the real starting development of the TWTs took place after 1946, when J.R. Pierce made the theory of these tubes and gave solutions to suppress many parasitic oscillations. The coupled cavity TWT appeared in 1950. The evolution of the TWTs is impressive, when we know that they are still nowadays used – in modern versions – for many purposes.

From that time, and because of important military and civilian needs, the microwave tubes entered into their industrial period. Of course the R&D was strongly going on, not only to improve the present devices and to replace them, according the new user requirements – higher frequencies, longer lifetime, greater power and bandwidth – but also to compete with the transistors and the solid state devices or, especially now, to collaborate with them.

The last 40 years period can be characterized by the following main events [1]:

- Coaxial magnetron, frequency agility magnetron.  
Mass production of magnetrons in the 1960s to provide the microwave ovens.
- Brazed and pressed helix TWTs, mainly used up to the 1980s in radar transmitters and ground radio-links.  
Variable pitch helix TWTs improving efficiency.  
Gridded electron guns and introduction of the impregnated cathodes in the 1970s.  
Then, development of TWT depressed collectors and radiating collectors.  
From 1962 space TWTs are used on satellites.
- Tunable klystrons or TV and communications. 10% instantaneous bandwidth klystrons. Inductive output tubes (IOTs).  
Multibeam medium power klystrons, mainly used in soviet countries from 1960 to 1980.  
Vapor cooled collectors, and 300 kV pulsed electron guns.  
High efficiency ( $\geq 65\%$ ), pulsed power (tens of MW) and CW ( $\geq 1.3$  MW) klystrons. Multibeam high power klystrons (MBKs) from 1995.

- Recently born gyrotrons, which are the only tubes capable of delivering very high power (MW) at very high frequencies ( $\geq 100$  GHz). In 1959, without knowledge of the astrophysicist R.Q. Twiss's work, J. Schneider in USA and A.V. Gaponov in Russia proposed an explanation for the amplifying mechanism based on free electron gyro radiation. But the first successful experiments took place in the 1970s and became really attractive in the 1980s, thanks to the support of the thermonuclear fusion plasma community, especially in Europe. And now after having solved many severe technological problems, such as the superconducting electromagnets and the sapphire or diamond windows, the gyrotrons and the associated low loss overmoded waveguides or quasi-optical transmission lines are manufactured and their development is still progressing.

From about 20 years, the market configuration is slowly changing and the requirements are now more specific, more severe and exacting, to the detriment of mass production. Nevertheless, after the merging and the reorganization of many tube manufacturers, the applications are mainly oriented as shown in Sect 1.1.

At the same time new research and developments are conducted in the direction of better performance [1] as higher frequencies and greater power, but also towards advanced technologies, such as the field emission and cold cathodes, nanotechnologies, compactness and optimization of the whole amplifiers.

### 1.1.3 Basic Operating Principles and Definitions

#### Basic Operating Principles

A microwave tube may be defined as an evacuated envelope (vacuum), inside which an electron beam interacts with an electromagnetic wave [2, 3]. This interaction means that the electrons of the beam give up a part of their kinetic or potential energy to the electromagnetic wave, thereby generating or amplifying this wave.

Since it is relatively known how to generate and then to accelerate or, in other words, to give energy to an electron beam – especially thanks to the high voltage electron guns – the objective of this book is to go further and to present the physics behind the interaction and the transfer of the beam energy to the electromagnetic wave. Such a process involves several separate or simultaneous physical phenomena as follows.

1. Formation and acceleration of an electron beam.
2. Periodic bunching of the electrons at a frequency  $f$ . This bunching is started up by the RF input or drive power  $P_d$  in the case of an amplifier, or by the electromagnetic noise in the case of an oscillator.
3. Deceleration of the bunches (or reduction of their relativistic mass) in such a way that their kinetic or potential energy is converted into an electromagnetic or a microwave energy at the frequency  $f$ .
4. Forwarding of this microwave energy outside the tube, which yields the tube's output power  $P_{OUT}$ .

### Characteristics and Definitions

To operate a microwave tube [4], the first step is to heat the electron-emitting cathode by connecting the attached filament to a source of electric power  $P_F = V_F I_F$ . Then a power supply ( $P_0 = V_0 I_0$ ) is connected between the cathode and the anode in order to generate the required energetic electron beam, which will travel at a velocity  $v_0$ , carrying a current  $I_0$ , given by the two non-relativistic expressions (the relativistic ones will be given in the following pages)

$$m v_0^2 / 2 = e V_0, \tag{1.1}$$

$$I_0 = P V_0^{3/2}, \tag{1.2}$$

with  $P$  being a factor related to the geometry of the gun, called perveance.

A magnetic field is used to focus the beam [5]. This field is created either with permanent magnet(s) or just by an electromagnet with a power consumption  $P_{FOC}$ . In the case of an oscillator, there is no RF input signal, and the tube directly converts the beam energy to microwave energy at the frequency  $f$ . Let  $P_{OUT}$  denote the tube output power. Then the overall tube efficiency is given by  $\eta = P_{OUT} / (P_F + V_0 I_0 + P_{FOC})$ , while the interaction efficiency is  $\eta_{interaction} = P_{OUT} / V_0 I_0$ .

The oscillation does not begin immediately with the application of the voltage  $V_0$ , but after a fluctuating starting time  $\tau_1$ , as shown in Fig. 1.2. Then, during the rise time  $\tau_2$ , the output power increases up to the nominal level  $P_{OUT}$ . The frequency  $f$  changes during this time  $\tau_2$  and then stabilizes.

The power  $P_{OUT}$  is dependent on the anode current  $I_0$  and on the load impedance  $Z_L$ , as shown in the Rieke diagram of Fig. 1.2. A pushing ratio  $\Delta f / \Delta I_0$  and a pulling ratio  $\Delta f / \Delta \varphi_L$ , measured at constant reflection coefficient from the load (or standing wave ratio, SWR), characterize the frequency sensitivities of the oscillator tube.  $\varphi_L$  is the phase of the load impedance  $Z_L$ . It is sometimes useful to lock or to control the oscillation frequency  $f$  by means of a controlling signal  $P_c < P_{OUT}$  at a frequency  $f_c$  (close to  $f$ ), which is injected into the tube via its output. For a given  $P_c$  setting, the Adler relationship gives the total range of frequencies over which this frequency locking is possible,  $\Delta f_{max} = 2 f_c / Q_x \sqrt{P_c / P_{OUT}}$ .

In the case of an amplifier, a microwave signal of power  $P_d$ , at frequency  $f$ , is injected at the tube input and is then amplified up to  $P_{OUT}$ . The amplifier overall efficiency is determined in practically the same way as for oscillators,  $\eta = P_{OUT} / (P_F +$

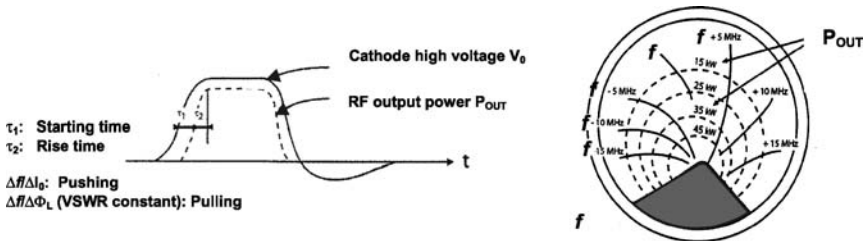


Fig. 1.2. Definitions: oscillators

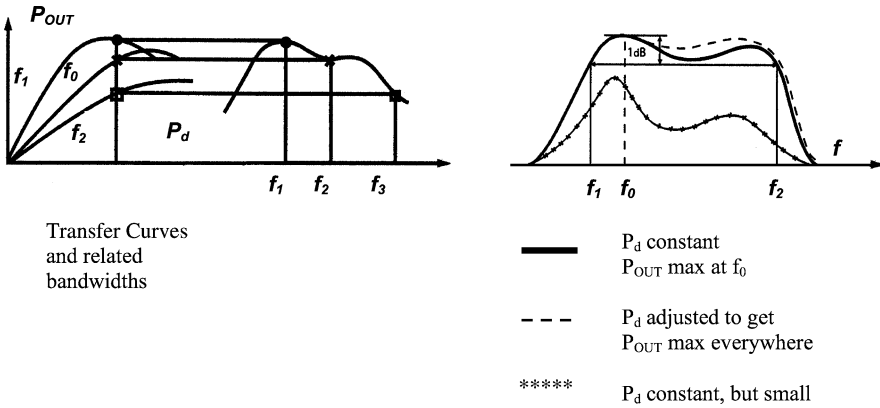


Fig. 1.3. Definitions: amplifiers

$V_0 I_0 + P_{FOC} + P_d$ ), and the interaction efficiency again is  $\eta_{interaction} = P_{OUT}/V_0 \cdot I_0$ . The ratio  $G = P_{OUT}/P_d$  is the gain, which is often written in decibels (dB) as  $G = 10 \log_{10}(P_{OUT}/P_d)$ . Usually, the  $P_{OUT}/P_d$  transfer curve (Fig. 1.3) shows an almost linear relationship at low signal levels and a saturation part at large signals. The bandwidth, generally measured at  $-1$  dB, is defined on the basis of the variation of  $P_{OUT}$  versus the frequency, with  $P_d$  adjusted, at each frequency, to maximize  $P_{OUT}$ . The bandwidth can also be defined with  $P_d$  constant and, for instance, adjusted to the value giving maximum  $P_{OUT}$  (Fig. 1.3).

The group delay  $\tau_g = d\varphi/d\omega$  represents the signal delay inside the tube amplifier,  $\varphi(f)$  being the phase shift between the input and the output. The influence of the load impedance  $Z_L$  is given by the Rieke diagram where the  $P_{OUT}(Z_L)$  curves are plotted.

### Basic Physical Laws of E-Beams

#### Equation of Motion and Relativistic Corrections

The only non-negligible forces which influence electrons in microwave tubes during their interaction with the RF wave are the electromagnetic Lorentz forces. All other forces, e.g. due to its spin or the gravitation, are typically 11 or 16 orders of magnitude lower, respectively.

From the relativistic equation of motion of a single electron

$$d(m_e \cdot v_e)/dt = -e(\mathbf{E} + v_e \times \mathbf{B}), \tag{1.3}$$

$$m_e = \frac{m_0}{\sqrt{1 - (v_e/c)^2}} = m_0(1 + V/V_n), \tag{1.4}$$

$$v_e = c\sqrt{1 - 1/(1 + (V/V_n))^2} \tag{1.5}$$

(with the charge  $e = 1.60 \times 10^{-19}$  C, the relativistic electron velocity  $v_e$ , the relativistic mass  $m_e$ , the rest mass of the electron  $m_0 = 9.11 \times 10^{-31}$  kg, the velocity of light  $c$ , the acceleration voltage  $V$  and  $V_n = m_0 c^2 / e = 511$  kV, the acceleration voltage to produce the equivalent of one electron rest mass as relativistic mass increase), we can easily conclude that the kinetic energy of an electron (or another charged particle) can only be changed by the electric field  $\mathbf{E}$  but not by the magnetic field  $\mathbf{B}$ , because the magnetic Lorenz force vector  $\mathbf{F}_L = -e(\mathbf{v} \times \mathbf{B})$  is perpendicular to both, the velocity  $\mathbf{v}$  and  $\mathbf{B}$ , and because the scalar product of two orthogonal vectors is always zero. Therefore, the energy transfer from an electron beam to a RF wave or vice versa employs always only the electric field components of the RF wave and space charge bunches

$$dE_{\text{kin}} = \mathbf{F} \cdot d\mathbf{s} = -e(\mathbf{E} + \mathbf{v} \times \mathbf{B}) \cdot \mathbf{v} dt = -e\mathbf{E} \cdot \mathbf{v} dt, \quad (1.6)$$

where  $d\mathbf{s}$  is the line path element along the trajectory. This does not mean that the magnetic fields  $\mathbf{B}$  are not very important. Conversely, magnetic fields are required to maintain the focused beam properties, as we will see in Sect. 1.3.

### Maxwell Equations

Since in a beam the number of electrons is far beyond the computation power of modern computers, the particle picture can be replaced for many considerations by the continuum theoretical approach of the Maxwell equations. Here the fields  $\mathbf{E}$  and  $\mathbf{B}$  are self-consistently determined by the local charge and current densities  $\rho$  and  $\mathbf{j}$ , which themselves depend on a set of differential equations, boundary and start conditions on the fields  $\mathbf{E}$  and  $\mathbf{B}$ . The Maxwell equations cannot describe localised collision processes or even the passing of particles, which occurs in RF tubes close to saturation. Nevertheless, they allow drawing helpful general conclusions and symmetry considerations and are also the platform for a lot of computer simulations and modelling.

$$\text{div } \mathbf{E} = \rho / \epsilon_0; \quad \text{Charge density is a source of } \mathbf{E}\text{-fields;} \quad (1.7)$$

$$\text{rot } \mathbf{E} = -\delta \mathbf{B} / \delta t; \quad \text{Induction law;} \quad (1.8)$$

$$\text{div } \mathbf{B} = 0; \quad \text{Magnetic field is source free, no magnetic} \\ \text{single poles;} \quad (1.9)$$

$$\text{rot } \mathbf{B} = -\mu_0 \mathbf{j} + \epsilon_0 \mu_0 \delta \mathbf{E} / \delta t \quad (= -\mu_0 \mathbf{j} \text{ for stationary beams).} \quad (1.10)$$

From the stationary Maxwell equations one can conclude that the electric and magnetic fields  $\mathbf{E}$  and  $\mathbf{B}$  can be derived from a *scalar potential*  $\phi$  and a *vector potential*  $\mathbf{A}$  in the form

$$\mathbf{E} = -\text{grad } \phi, \quad (1.11)$$

$$\mathbf{B} = \text{rot } \mathbf{A}. \quad (1.12)$$

Inserting these definitions into the Maxwell equations (1.7) and (1.10), one obtains equations for those potentials defined by the space charge density  $\rho$  and the beam current density  $\mathbf{j}$ , respectively:

$$\text{div grad } \phi = -\rho/\epsilon_0; \quad \text{Poisson's equation (the Laplace equation for } \rho = 0); \quad (1.13)$$

$$\text{rot rot } \mathbf{A} = -\mu_0 \mathbf{j}. \quad (1.14)$$

Since the influence of the beam current density  $\mathbf{j}$  on the magnetic field can be in most applications completely neglected compared to the externally applied magnetic fields, the fourth Maxwell equation (1.10) reduces for the stationary case simply to

$$\text{rot } \mathbf{B} = 0; \quad \text{For negligible current contributions to } \mathbf{B}\text{-field}; \quad (1.15)$$

$$\mathbf{B} = -\mu_0 \text{grad } \Omega; \quad \text{with } \mathbf{B}\text{-field defined by scalar potential } \Omega; \quad (1.16)$$

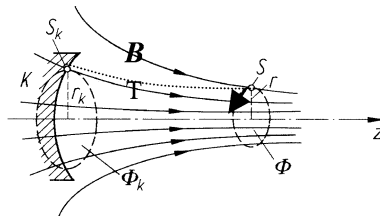
$$\text{div grad } \Omega = 0; \quad \text{Magnetic equivalent to the electric Laplace equation.} \quad (1.17)$$

In this case, like for the scalar electric potential  $\phi$ , one can define a magnetic scalar potential  $\Omega$ , and (1.17) becomes the magnetic equivalent to the electric Laplace equation (1.13).

*Busch's Theorem*

As a direct consequence of Maxwell equations in axially symmetric (rotational symmetric) systems, the Busch theorem is very useful for the analysis of magnetically focused linear electron beams (Fig. 1.4). It states a surprising conservation law, valid along an electron trajectory, by saying that the sum of its angular momentum  $m_e v_\theta r$  with respect to the  $z$ -axis and the magnetic flux  $\Phi$  parallel to the symmetry axis through a circle area with the trajectory radius  $r$  and multiplied by the factor  $e/2\pi$  is a constant.

$$\begin{aligned} m_e v_\theta r + e/2\pi \cdot \Phi &= \text{constant}; && \text{Busch's theorem, valid along trajectories} \\ m_e \dot{\theta} \cdot r^2 + \frac{e}{2\pi} \Phi &= \text{constant}; && \text{of charged particles in rotational} \\ &&& \text{symmetric systems (Fig. 1.4).} \end{aligned} \quad (1.18)$$



**Fig. 1.4.** Illustration for Busch's theorem in rotational symmetric systems



Since the angular velocity is zero at cathode emission, according to the Busch theorem (1.18) the angular velocity  $v_\theta$  or  $\dot{\theta}$  in S is just defined by the two flux values  $\Phi_K$ ,  $\Phi$  and the radius  $r$  (with  $\dot{\theta}$  = angular velocity around  $z$ -axis). There are a lot of other applications for the Busch theorem. Some of them will be introduced in the chapter on beam focusing.

### Scaling Laws

Geometrical scaling of microwave tubes is often appropriate when an approved existing design at a given frequency  $f_1$  has to be transferred to a new frequency  $f_2$ .

Since the tube dimensions scale with the RF wavelength  $\lambda$  or the reciprocal of the frequency  $f$ , the tube scaling factor  $\gamma$  for all linear dimensions is

$$\gamma = \lambda_2/\lambda_1 = f_1/f_2; \quad \text{Scaling with frequency.} \quad (1.19)$$

Now the question arises how the electromagnetic properties of the tube have to be scaled in order to get identical beam trajectories in the scaled coordinate system  $\mathbf{x}_2$ ?

The answer is obtained with the help of the Maxwell equations. It can be easily shown by insertion that the Maxwell equations remain invariant in the scaled, new coordinate system  $\mathbf{x}_2$  when the following scaling laws are applied.

$$\begin{aligned} \mathbf{x}_2 = \gamma \cdot \mathbf{x}_1; & \quad \text{Linear geometrical scaling of all dimensions in system} \\ & \quad \mathbf{x}_1 \text{ with the factor } \gamma \text{ in the} \\ & \quad \text{new coordinate system } \mathbf{x}_2; \end{aligned} \quad (1.20)$$

$$\mathbf{E}_2 = \gamma^{-1} \cdot \mathbf{E}_1; \quad \text{Electric field;} \quad (1.21)$$

$$\mathbf{B}_2 = \gamma^{-1} \cdot \mathbf{B}_1; \quad \text{Magnetic field;} \quad (1.22)$$

$$\phi_2 = \gamma^0 \cdot \phi_1; \quad \text{Electric potential;} \quad (1.23)$$

$$\mathbf{A}_2 = \gamma^0 \cdot \mathbf{A}_1; \quad \text{Vector potential;} \quad (1.24)$$

$$\mathbf{j}_2 = \gamma^{-2} \cdot \mathbf{j}_1; \quad \text{Current density;} \quad (1.25)$$

$$I_2 = \gamma^0 \cdot I_1; \quad \text{Total current (from gun);} \quad (1.26)$$

$$P_2 = \gamma^0 \cdot P_1; \quad \text{Perveance } P = I \cdot V^{-3/2}. \quad (1.27)$$

With the above scaling laws, we can easily understand why the power handling capability  $P_{\text{OUT}}$  of a given microwave tube design scales roughly with frequency  $f^2$  or  $P_{\text{OUT}} f^2 = \text{constant}$ .

Let us assume a tube scaled with  $\gamma = 1/2$  for the doubled frequency  $f_2 = 2f_1$ . If all the electrode potentials are kept constant, also the total currents and power consumptions are kept constant. But since the current densities are scaling with  $\gamma^{-2}$ , we get a 4 times higher thermal loading at the critical areas. Therefore, to maintain the same material loading at the thermal material limits, the power handling capability in the doubled frequency case is roughly only  $1/4$ . A reference for the topic of scaling is given in [6].

*Beam Formation in the Electron Gun*

First, we consider the emission of electrons at the cathode surface. Now mainly Ba-, Ca-Aluminates impregnated dispenser cathodes are used. Since they are in detail described in Chapter 10, we limit ourselves here to reproduce the emission laws of this type of thermionic emitters described by workfunction  $\phi$  and cathode temperature  $T$ .

*Thermal Cathode Emission*

In the temperature limited emission regime (all emitted electrons are drawn away from the cathode surface), the saturated emission current density  $j_s$  is given by the Richardson–Dushman equation (1911; Nobel Prize 1928)

$$j_s = A * (1 - r) \cdot T^2 \cdot e^{-\phi/kT}, \tag{1.28}$$

where  $A = 4\pi em_0k^2/h^3 = 120 \text{ A}/(\text{cm}^2 \text{ K}^2)$ ,  $k$  is the Boltzmann constant and the quantum-mechanical reflection coefficient  $r$  at the metal/vacuum surface is set to 0.

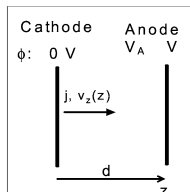
A more refined elaboration by Schottky includes the electric field  $E$  at the surface and is called the Richardson–Dushman–Schottky equation

$$j_s = A * T^2 * e^{-\phi/kT} * e^{Ka*E^{1/2}} \tag{1.29}$$

with  $Ka = (e^3/4\pi\epsilon_0)^{1/2}/kT$ .

*Space Charge Limited Emission*

Normally, due to space charge limitation the maximum emission current  $j_s$  is not obtained during operation of a linear beam microwave tube. The gyrotron cathodes only are operating in the temperature limited mode. The electron charges, emitted into a certain volume, defined by the boundary conditions for the electrostatic potential  $\phi$ , modify the potential distribution inside this volume. As a consequence, this volume is transparent or *perveant* only for a limited current, the space charge limited emission current. The following gives the space charge limited emission for a planar diode configuration (Fig. 1.5):



**Fig. 1.5.** Planar diode configuration

$$\begin{aligned}
 j_0 &= 2.335 \times 10^{-6} \cdot V_a^{3/2} / d^2; && \text{Child-Langmuir law for space charge} \\
 & && \text{limited current density in a diode;} \quad (1.30) \\
 I_0 &= F/d^2 \cdot 2.335 \times 10^{-6} \cdot V_a^{3/2}; && \text{Child-Langmuir law for total current;} \\
 P &= F/d^2 \cdot 2.335 \times 10^{-6}; && P = \text{diode perveance;} \\
 & && F = \text{diode area.} \quad (1.31)
 \end{aligned}$$

It is important to note that this space charge limited current does not depend neither on the cathode temperature nor the nature of the emitting cathode (workfunction  $\phi$ ), but only on the applied voltage and the gun geometry; here is the diode distance  $d$  and  $F$  is the diode area (see Figs. 1.6 and 1.7). The result (1.30) can be generalised as

$$I_0 = P \cdot V_a^{3/2}; \quad \text{Child-Langmuir law for total current.} \quad (1.32)$$

We remind of the result of the scaling laws (1.27) that the perveance  $P$  remains constant in case of a linear scaling in all dimensions.

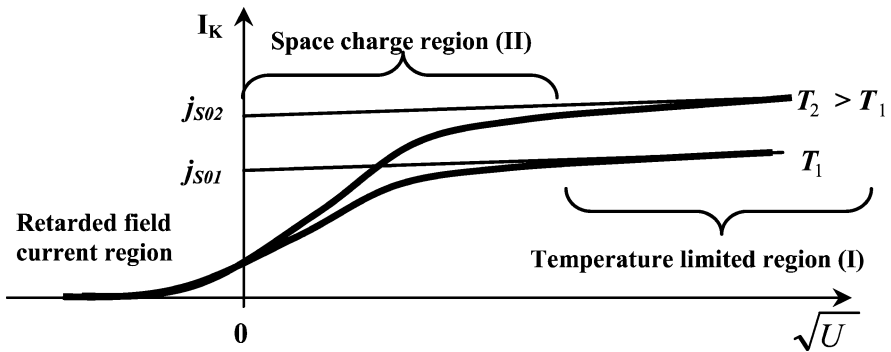


Fig. 1.6. Cathode emission vs the square root of applied anode voltage. For sufficiently high voltages the current is limited by the Richardson-Dushman-Schottky saturation current

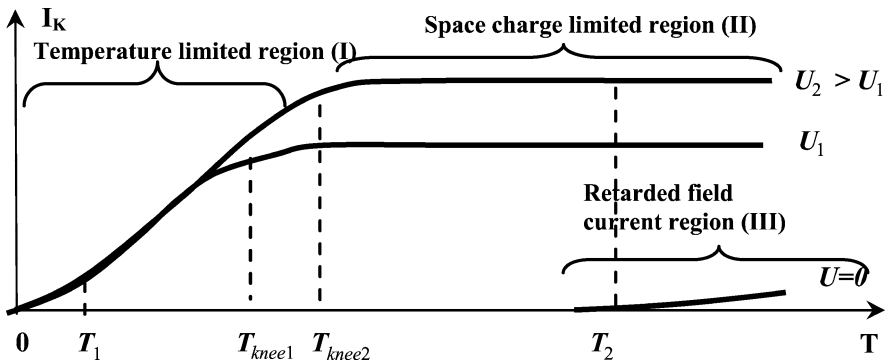


Fig. 1.7. Cathode emission vs the temperature. For low temperatures of the cathode the emission is in the temperature limited regime. At the so-called knee temperature the emission becomes space charge limited and independent of temperature

## 1.2 Klystrons

### 1.2.1 Klystron Amplifiers

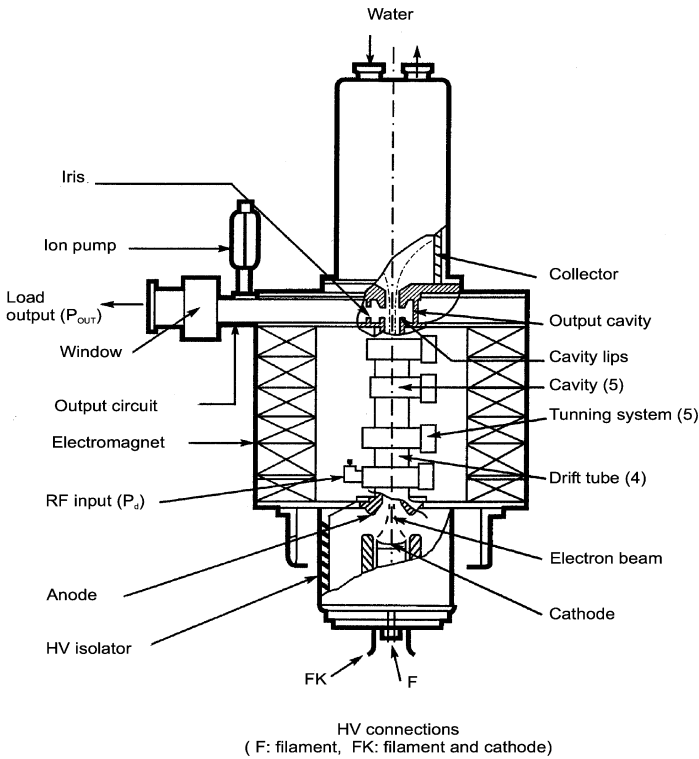
#### Introduction

Klystrons are amplifier microwave tubes, designed mainly for use at high frequencies from about 0.3 GHz to approximately 30 GHz. They are characterized by high gains (around 50 dB) and high output powers:

- 3 kW CW tunable from 14 to 14.5 GHz with efficiency  $\eta = 40\%$ ,
- 60 MW with 4  $\mu$ s pulses at 3 GHz ( $\eta = 38\%$ ),
- 1.3 MW CW at 352 MHz with  $\eta$  going up to 65%,
- 500 kW CW at 3.7 GHz with  $\eta = 45\%$ .

However, almost all klystron instantaneous bandwidths are fairly limited.

In a klystron (Fig. 1.8), the main functions are separated, which means that design and technology factors can be optimized for each function. These functions are the electron emission, the magnetical beam focusing, the electron bunching or the



**Fig. 1.8.** Klystron cross-section

beam density modulation, the extraction of the microwave energy and, lastly, the dissipation of residual energy.

**Interaction in a Klystron: Modulations and Energy Extraction**

Thanks to a high voltage  $-V_0$  applied to the cathode in regard the anode, a Pierce type electron gun generates an electron beam which carries the current  $I_0 = P V_0^{3/2}$  according to (1.2) and which is maintained approximately cylindrical thanks to a magnetic field  $B_z(z)$  over the entire length of the tube.

After leaving the anode, the electrons travel across the first cavity, or the input cavity. This cavity is excited by the weak input signal  $P_d$  which is to be amplified and whose frequency  $f$  is about  $f_0$ , the cavity's resonance frequency. This cavity is designed to resonate at its fundamental mode  $TM_{110}$  (rectangular) or  $TM_{010}$  (circular) with a maximum electric field  $E_1$  at the center where the electrons pass [7]. Moreover, this electric field is increased by the fact that the drift tubes, placed on both sides of the cavity, are reentrant (Fig. 1.9).

Electrons traveling across this narrow gap of the cavity are under action of the periodic electric field  $E_1 e^{j\omega t}$ . They are accelerated for a half of period and decelerated for the other half (Fig. 1.10). Consequently, the fast moving electrons from a given half-period catch up with slow moving electrons from the preceding half-period, resulting in the creation of electron bunches. In other words, the velocity modulation produced in the first cavity creates a beam current modulation in the following drift tube, which is expressed as  $I_b(z, t)$  [8, 9].

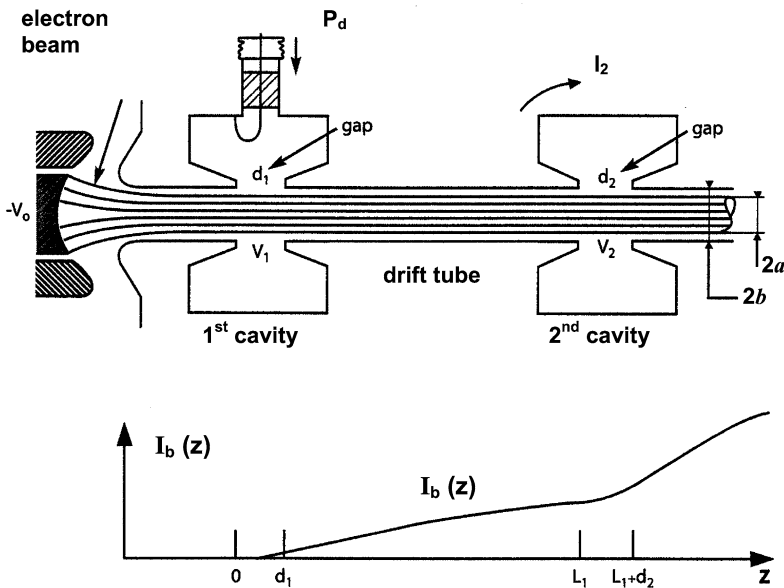
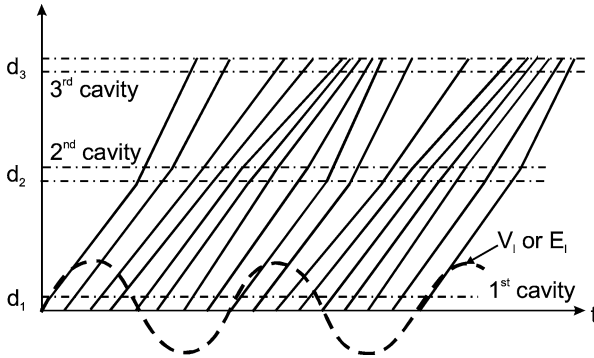


Fig. 1.9. Beam modulation along a klystron



**Fig. 1.10.** Applegate's diagram  $z(t)$

A second cavity (Fig. 1.9) is then added at the distance  $L_1$  where the bunches form. The beam current  $I_b(z, t)$  induces a current  $I_2$  in this cavity which gives rise to a voltage  $V_2 = Z_2 I_2$  (or an electric field  $E_2$ ) at the gap ends,  $Z_2$  being the cavity impedance. On its turn  $V_2$  (or  $E_2$ ) gives rise to a new velocity modulation, generally to an extent far exceeding the former modulation. Again, a third cavity is added at a distance  $L_2$ , etc.

The process is repeated at each drift tube and each cavity along the klystron, until the last, or the output, cavity is reached where the bunches are very narrow and dense. In this last cavity the very high induced current  $I_N$  gives rise to the large cavity voltage  $V_N = Z_N I_N$ . Then the bunches are strongly decelerated by this voltage  $V_N$  (or  $E_N$ ) so that they are themselves generating. In that way, they give up a large part of their kinetic energy to the electromagnetic field which builds up in this cavity and maintains  $V_N$  (or  $E_N$ ). This energy stored in the cavity yields the output power  $P_{OUT} = V_N^2 / 2Z_L$  routed to the load, through an iris or a coupling loop and a window (Figs. 1.8 and 1.11).  $P_{OUT}$  represents the power  $P_d$  which is amplified by the klystron. Typically, klystrons have four to six cavities, gains ( $P_{OUT} / P_d$ ) of about 50 dB, and interaction efficiencies ( $P_{OUT} / V_0 I_0$ ) of about 35% to more than 65%.

### From the First to the Second Cavity

Assuming several simplifications, the relationship between  $V_1$  and  $P_d$  is given by

$$V_1^2 = 8 \left( \frac{R}{Q} \right) Q(Q/Q_x) P_d \left[ 1 + Q^2 \left( \frac{f}{f_0} - \frac{f_0}{f} \right)^2 \right]^{-1} \quad (1.33)$$

with  $f_0$ , the cavity resonance frequency, and  $f$ , the operating frequency [8, 9, 11].

Solving the equation for the movement of an electron entering the gap of the cavity at a velocity  $v_0$  (1.1) yields the velocity  $v(d_1)$  at the output of the gap,

$$v(d_1) = v_0 \left( 1 + \frac{M_1 V_1}{2V_0} e^{j\omega t} \right), \quad (1.34)$$

where  $t$  is the time when the electrons pass the center of the gap and

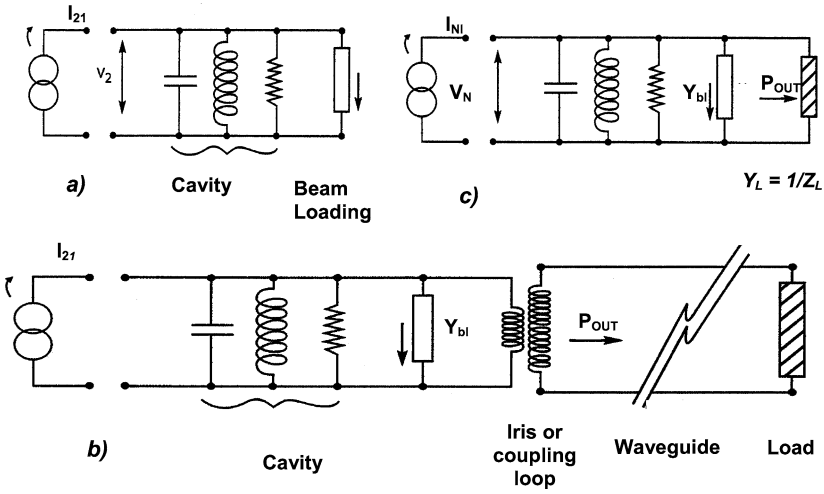


Fig. 1.11. Equivalent circuit of a klystron cavity

$$M_1 = \sin\left(\frac{\omega d_1}{2v_0}\right) \bigg/ \left(\frac{\omega d_1}{2v_0}\right).$$

$M_1$  is called the coupling coefficient. The electrons leave the cavity and travel in the following drift tube at the velocity given by (1.34).

Due to the periodicity of the modulation (Fig. 1.10), their respective positions change over time (some electrons bunch, other separate) and bunches form, once per period. The velocity modulation caused by the first cavity therefore results in electron spatial density modulation, i.e. current modulation in the drift tube. This current along the  $z$ -axis is given by

$$I_b(z, t) = I_0 + 2I_0 \sum_1^{\infty} J_n(nX) \cos n(\omega t - \omega z/v_0) \tag{1.35}$$

with  $X = M_1 \cdot (V_1/2V_0)(\omega z/v_0)$ ,  $J_n$  = Bessel function,  $I_0$  = DC or average beam current, and  $M_1$  given just above. Equation (1.35) shows harmonics. The first harmonic ( $n = 1$ ) maximum is  $1.16I_0$  and is located at a distance  $z = L_1$  from the center of the gap of the first cavity such that  $X = 1.84$ . The second harmonic ( $n = 2$ ) maximum is  $0.96I_0$  and it is located at  $z = L_2$  such that  $X = 1.54$  [8, 9]. The second cavity is usually located near  $z = L_1$  where the electron bunches are strongly formed.

Contrary to the first cavity entrance, both the electron velocity  $v(L_1, t)$  from (1.34) and the current  $I_b(L_1, t)$  from (1.35) at the entrance of the second cavity change over time and are time-modulated. The beam current  $I_b(z, t)$  travels inside the gap (width  $d_2$ ) of the second cavity.  $I_b(z, t)$  is an instantaneous current along  $z$  at time  $t$ .

Each electron induces a positive image charge in the walls at the ends of the drift tubes and especially in the cavity. Thus, at time  $t$ , the current  $I_2(t)$  induced inside

the cavity is the sum of all the charges induced by the electrons in the gap at time  $t$ . This can be expressed mathematically by stating that  $I_2(t)$  is the integral of  $I_b(z, t)$  from  $L_1$  to  $L_1 + d_2$ .

After calculations,  $I_2(t)$  comprises the three main terms:

- $I_0$ , the average current, which does not interact with the cavity;
- 

$$I_{21} = M_2 \cdot I_{b1} e^{j\omega t} \quad (1.36)$$

with  $I_{b1} e^{j\omega t}$  = the first harmonic of the beam current  $I_b(z, t)$  at  $L_1 + d_2/2$  and  $M_2$  the coupling coefficient given by (1.38) below;

- 

$$I_{22} = jG_0(V_2/D_2)[\exp(-jD_2/2)][\cos(D_2/2) - \sin(D_2/2)/(D_2/2)] \quad (1.37)$$

with  $G_0 = I_0/V_0$  and  $D_2 = \omega d_2/v_0$ . The voltage  $V_2$  induced in this second cavity (between the ends of gap  $d_2$ ) is given further in the Sect. 1.2.1.

### Behaviour of the Second Cavity

The coupling coefficients, for instance  $M_2$ , are always  $<1$  and express the fact that the field  $E_2 = -V_2 e^{j\omega t}/d_2$  experienced by an electron is a function of time and changes during the traveling of this electron through the gap.

Up to now, the above calculations assumed an ideal gap with imaginary grids [9]. If we now consider a real gap with the electric field extending inside the adjacent drift tubes on the left and right and varying in both the axial and radial directions, the general expression of  $M_2$  is given by

$$M_2 = \frac{1}{\int_0^a \int_{-\infty}^{\infty} E_2(z, 0) r dr dz} \int_0^a \int_{-\infty}^{+\infty} E_2(z, r) e^{j\omega z/v} r dr dz, \quad (1.38)$$

where  $\int_{-\infty}^{+\infty} E_2(z, 0) dz = V_2$ .

The narrower the gap  $d$  and the smaller the radii  $a$  or  $b$ , the more  $M_2$  approaches 1, and only when  $D_2 \geq 1.2$  rad and  $\omega b/v_0 \geq 1$  rad,  $M_2$  drops off to any large extent. These factors determine the orders of magnitude of the gap  $d_2$ , the drift tube diameter  $2b$ , and the electron beam width  $2a$ , given that the filling coefficient  $a/b \approx 0.6$  and that  $b$  and  $d_2$  are also related to the  $R/Q$  values of the cavity.

$I_{22}/V_2$  looks like a conductance  $Y_{bl} = G_{bl} + jB_{bl}$ . This is known as the beam loading conductance. A positive  $G_{bl}$  value means that an energy is taken from the modulated electron beam, whereas a negative one means that an energy is given to the electron beam.  $G_{bl}$  is at a maximum for  $D_2 = \pi$  and becomes negative after  $D_2 = 2\pi$ . Thus, if a cavity has a gap such that  $D_2 = (\omega d_2/v_0) > 2\pi$ ,  $G_{bl}$  is negative,  $G_{bl} + G_c$  can be also negative, and an oscillation (known as ‘‘monotron’’ oscillation) can occur.  $G_c$  is the conductance representing the cavity losses.  $\omega = 2\pi f$  is related not only to the operating fundamental mode of the cavity, but also to anyone of the numerous resonances at higher frequencies.



The expressions given above determine the equivalent schema for the second cavity as for any of the other intermediate cavities. This equivalent schema is an oscillating circuit, as represented in Fig. 1.11a, driven by the induced current  $I_{21}$  and loaded by the “losses” conductance  $G_c$  and the beam loading conductance  $Y_{bl}$ .

### Space Charge

Up to now, we have neglected the space charge, i.e. the repelling force between electrons which naturally tends to separate them, thereby hindering bunching. If we disturb an electron beam in a state of equilibrium by moving an electron in relation to the other ones, this electron is firstly repelled by its neighbours and then returns to its position of equilibrium, which it overshoots, before turning back again towards the equilibrium position, like a swinging pendulum. This movement takes place within a beam moving at a velocity  $v_0$ . The frequency of this oscillation phenomenon (known as the plasma frequency  $f_p = \omega_p/2\pi$ ) is given by  $\omega_p^2 = (e/m)(\rho_0/\epsilon_0)$  with  $\rho_0 = J_0/v_0$ , the beam charge density, and  $J_0 \approx I_0/\pi a^2$ , the current density [10]. Nevertheless, this expression is somewhat inexact because the true plasma frequency  $f_q$  must take into account the metal or conducting walls of the drift tubes.

Taking the space charge into consideration, it changes the second term of  $v(d, t)$  in the expression (1.34), which has to be multiplied by  $\cos(\omega_q z/v_0)$ . Furthermore, the expression (1.35) also changes when the space charge is included.  $X$  becomes

$$M_1(V_1/2V_0) \frac{\omega}{\omega_q} \sin\left(\frac{\omega_q z}{v_0}\right).$$

At  $\omega_q \Rightarrow 0$ , this yields the original expression.

### From the Second Cavity to the Output Cavity

The current  $I_2$  creates a voltage  $V_2 = Z_2(f) \cdot I_2$  across the gap of the second cavity. This voltage in turn modulates the velocity of the electrons, whereby this modulation is not necessarily in phase with the preceding modulation but is considerably greater in magnitude. In the drift tubes between cavities 2 and 3, the new velocity modulation is transformed on its turn into a density or a current modulation (Fig. 1.10). This iterative process continues until the addition of another cavity has quite no effect on the modulation [9].

This last cavity is the output cavity and is characterized by a high degree of coupling to the external load, that is the user’s device to which the tube is connected. In practical terms, a loop or an iris is used for this coupling (Fig. 1.8).

The equivalent circuit presented above applies to all cavities, including the last cavity which is coupled to the load (Fig. 1.11b and Fig. 1.11c). If we now assume that the beam loading expression has no imaginary part ( $Y_{bl} = 1/Z_{bl} = G_{bl}$ ) and the load too ( $Y_L = 1/Z_L = G_L = 1/(R/Q)Q_L$ ), this yields

$$Y_N = (1 + 2jQ_N\Delta)/(R/Q)Q_N \quad (1.39)$$

with  $\Delta \approx (\omega - \omega_0)/\omega_0 = (f - f_0)/f_0$  and  $1/Q_N = 1/Q_c + 1/Q_{bl} + 1/Q_L$ . Then

$$V_N = I_N/Y_N. \quad (1.40)$$

Therefore,  $P_{OUT}$  can be written as,

$$P_{OUT} = \frac{1}{2}V_N^2G_L = \frac{1}{2}I_N^2G_LQ_N^2(R/Q)^2/(1 + 4Q_N^2\Delta^2). \quad (1.41)$$

This expression can be used to yield the gain  $G = P_{OUT}/P_d$  and the interaction efficiency  $\eta = P_{OUT}/V_0I_0$ .

The methodology we have applied since the Sect. 1.2.1 shows how  $P_{OUT}$  can be deduced from  $P_d$  throughout the formulae (1.33) up to (1.41). However, it is important to bear in mind that these expressions hold only at “weak fields or signals”. As soon as  $P_d$  increases in magnitude (i.e. modulation increases), we are no longer dealing with linear problems and the equation for  $P_{OUT}$ , as given by (1.41), becomes more complex, and in fact, even ceases to be analytical. The nonlinearities are primarily due to electron bunching and space charge forces.

This being the case, more complete and complex calculations are required, necessarily drawing on computer processing power. In fact, computer permits us to analyze considerably more than just the non-linear phenomena; it also allows us to incorporate radial movements (neglected in previous calculations), the 3D nature of certain events, relativistic effects and reflected electrons. Schematically speaking, this involves solving the electron movement equation for varying electromagnetic fields and space charge fields.

## Output Power Optimization

Most of the time klystrons use 4, 5 or 6 cavities. These cavities gradually increase the RF beam current  $I_b$ , then  $I_N$  and  $P_{OUT}$ , despite the space charge forces, which become very disturbing when  $I_b$  is more and more large. At the same time, to optimize  $P_{OUT}$ , the velocity dispersion must be kept low,  $(v - v_0)/v_0 \leq 10$  to 20%, in order to avoid reflected electrons from the output cavity. Therefore, the intermediate cavities are carefully frequency tuned to adjust the gap voltages in amplitude and in phase and, at the same time, to control the RF beam current and the velocity dispersion.

Some klystrons use a second harmonic cavity which resonates at a frequency slightly lower than  $2f_0$ . Such a cavity is excited by the second harmonic of the beam current and generates a voltage which reinforces the bunching and the efficiency. This cavity is usually located after the second one, where the electrons are already concentrated in a phase extension  $\leq \pi$ .

Due to the values of the impedance  $Z_L$ , the absolute value of  $V_N = Z_N I_N$  can exceed  $V_0$ , which is the voltage corresponding to the average electron velocity. Were  $V_N$  to exceed  $V_0$ , the electrons would be decelerated, but some would even be reflected back towards the cavities and the cathode, which would generate beam interception and lead to klystron malfunction or even permanent damage.

The output cavity behaves at large signals like a current generator with an internal impedance  $R^*$  around the operating point. Therefore,  $P_{\text{OUT}}$  is maximum when  $Z_L = R^*$ . Since the coupling iris or the loop transform the load impedance at the user device (radar or transmitter antenna, accelerator structure) to the load impedance at the cavity, these coupling devices have to be adjusted so that  $Z_L = R^*$ , in order to maximize the output power.

## Klystrons Engineering and Technologies

This presentation of different steps of the interaction in a klystron allows us to understand the klystron structure which is designed around the electron beam on one hand and the cavities and the drift tubes on the other hand.

From a technological point of view, as shown in Fig. 1.8, the constitutive elements of the klystron tube are:

- The Pierce type electron gun, especially with the high voltage insulator and the cathode. The high voltage insulator is a cylinder made of alumina located between the anode and the cathode. Its dimensions are such that the DC electric fields are smaller than the breakdown limit. The electron emissions from the triple point are minimised thanks to a screen, called anticorona ring. The anode is grounded for electrical safety reasons, explaining why the gun and the cathode are usually raised to a negative voltage;
- The modulating cavities (usually frequency tunable in a factory);
- The last or output cavity coupled to the output waveguide thanks to a coupling loop or iris;
- The output window(s) which is located in the waveguide(s) and which separates the external atmosphere from the internal vacuum ( $\approx 10^{-8}$  Torr) inside the tube. The drive power to be amplified is usually injected inside the first cavity through a coaxial connection which is also vacuum tight thanks to a small input window;
- The collector whose function is to collect the electrons after their interaction in the last cavity and to dissipate their remaining energy. Moreover, it must be able to dissipate the whole electron beam energy, when  $P_d = 0$  and then  $P_{\text{OUT}} = 0$ . Therefore, it has to be efficiently cooled. The collector is usually at the same potential than the body or the anode;
- The magnetic circuit including an electromagnet, or permanent magnet(s), and the two pole pieces located near the anode and between the collector and the output cavity. These pole pieces concentrate the magnetic flux to get the required focusing  $B_Z$  parallel to the axis ( $B_R/B_Z$  better than several ‰).

The vacuum is usually maintained thanks to a small ion getter pump. However, this pump is not always necessary, because the beam itself has also a pumping function. The accelerated electrons ionize the residual gases. Then the generated ions are electrically attracted by the beam and slowly drained toward the cathode.

## 1.2.2 Multibeam Klystrons

### Limitations in the Increase of $P_{\text{OUT}}$ in a Klystron

As explained in Sect. 1.2.1, the space charge forces are opposed to a perfect electron bunching. These repulsion forces appear in the form of the plasma frequencies  $\omega_q$  or  $\omega_p$ , which is proportional to the square root of the perveance  $P$ .

In a conventional klystron, the perveance of the beam is in the range 0.5 to  $2.5 \times 10^{-6} \text{ A V}^{-3/2}$ . A perveance  $P = 2.5 \times 10^{-6} \text{ A V}^{-3/2}$  is the practical limit, beyond which the electron beams are difficult to be maintained fairly cylindrical and to be focused without notable body interception. When the perveance is high, the efficiency is low. At the same time the instantaneous bandwidth is enlarged to  $\approx 5\%$  or more, instead of the usual 1 to 2%. This last point is explained by the high value of the beam loading conductance  $G_{\text{bl}}$  proportional to  $P V_0^{1/2}$ , which damps all the cavities.

On the contrary, a perveance  $P = 0.5 \times 10^{-6} \text{ A V}^{-3/2}$  is the practical lower limit under which the smallness of the current  $I_0$  dictates unacceptable high beam voltages  $V_0$  and involves many electrical insulation difficulties on the tube itself and on the whole transmitter or equipment. But the low perveances are favourable for high interaction efficiencies because a strong bunching can be achieved.

In conclusion, larger output powers are obtained by increasing either the beam current  $I_0$  or the high voltage  $V_0$ . In the first case the perveance is important; the efficiency notably decreases, but the instantaneous bandwidth is enlarged and the limitations are the control and the focusing of the beam. In the second case the perveance is kept low; the efficiency is therefore high, but the main limitations are the breakdowns and the practical use of high voltages.

### The Multibeam Klystrons (MBKs)

The MBKs give the possibility to reach larger RF output powers with high efficiencies and, at the same time, acceptable high beam voltages, despite very high perveances. A conventional or one beam klystron (OBK) uses just a single electron beam which travels along the common axis of the tube and the magnet. On the contrary, the MBK, as shown in the Fig. 1.12, uses several ( $N$ ) electron beams which travel all together through the same cavities, but each one has its own drift tube. Therefore, each electron beam has a low current  $i_0$  giving rise to a high efficiency  $\eta$ . The whole current  $Ni_0$  is important; then, for the same RF output power  $P_{\text{OUT}} = V_0 \eta N i_0$ , the cathode voltage is modest and even small. For example, the number of beams is 6 or 7. The perveance of a single beam is about 0.5 to  $0.6 \times 10^{-6} \text{ A V}^{-3/2}$  and the total perveance  $P = N i_0 V_0^{-3/2} \approx 3$  to  $4 \times 10^{-6} \text{ A V}^{-3/2}$ . The interaction efficiency is around 65%.

In comparison with a OBK, the cathode voltage  $V_0$  is usually reduced by  $\approx 40\%$ . Consequently, the electrical fields  $E_0$  are decreased and the product  $E_0 V_0$  ( $\text{kV}^2/\text{mm}$ ),

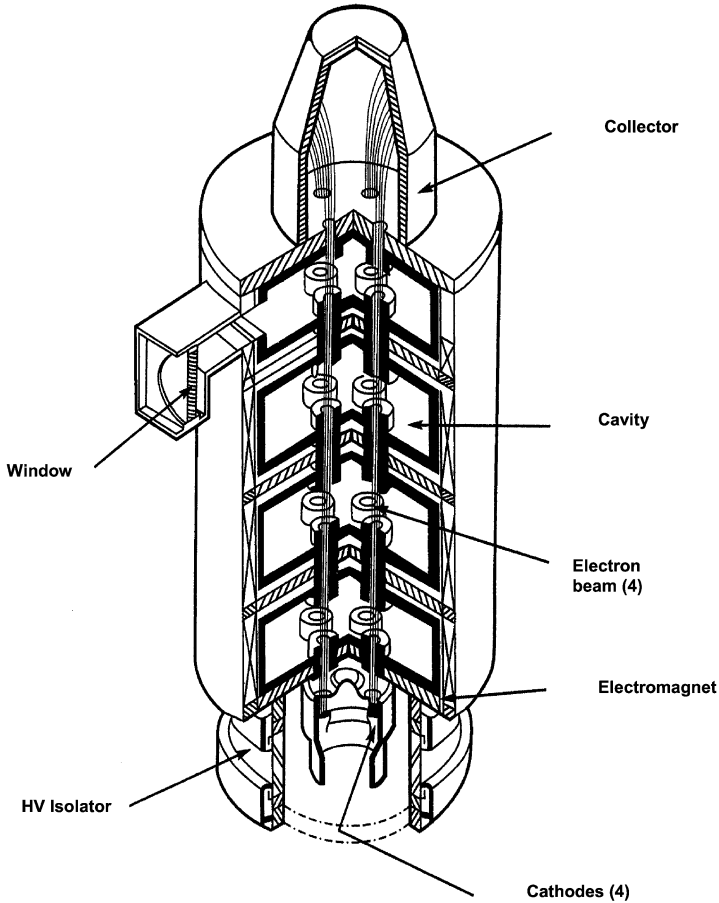


Fig. 1.12. Multibeam klystron cross-section (4 beams)

which interprets the breakdown occurrence, is also reduced by more than 50%, giving rise to the possibility of much more safe and reliable operations in longer pulses or DC voltages.

The cavities are cylindrical. The RF resonant mode is generally the conventional one, the  $TM_{010}^O$ , and the re-entrant drift tubes, where the beams are passing through, are concentrated around the axis [7], as shown in Fig. 1.13. The RF field pattern allows, of course, an in phase interaction of each electron beam, but also high coupling factors  $M$  between the electrons and the RF electric field  $E$ , despite a non-negligible variation of  $E$  versus the radius and the possible influence of the RF magnetic field.

The overall high perveance of the electron beams increases the conductance of the beam loading of the cavities. Consequently, the instantaneous bandwidths become larger, by a factor of 5. Finally, the cavities are designed in such a way that

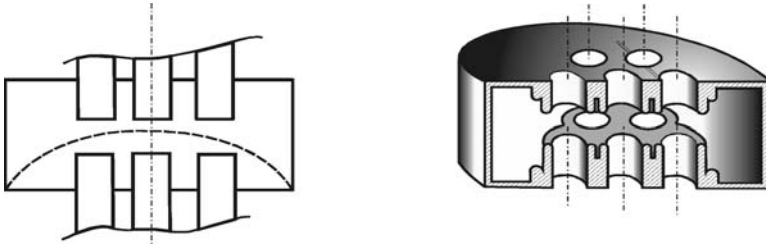


Fig. 1.13. MBK cavity (7 beams)

the adjacent modes are very far from the operating one. The reason is to prevent monotron oscillations (see Sect. 1.2.1), encouraged by the large whole beam current  $Ni_0$ .

The focusing of the electron beam is difficult because the beams axes are offset and not identical with the tube axis, generating an important radial magnetic field  $B_R$ . Therefore, the electromagnet is equipped with specific multiple pole pieces. Between those the axial field is nearly constant, and the relative radial components  $B_R/B_Z$  smaller than a few %.

In short, the main characteristics of the MBKs are the significantly lower cathode high voltages and the larger efficiencies and/or the broader bandwidths. The results are:

- Smaller dimensions and size and reduced electrical supplies;
- Lower breakdown or arcing risks. HV insulation in air and less and less in oil;
- Less X-rays parasitic radiations;
- Better reliability.

However, the designer has to take into account the following two difficulties:

- Focusing and transmission of the  $N$  beams,  $N - 1$  of which (at least) being offset in respect to the axes of the tube and the magnetic field;
- Elimination or damping of parasitic oscillations in the cavities, which can present many high order modes.

### 1.2.3 Inductive Output Tubes (IOT)

In the lower part of the frequency spectrum, for instance around 500 MHz in the TV bands, the ground transmitters are now equipped with Si and SiC transistors in parallel. But the RF output power is limited to several hundreds of W. To achieve much higher output power in the range of tens of kW, vacuum tubes are still used – and for a long time – thanks to their proven reliability and great efficiency. The tubes are triodes, tetrodes [11], klystrons and now mainly IOTs.

The gains of about 13 to 15 dB of triodes and tetrodes are very low. On the other hand, the large size and the unpracticable frequency tuning of the TV klystron cavities are not very attractive. That's why a hybrid tube, the IOT, has been developed about 20 years ago for the main use with transmitters operation in the 470–830 MHz

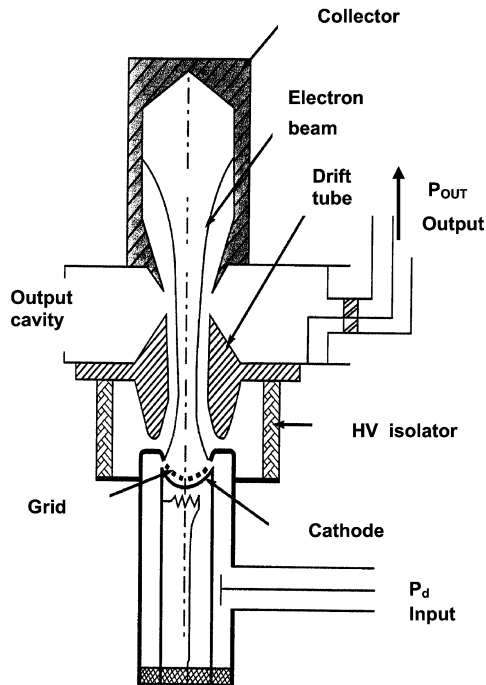


Fig. 1.14. Inductive output tube (IOT)

range, at power of several dozen kW and gains of 20 to 23 dB compatible with solid-state drivers.

IOTs represent a modification from conventional coaxial grid tubes towards a linear beam structure close to the one of the klystrons, but with just one cavity (Fig. 1.14). A Pierce type electron gun fitted with a cathode and a spherical modulation grid  $G_1$  creates a converging electron beam, with an average current  $I_0$ , modulated by a periodic voltage  $V_G$  at the microwave frequency  $f$ .

To avoid any malfunction, no microwave interaction must take place in the large accelerating gap between the grid and the anode. This is why the gun is designed so that no microwave energy enters this gap. Such an energy could come from the tube outside or because of leakages from the coaxial cathode-grid resonator and from the output cavity through the anode. Also, no oscillation may occur in this gap; therefore, microwave resonances must be eliminated.

The electron bunches between the grid and the anode are accelerated by high voltages  $V_A$  going up to 30 kV or more, which is considerably higher than the 8–10 kV limit of triodes. After the anode, the bunches are traveling across a klystron type resonating cavity where much of their kinetic energy is transferred to a waveguide or coaxial cable, in order to yield the output microwave power  $P_{OUT}$ . The process is exactly the same as in the output cavity of a conventional klystron. It should be

noted that a too high deceleration voltage in the cavity can reflect electrons towards the cathode and damage the tube.

Finally, the remaining energy of the electrons is dissipated in the collector. Because the beam is short and don't include any cylindrical part, the focusing is simplified; just a permanent magnet around the anode is needed.

From a technological point of view, the most critical part is the grid gun, not only because the grid is located very close ( $\approx 1$  mm) to the hot cathode, but also because the drive power  $P_d$  must be injected in the gun assembly which is raised to a high potential of  $-V_A \approx -30$  kV. This is done thanks to a coupling loop and RF traps that are difficult to design. By the way we note that, in most of the tubes, the anode is grounded for electrical safety reasons, explaining why the gun and the cathode are raised to  $-V_A$ .

Before to conclude it should be point out that:

- the presence of a grid close to the hot cathode and the design of the coaxial resonator limit the operating frequencies to 1.5 GHz maximum,
- and the high voltage  $V_A$  is practically limited by the necessary use of air – and not of oil – to insulate the gun including the cathode–grid resonator.

Finally, IOTs are very attractive specific grid tubes operating below 1.5 GHz, at high voltages of about 30 kV. The gains are around 22–23 dB and efficiencies around 55%, for microwave output power of 10 to 100 kW.

## 1.3 Traveling Wave Tube (TWT)

### 1.3.1 Introduction

Looking back from the beginning of the 21st century to the history and evolution of microwave tubes (as described in Sect. 1.1.2 of this book), we might wonder why the TWT (Lindenblad, 1940; Kompfner, 1942), as the purest realization of the microwave generation principle in electron tubes, was invented after the magnetron (A.W. Hull, 1921, to K. Posthumus, 1933) and after the klystron (R.H. & S.E. Varian, 1937). The limited information exchange during the war might have been the reason why the U.S. patent of Lindenblad [12] was not known by Dr. Rudolph Kompfner, an Austrian refugee working on microwave tubes for the British Admiralty, and why it took again years from their documented inventions of the TWT principle to Kompfners publication [13] in 1946.

In fact, the TWT shows all the necessary elements for RF generation in a tube in a pure, geometrically separated and physically subsequent form. Those elements are electron beam formation and acceleration in an electron gun, power transfer from the electron beam to the amplified RF wave in an interaction section and collection of the decelerated spent electron beam in a collector. Additional elements are the RF input and output couplers at the beginning and the end of the interaction section and the magnetic beam focusing system.



In contrast to its clear physical principle, the TWT employs the most challenging manufacturing technology amongst the microwave tubes. The necessity to focus a high power density electron beam through a tiny helix with length more than 100 times the diameters ranging from 0.3 mm (60 GHz) to 4 mm (1.5 GHz) requests mastering of very small tolerances between beam forming structures and the magnetic focusing system. The fragile delay line structures limit the obtainable RF power compared to the bulk resonator structures of magnetrons or klystrons. The difference in technological maturity and power handling capability at time of TWT appearance is shown in Table 1.1.

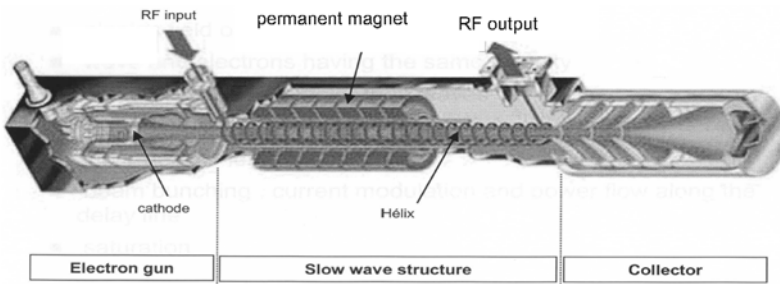
Though the basic difference in the power handling capability was remaining over the years (see Fig. 1.1), TWTs have developed since that time, due to their excellent linearity and broadband capability, to the major microwave amplifier used in terrestrial and especially in space telecommunication. Other TWT applications are: coherent microwave sources for radar surveillance and guidance systems, satellite based Earth observation radars and as broadband Electronic Counter Measurement (ECM) amplifiers.

### 1.3.2 TWT Design and Operation Principle

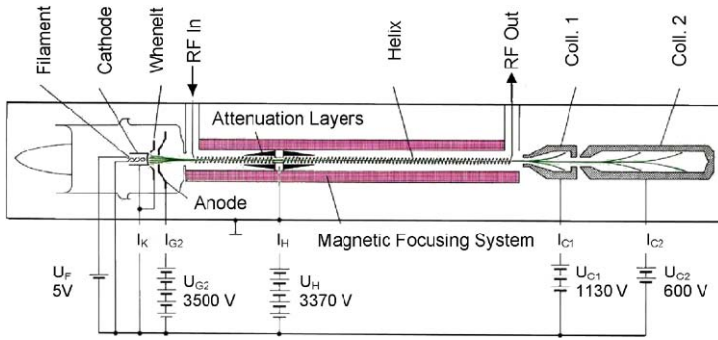
Figure 1.15 gives a cross-section through a permanent periodic magnet (PPM) focused electrostatic 4 stage collector TWT showing the essential functional elements.

**Table 1.1.** Output power and application of early C-band magnetrons, klystrons and TWTs around the time of first industrial production of TWTs. Data are from [14–16] for magnetron, klystron and TWT, respectively

Parameter	Magnetron	Klystron	TWT
Year	1942	1949	1952
Manufacturer	Western Electric	Stanford University, Varian	STC
Type	WE 718	Mark III	
Application	Radar	Linear Electron Accelerator	TV, Ground Link Communication
Frequency	2.7–2.9 GHz	2.85 GHz	3.6–4.4 GHz
Output power	193 kW, pulsed	12 MW, 1 μs pulses	2 W, CW



**Fig. 1.15.** Cut through a PPM focused, electrostatic 4 stage collector TWT



**Fig. 1.16.** Electric circuit of a CW-TWT with double stage collector

Figure 1.16 provides the electrical circuit needed for its operation (only 2 collector stages are shown). A vacuum envelope, comprising the electron gun, the RF interaction section and the collector is evacuated to the  $10^{-9}$  mbar range. Metal/ceramic brazing technology is used for the electrical feed-through to the electron gun and collector and for the windows at RF in- and output. In the further description we follow the electrons from emission to collection.

**Electric Circuit and Electron Gun**

To emit the electron current  $I_K$  from the cathode surface, a thermionic cathode is heated to its operating temperature  $T_C$  of about  $1000^\circ\text{C}$  brightness by a filament power supply which provides filament voltage  $V_F$  and filament current  $I_F$  on a negative cathode potential  $V_K = -V_H$ . Application of positive voltages  $V_{G2}$ ,  $V_H$ ,  $V_{C1}$ ,  $V_{C2}$  let the electrons flow through the vacuum to the respective electrodes and from there in closed circuits through their respective power supplies back to the cathode. Looking closer, they first form an accelerated electron beam which is focused by a PPM focusing system through the helix and is mainly collected by the collector electrodes. The kinetic beam power  $P_{\text{beam}} = I_K \cdot V_H$  of the accelerated electron beam entering the delay line section at ground potential had to be spent as potential power by the various electrode power supplies when pumping the negative charged electrons from their electrode potentials  $V_{G2}$ ,  $V_H$ ,  $V_{C1}$ ,  $V_{C2}$  to the negative cathode potential  $V_K = -V_H$ . Thus the major power supplies are the collector power supplies because anode and helix supplies have to provide only very small powers  $P_{G2} = I_{G2} \cdot V_{G2}$  and  $P_H = I_H \cdot V_H$  due to the small interception currents  $I_{G2}$  and  $I_H$ .

The electron beam entering the delay line is formed by the electron gun optics to a small diameter electron beam characterized by the area beam convergence factor CF as the ratio of cathode surface to beam cross-section area. For various TWT applications CF can vary in the range 1–100. For very good beam focusing properties CF should be maintained below around 30.

## Focusing System and Delay Line/RF Interaction Section

The delay line, as the structure with the largest interface to the TWT environment, is kept on ground potential. This has the advantage that the interception current  $I_H$  with the electron beam, which needs to be controlled in safe operational limits, can simply be monitored on ground potential. Here the subscript “H” reminds of “helix”, the RF delay line used in many TWT designs. To avoid the interception with the delay line due to the repulsive radial space charge forces in the beam, compensating magnetic forces have to be introduced by a focusing system. Constant axial fields produced by solenoids or periodic fields created by alternating permanent magnets can be used. Sufficient details of the focusing concepts will be discussed later in Sect. 1.3.2.

The RF power  $P_1$  is fed through the RF input window to the delay line. It travels on the delay line with reduced phase velocity  $v_p$  approximately equal to the velocity of the electrons in the beam. Interacting with the electron beam, the RF wave gets amplified towards the output to the RF power  $P_2$ . Normally, the delay line is divided into an input and output section to limit the gain in each section. At the centre sever of the delay lines the RF wave is attenuated to avoid reflections and oscillations in the sections.

The maximum RF gain can be obtained when the electrons are slightly faster than the RF wave. At that condition the phase velocity is equal to the moving electron density bunch  $v_{\text{bunch}}$  which is forming in the decelerating phase of the RF wave. It is the velocity of the slow space charge wave on the electron beam moving backwards with the velocity  $-v_{\text{sc}}$  or, looking from outside, with the velocity  $v_e - v_{\text{sc}}$ . Thus

$$v_p = v_e - v_{\text{sc}} = v_{\text{bunch}} \quad (1.42)$$

is the fundamental synchronism condition of a TWT. The understanding of this interaction and RF amplification process can be enlightened by the following everyday observation. Assume that electrons, moving across the decelerating and accelerating phases of the RF field, behave like a steady stream of cars moving over a hilly highway. On the uphill side the cars become decelerated and the car density becomes higher. The opposite occurs on the downhill side. Thus we create a bunching of cars on the uphill side, which can remain with time at the same hillside position even when the single cars move over the hill. Back in our electron picture this means that the electron bunch remains and growth for some time in the same decelerating phase with respect to the RF wave. Due to deceleration of bunch electrons, resulting in a growing of bunch space charge density and thus growing of RF current, a maximum amount of kinetic electron energy is at this synchronism condition transferred to the amplified RF wave. Thus at ideal synchronism we get the maximum power gain of the TWT. A quantitative approach to the beam/RF interaction process was given by Pierce, see Sect. 1.3.3.

At the end of the delay line we find: (a) an amplified RF wave with power  $P_2$  coupled via the RF output coupler to a load, and (b) a decelerated spent electron beam with a wide electron velocity spectrum. Depending on the interaction efficiency, the

beam has still about 65% to 95% of its initial kinetic power left, which can be recovered up to approximately 80% in the electron collector.

To support the understanding of the interaction physics further, it is mentioned here that a linear accelerator (LINAC), which transfers power from a propagating RF wave to a stream of charged particles (e.g. electrons), can be understood as an inverted TWT. To accelerate electrons in a growing bunch, it requests for its optimal operation the coupling of the RF wave to the fast space charge wave on the particle beam, and thus the LINAC synchronism condition is given by

$$v_p = v_e + v_{sc} = v_{\text{bunch}}. \quad (1.43)$$

That means, in a LINAC the RF wave has to be faster than the charged particles (e.g. electrons) in order to maintain synchronism with the growing bunch during acceleration of single particles in the bunch. In other words, the accelerating phase of the wave front densifies the slower moving single particles in a growing bunch moving with the RF phase velocity.

Having this inversion in mind, we might wonder again why the TWT was invented only in 1942, because the LINAC principle was described already in 1924 by Gustaf Ising, a Swedish physicist, and it was built already in 1928 by the Norwegian engineer Rolf Wideröe.

## Collector

The first TWT collectors built were like klystron collectors, single stage collectors on ground potential ( $V_C = V_H$ ). At the grounded collector electrode the current loop is closed for the dominant portion  $I_C$  of the electron beam current  $I_{\text{beam}}$ . Since the spent electron beam entering the collector carries still a lot of kinetic power, this power is thermally dissipated when the electrons hit the collector walls. Now we want to know this dissipated power  $P_{C,\text{diss}}$ .

Assuming that the generation of the RF power  $P_2$  has slowed down only the electrons entering the collector, we can write, because of conservation of energy for the dissipated power in the single stage collector,

$$P_{C,\text{diss}} = I_C \cdot V_C - P_2, \quad (1.44)$$

where  $P_2$  is the RF power (fundamental and harmonics) created in the delay line circuit. The goal of TWT designers is to reduce all losses, but due to its dominance especially the collector losses. According to (1.44) this can be done for a given output power  $P_2$  in two directions: first, by reducing the beam current and thus the collector current  $I_C$  required to produce the output power  $P_2$ , which needs improvements of the beam to RF interaction in the delay line section; second, by reducing the collector voltage  $V_C$  with respect to the cathode. This collector voltage depression is possible as long as the slowest electrons in the spent beam entering the collector have sufficient kinetic energy  $E_{\text{kin},\text{min}}$  to arrive at the electric potential of the collector surface,

$$E_{\text{kin},\text{min}} > |e \cdot (V_H - V_C)|. \quad (1.45)$$

Here  $e$  is the elementary charge of the electron. In modern space application TWT's a depression ratio up to  $(V_H - V_C)/V_H = 0.55$  can be obtained. Since for a constant pitch helix the beam power efficiency  $\eta_0$  is about 13%, it was a breakthrough, when H. Wolkstein [17] reached in 1958 with a single stage depressed collector TWT 30% efficiency.

Similar consideration can be made when  $i$  collector stages are introduced to further decelerate the fast electrons in subsequently depressed collector voltage stages. In the formula (1.44) the term  $I_C \cdot V_C$ , the electric power provided by the single stage power supply, can be replaced by the much smaller sum over the electric power supply stages  $i$ , and the dissipated power in a multi stage collector becomes

$$P_{C,diss} = \sum_i I_{C_i} \cdot V_{C_i} - P_2, \quad (1.46)$$

$$E_{i,kin} > |e \cdot (V_{C_i} - V_{C_{i+1}})|. \quad (1.47)$$

In (1.47) the entrance condition for the residual kinetic energy of electrons in stage  $i$  is related to the increase of potential energy of electrons entering the stage  $i + 1$ .

An exotic extreme with 10 depressed collector stages was reached by Neugebauer and Mihran [18] in 1972. It allowed increasing the efficiency of a certain klystron from 54% (single stage) to 70.9%. In modern space TWTs the best compromise between efficiency improvement and complexity is found in the range of 3 to 5 depressed collector stages depending on the width of the spent beam velocity spectrum. There, with 4 collector stages a total TWT efficiency up to 74% can be obtained.

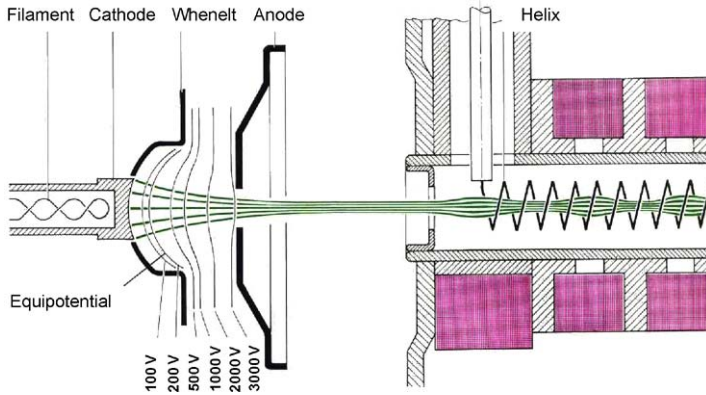
### 1.3.3 TWT Physics

After the qualitative introduction to the TWT concept and its global DC-power operation, we give in here a basic description of the TWT physics and a deeper review of the TWT components. For a detailed study additional textbooks are required. Amongst others, the three English language books [6, 19, 20] are recommended.

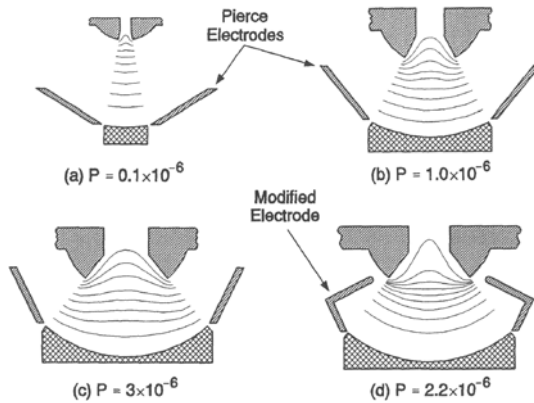
#### Pierce Electron Gun for Space Charge Limited Beams

The Pierce electron gun starts a beam from a cathode surface which is larger than the final beam cross-section in order to keep the cathode current density in the order of a few A/cm<sup>2</sup>, and thus the required operating temperature as low as possible. As Fig. 1.17 shows, this can be obtained with a spherical concave shaping of cathode surface. The equipotential lines are concentric, and the electron trajectories start perpendicular on those from cathode surface.

The perveance of such a Pierce gun can be analytically approached by the model of a conical segment of a spherical diode as calculated by Langmuir and Blodgett [21]. Here we limit ourselves to show in Fig. 1.18 the dependence of the gun perveance on the geometrical properties.



**Fig. 1.17.** Launch of an electron beam in a modified Pierce optic electron gun



**Fig. 1.18.** Perveance  $P$  of different electrode configurations measured in  $A/V^{3/2}$ . The Wehnelt (Pierce) electrode is kept on cathode potential in all cases. The perveance increases with smaller cathode to anode distance and larger half-cone angle  $\theta$  (width of cathode)

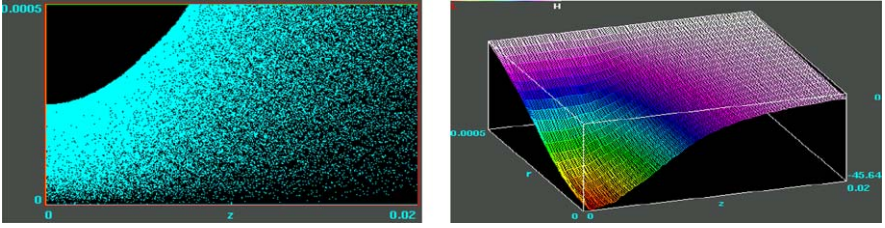
Now computer codes allow to calculate the perveance and the electron trajectories of all wanted gun geometries.

**Beam Focusing Over Delay Line Length**

Before dealing with the external measures to focus an electron beam, we look to the self-forces acting on the beam due to its charge and current density.

*Repulsive Space Charge and Attractive Magnetic Forces in a Beam*

For a uniform cylindrical beam with uniform axial velocity  $v$ , it can be shown that the radial forces at radius  $r$  on a charged particle are given by



**Fig. 1.19.** Electron distribution and space charge potential using XOOPIC, a 2.5 dimensional particle in cell code developed by the Berkeley University in California. Simulation parameters:  $I_{\text{beam}} = 110 \text{ mA}$ ,  $V_{\text{beam}} = 7.5 \text{ kV}$ ,  $r_{\text{beam}} = 0.25 \text{ mm}$  radius beam  $r_{\text{tube}} = 0.5 \text{ mm}$  radius grounded tubing

$$F_{\text{sc}} = Qe/(2\pi r\epsilon_0); \quad \text{outward radial space charge force;} \quad (1.48)$$

$$F_{\text{m}} = Qe\mu_0 v^2/(2\pi r); \quad \text{inward radial magnetic force,} \quad (1.49)$$

where  $Q$  is the total charge per unit length *inside* the radius  $r$ .

Inserting the physical identity  $\epsilon_0\mu_0 = 1/c^2$  into the ratio of both self forces one simply obtains

$$F_{\text{sc}}/F_{\text{m}} = c^2/v^2. \quad (1.50)$$

Above equations have two noteworthy consequences:

- The radial outward space charge force is dominating the magnetic pinching effect for all beam velocities, since  $v < c$ . But, there can be the exception that positive ions are neutralising the electron beam space charge which then can lead to a dominance of the contractive magnetic self force. (Example: vacuum switches, there this destructive effect is counteracted by an applied axial magnetic field.)
- At the inner edge of a cylindrical hollow beam the inside charge  $Q$  is zero, thus electrons on the inner radius of a hollow beam do not see a radial space charge force!

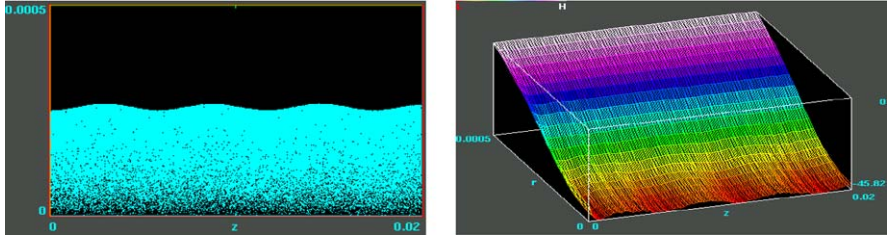
### *Universal Beam Spread*

In Fig. 1.19, we plot the beam expansion and potential depression of an unfocused, typical beam required for a 200 W Ku-band TWT in a grounded tubing with 1 mm diameter and 20 mm length. We see that within 1 cm length the beam would expand to hit the inner diameter of a helix. The potential depression at the origin is  $-45.6 \text{ V}$  and reduces due to the beam expansion.

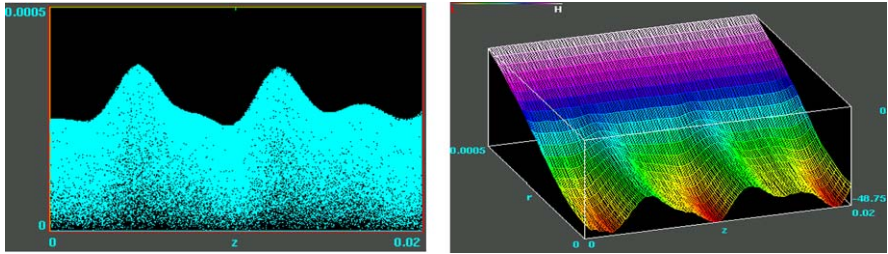
### *Magnetic Focusing*

Inserting the same beam into an axially constant magnet field with  $B_z = 0.33 \text{ T}$ , as it could be produced by a solenoid, we get a beam with a small so-called scalloping ripple, as seen in Fig. 1.20. The potential depression is now almost uniformly  $45.8 \text{ V}$ .





**Fig. 1.20.** Particle in cell simulation of a 110 mA, 7.5 kV, 0.25 mm radius beam in a 0.5 mm radius grounded tubing as simulated with XOOPIC, in a homogeneous magnetic field with  $B_z = 0.33$  T



**Fig. 1.21.** Particle in cell simulation of a 110 mA, 7.5 kV, 0.25 mm radius beam in a 0.5 mm radius grounded tubing as simulated with XOOPIC in a PPM magnetic field with 0.33 T peak field

Figure 1.21 shows the overlay of scalloping and PPM ripple period (7 mm magnet period) for the same beam and a periodic peak field of 0.33 T. In comparison to the uniform magnetic field case, we recognise a much stronger beam ripple due to the overlay of scalloping and magnetic field periodicity with a pronounced potential variation on the axis of 16 V compared to 3 V, respectively. *Note:* The potential traps along the axis can cause ion oscillation phenomena by ionisation of residual gas in a TWT. In practical life, small disadvantages of a PPM magnet system are more than compensated by large savings with respect to mass, power, reliability and interface complexity.

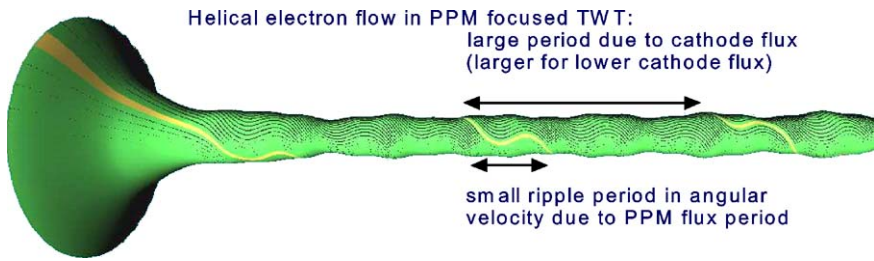
*Brillouin Flow*

There is only one special case, known as the Brillouin flow, without any beam and potential ripples. A straightforward derivation from the Busch theorem gives the Brillouin flow field  $B_{zBr}$  as function of beam current  $I$ , beam voltage  $V$  or electron velocity  $v_e$  and beam radius  $a$ :

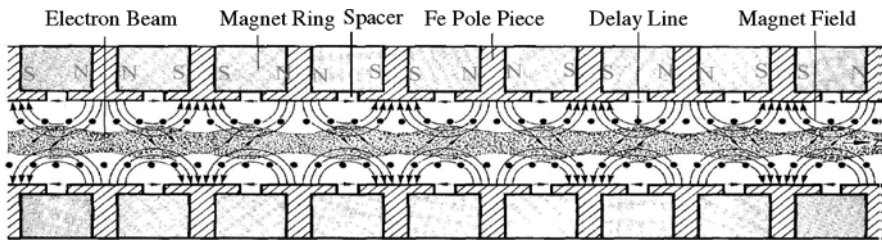
$$B_{zBr} = \sqrt{\frac{2 \cdot I}{\epsilon_0 \cdot \pi \cdot a^2 \cdot v_e} \cdot \frac{m_e}{e}},$$

$$\frac{B_{zBr}}{\text{Vs/cm}^2} = 8.3 \times 10^{-6} \frac{(\text{IA})^{1/2}}{\left(\frac{a}{\text{cm}}\right) \left(\frac{V}{\text{V}}\right)^{1/4}}. \tag{1.51}$$





**Fig. 1.22.** Envelope of an electron beam with a “golden edge trajectory” from cathode surface into the PPM focused interaction region of a typical Ku-band space TWT. Parameters of the modified Pierce gun are:  $I = 150$  mA,  $V = 7.5$  kV into a  $\phi = 1$  mm, • grounded tunnel,  $B_{\text{peak}} = 0.325$  T. (Simulated with 2D-gun program and visualised with virtual reality shareware code by W. Schwertfeger, TED, Ulm. Different relative scaling,  $r = 8 \times z$  direction)



**Fig. 1.23.** PPM magnet stack with Fe-pole pieces and nonmagnetic spacers braced to a tight vacuum envelope

Equation (1.51) is used as a design rule for TWT magnet systems: the peak PPM magnetic field should be 1.2 to 2 times the Brillouin field to guarantee a save focusing of an electron beam over the interaction length of a TWT.

Another design rule, the focusing stability requirement, is valid for the length of the magnetic field period  $l_m$  in a PPM system:

$$l_m \leq 418 \cdot \frac{V}{B_{zBr}^2} \cdot \frac{m_e}{e}. \tag{1.52}$$

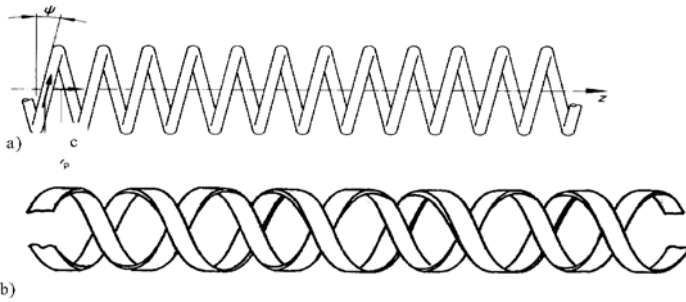
Figure 1.22 visualises the helical movement of the electrons in the PPM focused beam. A technical realisation of a PPM focusing system is sketched in Fig. 1.23.

### Delay Line System and RF Interaction

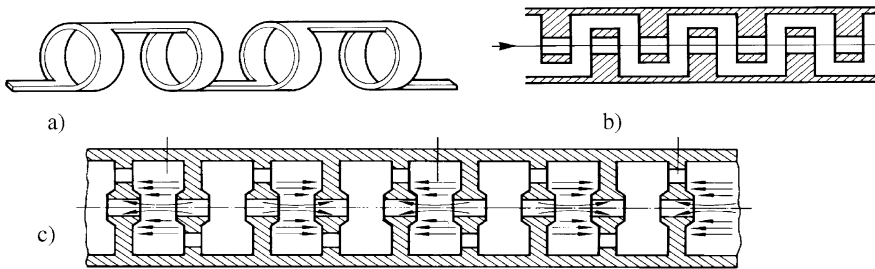
#### Types of Delay Lines

Depending on the application and power level, several types of delay lines are used:

- Helix; low power, very broadband (up to several octaves), needs ceramic supporting rods.



**Fig. 1.24. a** Helix delay line: the pitch angle  $\psi$  defines the RF phase velocity  $v_p = c \cdot \tan \psi = c \cdot 2\pi a / p$ ,  $c =$  speed of light,  $p =$  axial pitch; **b** Double helix delay line



**Fig. 1.25. a** Ring and bar line; **b** Interdigital or comb line; **c** Coupled cavity line

- Counter wound double helix; suppresses backward wave oscillations (due to mechanical complexity scarcely used), needs ceramic supporting rods.
- Ring and bar line; suppresses backward wave oscillations, needs ceramic supporting rods.
- Interdigital line; rugged and compact delay line for high power high frequency TWTs, reduced bandwidth.
- Coupled cavity; low bandwidth, high power capability.

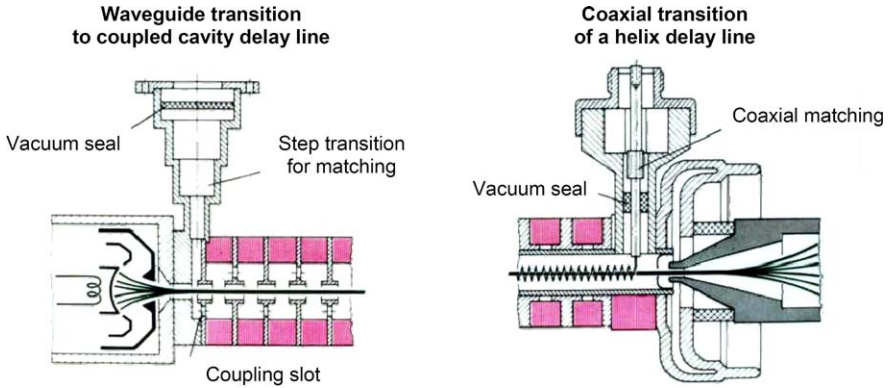
Figures 1.24 and 1.25 give a survey on the major types.

*RF Input and Output*

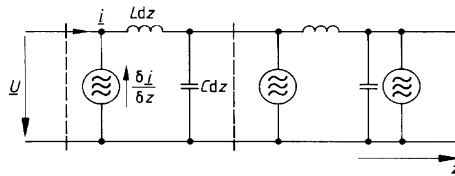
Depending on the delay line concept, several configurations for the RF input and output are known. We give in Fig. 1.26 only two examples for waveguide windows, as used, e.g. for a coupled cavity TWT input, and a coaxial feed through, as often used for low power helix TWT input and output.

*Small Signal Theory (Pierce)*

At the time Pierce developed his TWT theory, the Eulerian approach was the only success promising approach. It treats the electron beam as a charged fluid, characterised by a current  $I$  with beam velocity  $v_0$  or beam voltage  $V_0$  and the space charge



**Fig. 1.26.** *Left:* waveguide input transition with a Chebyshev step transformer for matching. *Right:* coaxial output transition from a helix with coaxial matching and  $\lambda/4$  ceramic window for the vacuum seal



**Fig. 1.27.** Equivalent transmission line model for a helix delay line

bunches as an AC current  $i$  propagating with the same frequency as the RF wave. As indicated before, this approach is limited to the small signal behaviour of the TWT because saturation effects cannot be treated. The ingenious concept of Pierce combined this Eulerian view of the electron beam with the replacement of the delay line as propagation structure by an equivalent transmission line model consisting of distributed inductances  $L$  and capacitances  $C$ , as shown in Fig. 1.27.

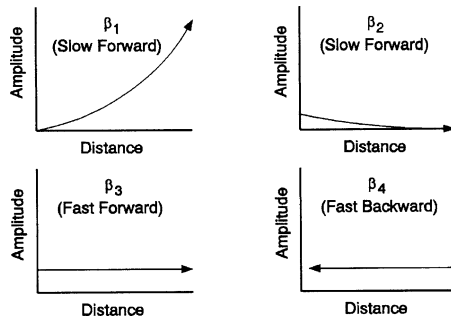
As a result of his derivation, he obtained a fourth degree equation for the wave propagation constant  $\beta$  which is known as the so-called determinantal equation

$$0 = 1 + \frac{\beta_e}{(\beta - \beta_e)^2} \cdot \frac{\beta^2 \beta_c}{(\beta^2 - \beta_c^2)} 2C^3, \tag{1.53}$$

$$C^3 = \frac{I \cdot Z}{4V_0}, \tag{1.54}$$

where  $C$  is the Pierce parameter. It has four roots corresponding to (1.55)–(1.57),

$$\beta_{1,2} = \beta_e + \beta_e C/2 \pm j\sqrt{3}\beta_e C/2; \quad \text{Solutions for exponentially increasing and decreasing slow waves;} \tag{1.55}$$



**Fig. 1.28.** The four waves propagating along the delay line of a TWT

$$\beta_3 = \beta_e(1 - C);$$

Solution for a fast forward wave with constant amplitude; (1.56)

$$\beta_4 = \beta_e(C^3/4 - 1);$$

Solution for a fast backward wave with constant amplitude. (1.57)

The meaning of the solutions becomes clear by reminding that the waves vary proportional to  $e^{j(\omega t - \beta z)}$ . Figure 1.28 sketches the four solutions. Considering only the exponentially increasing solution, we get from (1.55) the linear power gain  $G$  over  $N$  wavelengths of the TWT in dB

$$G = 10 \log 10e^{\sqrt{3}\pi CN} = 47.3 \cdot CN. \tag{1.58}$$

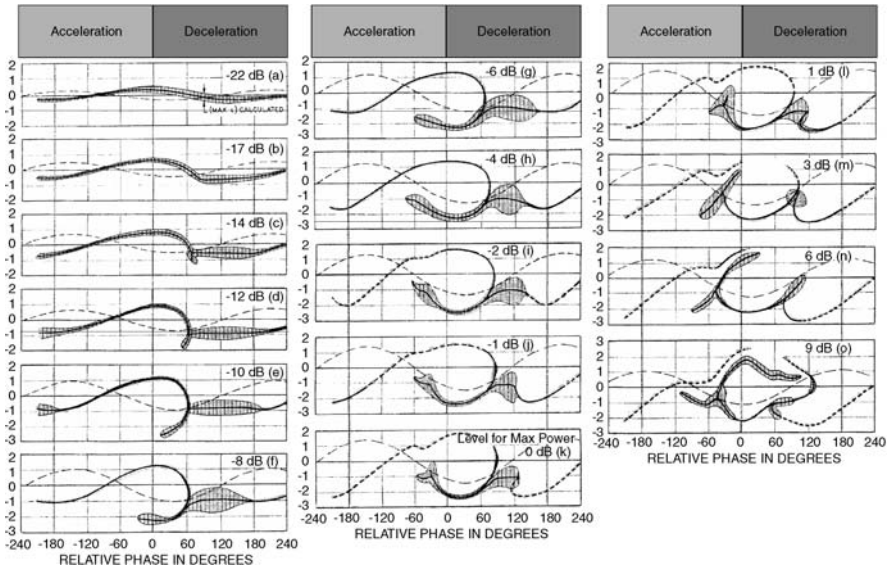
To satisfy the boundary conditions when launching the four waves at the tube entrance, one gets an additional so-called distribution loss, and (1.58) becomes

$$G = -9.54 + 47.3 \cdot CN, \tag{1.59}$$

which is the total linear power gain of the tube with distribution loss. It should be mentioned here that above solutions are not limited to helices, but are valid for all type of delay lines when introducing their respective equivalent circuit properties.

### *Cutlers Beam and RF Signal Characterization up to Saturation*

A great improvement in the understanding of the nonlinear behaviour of the TWT was reached when Cutler [22] published his test results on RF circuit voltage (dashed line), beam velocity (solid line) and beam current (vertical width of shaded area) at the TWT output relative to the undistorted signal phase as function of drive level (see Fig. 1.29). His findings for the 15 drive conditions from  $-22$  dB input back off to  $+9$  dB overdrive level are interpreted as follows. With respect to the circuit voltage, one can define an acceleration and a deceleration zone for the beam electrons.



**Fig. 1.29.** Results of Cutler experiment in 1956

Due to the acceleration or deceleration we find the relative velocity  $v_r$  of the electrons to be increased between acceleration and deceleration zone and smaller than zero in the other regions. Also, we see that  $v_r$  starts to become double-valued for drive levels larger than 14 dB input back off because some electrons are reflected back from the deceleration zone into the acceleration zone. The amount of beam current (shaded area) is larger in the deceleration zone till saturation, where the electron bunch in acceleration zone becomes about equal due to decelerated electrons moving into this zone. Two bunches in one period means that a harmonic frequency wave has been created on the circuit. This reaches its maximum after saturation. At higher overdrive level, the electrons are smeared out again more uniformly over the relative phase. If one makes a vertical cut through the electron velocity body and integrates that over various relative phases, one gets the electron velocity spectrum at the tube exit as a function of drive. This exit velocity spectrum is entering into the collector and plays an important role for the total efficiency of the TWT as we will see in the next section. Here, it can be summarised that most of the electrons are decelerated, but few of them are accelerated compared to the start velocity  $v_0$ .

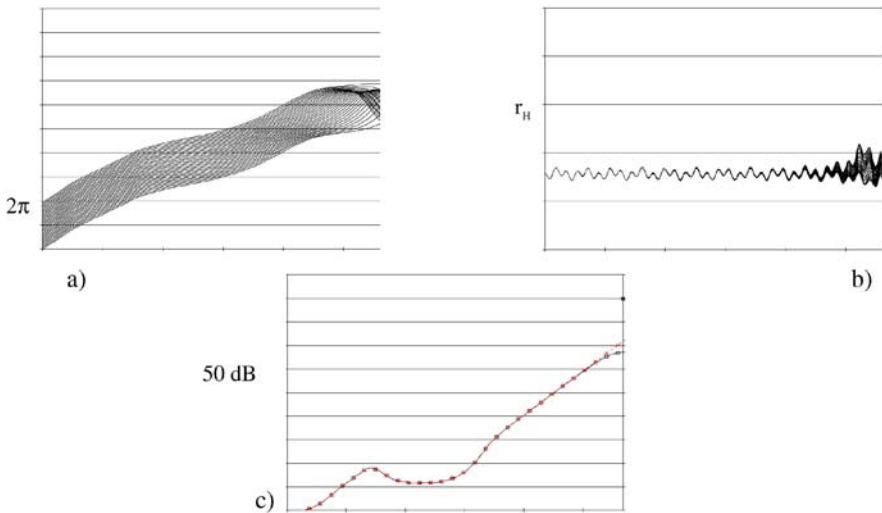
*Large Signal Theory (Rowe) and Simulation Results*

It is not space enough to report on the numerous theoretical approaches which deal with the nonlinear effects occurring closer to saturation drive of a TWT or even in overdrive. It should be sufficient to refer the reader to the compendium of Rowe [23] and to declare that no analytical solutions exist for the large signal operation of the TWT. The theoretical approaches are mainly based on the Lagrangian concept

which treats the electrons as particles or as representative particles and which allows multi-valued velocity distributions of electrons at a given space or phase location. Still today, fully 3-dimensional numerical simulations are too heavy for useful design work. A lot of 2.5-dimensional codes (2-dimensional axially symmetric electric and magnetic fields and 3-dimensional movement of representative electrons) (layers and shells of electrons, or statistically distributed “heavy electrons”), are providing reliable design information on gain, output power, nonlinear phase shift and even intermodulation distortions as a function of input drive and frequency as well as the trajectories of the representative electrons in the real space and phase space. As an input information to the code, they need from the delay line side only the coupling impedance  $K(f, r, z)$  as a function of frequency, radius and position, the phase velocity  $v_p(f, z)$  as a function of the frequency  $f$  and the axial position, the RF attenuation  $\alpha(f, z)$  as a function of the frequency  $f$  and the axial position.

For the beam, the representative charge  $\rho(r, z_0)$  and current density  $\mathbf{j}(r, z_0)$  information is required at the entrance  $z_0$  of the delay line. Figure 1.30 gives for a modern Ku-band space TWT the simulated relative phase of the electrons, being uniformly distributed over  $2\pi$  at the delay line entrance, the outer electron beam diameter and the small signal and saturation drive gain over the length of the delay line.

For Fig. 1.30a we note the crossing of electrons approaching saturation at the very last centimetres before the delay line end. From Fig. 1.30b we see again the magnetic ripple on the beam and the moderate increase of the beam radius as the electron velocity slows down close to the exit. From Fig. 1.30c we recognise the in-



**Fig. 1.30.** **a** Applegate diagram of electrons (relative phase with respect to RF wave); **b** Outer diameter of electron beam inside delay line; **c** Small signal (crosses) and saturation (circles) gain along tube axis

sertion loss at the delay line entrance, the extended sever region where RF power is transported by the electron beam and the difference between small signal and saturation gain of less than 5 dB, which is important for excellent linearity characteristics of the tube.

### Electron Beam Collector

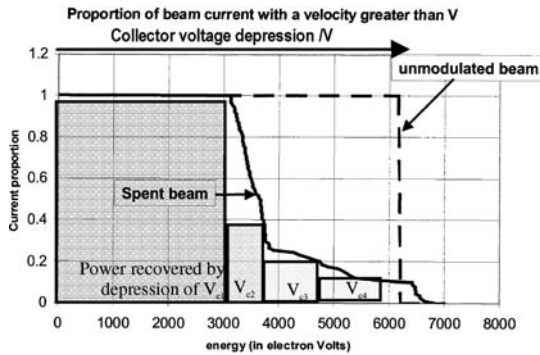
#### Collection of an Electron Beam with Distributed Velocities

Figure 1.31 shows a typical velocity spectrum of a highly efficient Ku-band space TWT at saturation drive as a cumulative distribution function. It gives on the ordinate the amount of the current ratio  $I/I_0$  which has a higher axial velocity than that corresponding to the reference acceleration voltage given on the abscissa. The original zero drive velocity distribution corresponds to the depicted rectangular distribution (all electrons have uniform velocity corresponding to helix voltage of 6250 V). The shaded areas correspond to the recovered power  $P_{\text{recover}}$  in the collector if the respective current contributions are gathered at their corresponding reduced collector potentials of a multistage collector.

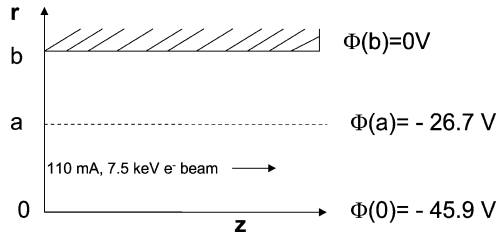
#### Potential Depression in an Ideally Focused Cylindrical Beam

Assume an ideally focused cylindrical beam with  $I = 110 \text{ mA}$  in a metallic tube at potential  $\phi(b) = 0$  with the mono-energetic beam voltage corresponding to the negative cathode potential  $\phi_c = -7500 \text{ V}$ , as shown in Fig. 1.32. With the beam velocity

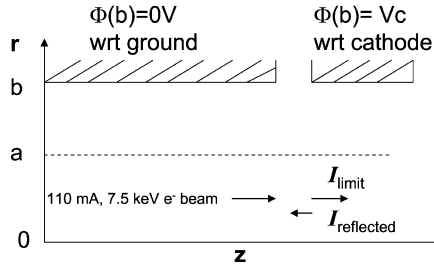
$$v_z = (2\eta(\phi_b - \phi_c))^{1/2}, \tag{1.60}$$



**Fig. 1.31.** Typical velocity/energy spectrum of the spent beam at the collector entrance and recovered power proportions (shaded area) of a Ku-band TWT with  $V_H = 6250 \text{ V}$ ,  $V_{C1} = 3250 \text{ V}$ ,  $V_{C2} = 2500 \text{ V}$ ,  $V_{C3} = 1750 \text{ V}$  and  $V_{C4} = 450 \text{ V}$  with respect to cathode. The collector efficiency is represented by the ratio of the shaded area to the total area below the spent beam distribution curve



**Fig. 1.32.** Cylindrical electron beam of radius  $a$  in a tube with radius  $b$  and potentials  $\phi(0)$  at the beam centre,  $\phi(a)$  at the beam edge and  $\phi(b)$  at the grounded tube



**Fig. 1.33.** Focused beam with voltage  $\phi_{\text{beam}}$  entering a collector iris at a reduced collector potential  $V_C$

we write the approximately valid analytical formulas for the depressed beam potential:

$$\phi(a) = \phi(b) - I \cdot \ln(b/a) / 2\pi \epsilon_0 v_z; \quad \text{Potential at beam edge;} \tag{1.61}$$

$$\phi(0) = \phi(b) - I \cdot (\ln(b/a) + 1/2) / 2\pi \epsilon_0 v_z; \quad \text{Potential at beam centre.} \tag{1.62}$$

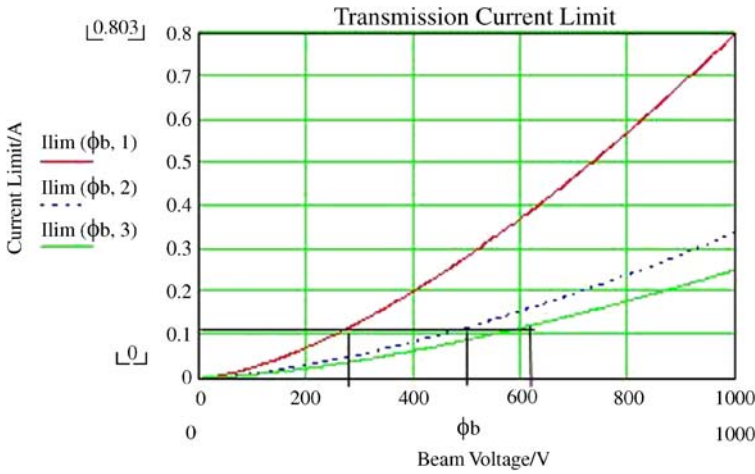
It is quite satisfying that the results for the potential depression at the beam edge and the beam centre,  $\phi(a) = -26.7 \text{ V}$  and  $\phi(0) = -45.9 \text{ V}$ , is in agreement with those from the particle in cell code XOOPIC simulation (see Figs. 1.19–1.21), where we used the same parameters  $I = 110 \text{ mA}$ ,  $\phi(b) = 0$ ,  $\phi_c = -7500 \text{ V}$  and  $b = 2a = 0.5 \text{ mm}$ .

*Collector Current Limitation by Space Charge Effects*

Assume the beam of Fig. 1.32 approaching a collector entrance iris at a reduced potential, as shown in Fig. 1.33. The question arises about the limited beam current  $I_{\text{limit}}$  which can pass without reflections into the collector tunnel at a depressed collector potential  $V_C$ . Note:  $V_C$  is measured with respect to the cathode potential.

As we see from (1.63) below, the maximum current depends on the ratio of the collector tunnel radius to the beam radius  $b/a$  pressed to avoid reflection of parts of the beam for a given beam current and the ratio of the collector entrance radius  $b$  to the beam radius  $a$  (Fig. 1.34),





**Fig. 1.34.** Transmission current limit as a function of beam (collector) voltage for 3 values of tunnel to the beam radius ratio  $b/a = 1, 2,$  and  $3$ . As we see for the example of a 110 mA beam, the lowest beam voltage (depressed collector voltage) can be achieved if the beam is uniformly filling the collector tunnel ( $b/a = 1$ )

**Table 1.2.** Minimum collector voltage for a 110 mA electron beam as function of the tunnel-beam radius ratio

Ratio $b/a$	1	2	3
Minimum collector voltage for a 110 mA beam	260 V	500 V	620 V

$$I_{lim}(b/a) = 4\pi\epsilon_0\sqrt{e/m_0} \cdot \frac{1}{1 + 2\ln(b/a)} \cdot \left(\frac{2}{3}(\phi_{beam} - V_C)\right)^{3/2}. \quad (1.63)$$

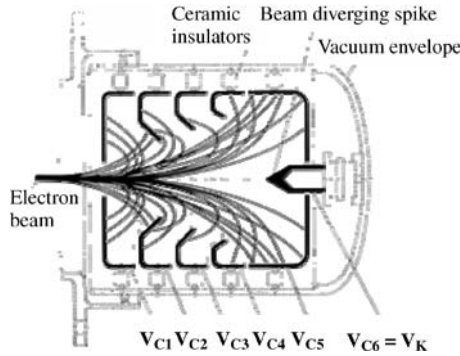
Equation (1.63) has again the form of a perveance or here acceptance,  $I_{lim} = A(b/a) \cdot (V_C)^{3/2}$ , which means that the scaling laws apply (see Table 1.2).

The findings imply a theoretical limit to the collector efficiency. Depending on the width of the electron velocity spectrum, 3 to 5 collector stages are found to give an optimal compromise between the total tube efficiency and system complexity. Amongst the MDCs the two categories, electrostatic collectors and magnetically focused collectors, are distinguished.

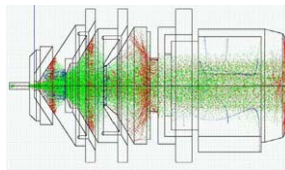
### Electrostatic Collectors

Due to the deceleration of the beam at the collector 1 entrance, the radial space charge force in the beam increases and the beam expands radially. This beam expansion affects the slower electrons more than the faster ones and is therefore used to separate the slower electrons from the faster ones which land further downstream.

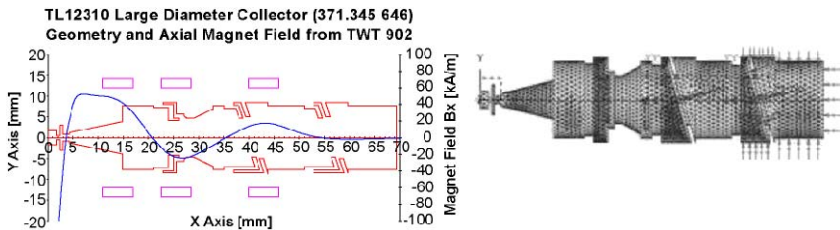
Figure 1.35 sketches the electron trajectories in a 6 stage (5 stages +1 spike on cathode potential) collector as it was used in the 1980s for the 250 W space TWT TL



**Fig. 1.35.** Electrostatic 5 stage + spike collector used for radiation cooled space TWT



**Fig. 1.36.** Distribution of primary reflected and secondary electrons in an *electrostatic* 4 stage collector simulated with the Thales Electron Devices PIC program Collect 3D for a 150 W Ku-band TWT

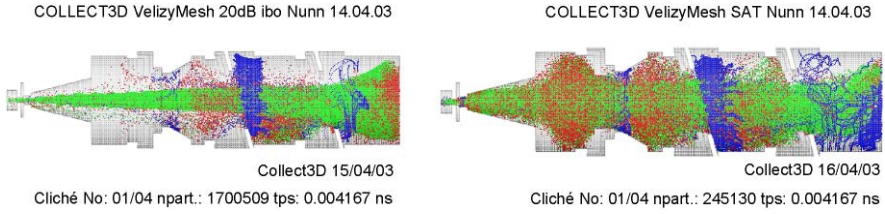


**Fig. 1.37.** Collector geometry, axial magnetic field and simulation mesh of a magnetically focused 4 stage collector for a 300 W Ku-band TWT (the transverse magnetic fields are not shown)

12250. It achieved typically 48% total efficiency. Figure 1.36 shows the design of a modern electrostatic 4 stage collector used in some Thales Ku-band TWTs with the simulated distribution of primary (green), reflected (blue) and secondary electrons (red) in the collector volume, which achieves about 68% total efficiency.

*Magnetically Focused Collectors*

These collectors minimise the radial dimensions of the collector by continuing the magnetic PPM focusing of the electron beam with an adapted periodicity and strength of the magnetic field into the various collector stages. Figure 1.37 shows the principle for a modern 4 stage collector used for a Thales 300 W Ku-band TWT.



**Fig. 1.38.** PIC-simulation of electron distribution in the *magnetically focused* 4 stage tilted field collector at zero drive (*left*) and saturation. Primary electrons (*green*), reflected (*blue*) and secondary (*red*) simulated with the Thales Electron Devices PIC program Collect 3D

The magnetically focused collector allows an optimised beam filling of the collector at saturation drive as shown on the right side of Fig. 1.38 and thus a maximum efficiency up to 74%. To minimise backstreaming of electrons, the most advanced magnetically focused collectors are using tilted electric and magnetic fields producing compensating deflection effects in downstream direction to focus the fast electrons into the collector 4 tunnel and enhanced deflection in backstreaming direction.

#### *Relation between TWT Total-, Beam- and Collector Efficiency*

The TWT total efficiency  $\eta_{\text{tot}}$  and the beam power efficiency  $\eta_{\text{beam}}$  (or basic efficiency  $\eta_0$ ) can be simply defined and rewritten as

$$\eta_{\text{tot}} = \frac{P_{\text{fund}}}{P_{\text{el}}} = \frac{\eta_{\text{beam}} \cdot P_{\text{beam}}}{P_{\text{RF}} + P_{\text{losses}}} = \frac{\eta_{\text{beam}} \cdot P_{\text{beam}}}{P_{\text{beam}} - (P_{\text{beam}} - P_{\text{RF}} - P_{\text{losses}})}, \quad (1.64)$$

where  $P_{\text{fund}}$  is the fundamental RF power at the TWT output,  $P_{\text{RF}}$  is the total RF power (including fundamental and harmonic RF power and RF losses),  $P_{\text{beam}} = V_{\text{H}} \cdot I_{\text{K}}$  is the electron beam power and  $P_{\text{losses}}$  are the thermal losses produced in the tube. A short analysis of the thermal TWT losses  $P_{\text{losses}}$  provides

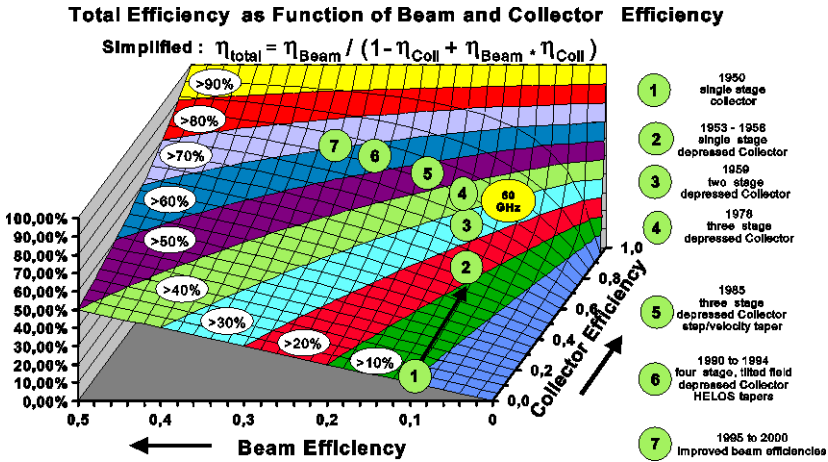
$$P_{\text{losses}} = P_{\text{Coll,losses}} + P_{\text{H,therm}} + P_{\text{A,therm}} + (P_{\text{filament}}). \quad (1.65)$$

Neglecting the small quantities (filament power, helix and anode losses), the term  $P_{\text{recover}} = (P_{\text{beam}} - P_{\text{RF}} - P_{\text{losses}})$  in (1.66) becomes approximately equivalent to the recovered kinetic electron beam power by reduced collector voltages. With the definition of the collector efficiency  $\eta_{\text{C}}$  as the ratio of the recovered power to the entering beam power

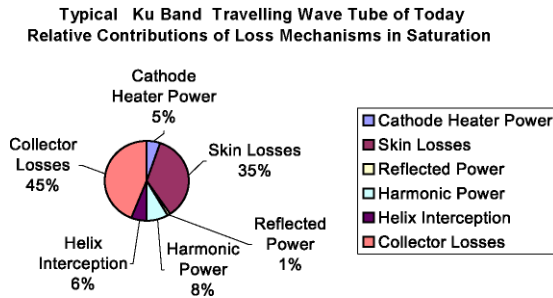
$$\eta_{\text{C}} = \frac{P_{\text{recover}}}{P_{\text{enter}}} = \frac{P_{\text{beam}} - P_{\text{RF}} - P_{\text{losses}}}{P_{\text{beam}} - P_{\text{RF}}}, \quad (1.66)$$

we get a simplified relation between the total beam power and collector efficiency by the further neglecting the harmonic power and the RF losses in  $P_{\text{RF}}$  and by division with  $P_{\text{beam}}$

$$\eta_{\text{tot}} = \frac{P_{\text{fund}}}{P_{\text{el}}} = \frac{\eta_{\text{beam}} \cdot P_{\text{beam}}}{P_{\text{beam}} - \eta_{\text{C}}(P_{\text{beam}} - P_{\text{RF}})} = \frac{\eta_{\text{beam}}}{1 - \eta_{\text{C}}(1 - \eta_{\text{beam}})}. \quad (1.67)$$



**Fig. 1.39.** Total efficiency as function of the two variables beam efficiency and collector efficiency. The historical path from single stage collector tubes (station 1, 10%) to 4 stage tilted field collector tubes with enhanced beam efficiency (station 7, 70%) is sketched for Ku-band TWTs. The figure is adapted from Kornfeld et al. [24]



**Fig. 1.40.** Total distribution of thermal losses in a modern TWT

The failure in making these simplifications can be estimated from Fig. 1.39. In Fig. 1.39 the relation (1.67) is plotted. It indicates further the historical development axes for TWT efficiency. First this occurred via the collector efficiency improvement and later by essentially improving the beam efficiency with tapered helix concepts. Though Fig. 1.39 seem to imply that beam and collector efficiency are independent, this is physically not the case. The larger the beam efficiency becomes, the wider is the electron velocity spectrum entering the collector with detrimental effects on the collector efficiency.

*Loss Analysis of a Typical Ku-Band Space TWT*

From Fig. 1.40 we can see, that further efficiency improvements need to reduce mainly the collector losses (45%) and the skin effect losses (35%). The other losses

in a developed space TWT are well below 10%: harmonic power 8%, helix interception losses 6%, cathode heater 5%, and reflected RF power 1%.

### 1.3.4 TWT Applications

Table 1.3 gives a survey on the different application fields of TWTs. We note that the helix is the most used type of delay line. For communications the reason is its large bandwidth and very good linearity. For military radar and ECM, again its extreme bandwidth, which for some type of ECM tubes can achieve up to 3 octaves. In the following we provide application examples based on the Thales Electron Devices product spectrum.

#### Communication TWTs

##### *TWTs for Ground Station, Airborne and Shipboard Communication*

Following an internal TED communication of Francis Payen, we give a review of these TWT applications.

Depending on the system architecture, the microwave tubes used in ground-based, airborne or shipboard communications system transmit signals to a satellite (up-link) or to a ground based receiver (point to point or point to multipoint communication). Though in some communication systems, due to power requirements, also klystrons are used, TWTs are becoming predominant, because the relative bandwidth requirements are becoming more and more demanding (usually more than 10% are required). Table 1.4 presents the relative bandwidth and the output power capability, as a function of frequency, for the TWTs made by TED for up-link communications systems.

Some examples of ground-based or airborne communication systems using TED microwave tubes are DirecTV, Echostar and Astra for DBS, Iridium for commercial systems and Milstar, Syracuse, Stentor, SBIRS for military systems.

**Table 1.3.** Application fields for different types of TWT delay lines

Application	Communication		Radar and ECM				
Sub-application	Ground station	Space	Earth Observation	Ground & Ship Radars	Airborne Radars	Missile Seekers	ECM
Helix	•	•	•	•	•	•	•
Ring & Bar	•		•				
Coupled Cavity	•			•	•		
Interdigital Line	•			•	•	•	

**Table 1.4.** Survey on up-link TWTs

Frequency band	C	X	Ku	Ku	Ka	Q
GHz	5.85–7.1	7.9–8.4	12.75–14.5	17.3–18.4	25.5–31.5	43.5–45.5
Relative bandwidth	Up to 20%	6%	Up to 13%	6.2%	Up to 20%	4.5%
CW output power	3 kW	2.5 kW	1 kW	500 W	350 W	250 W

**Table 1.5.** Comparison of historic C-band tubes

	First TWT in Use	First Space TWT	First European Space TWT	Modern Space TWT
Program	TV-Ground Link	Telstar 1	Symphonie	Measat
Manufacturer	STC	Bell Lab	AEG	TED
Year	1952	1962	1973	2003
Frequency	3.6–4.4 GHz	3.7–4.2 GHz	3.7–4.2 GHz	3.4–4.2 GHz
Output Power	2 W	2 W	13 W	70 W
Gain	25 dB	40 dB	46 dB	56 dB
Efficiency	≈1%	<10%	34%	71%
Nonlinear Phase	?	50°	50°	38°
Mass	>5000 g	>1000 g	640 g	800 g
Collector	1 stage	1 stage	1 stage depressed	4 stage depressed
Focusing Syst.	Solenoid	PPM PtCo	PPM PtCo	PPM SmCo
Cathode	Oxide	Oxide	Oxide	MM Dispenser

*TWTs for Space Communication*

The major requirements for microwave tubes used in satellite transponders for transmitting down-link signals are:

- long useful operating life and high reliability (> 15 years, <100 FIT, respectively; more than 35 000.000 h accumulated in orbit),
- high total electrical efficiency (>60%),
- high linearity (nonlinear phase shift <48°),
- low mass (depending on output power and radiation or conduction cooling).

TWTs meet all these demanding requirements and beat by far the competition from solid state amplifiers especially with respect to life, reliability and efficiency. The driving force for the impressive improvements in all those parameters was in the past and is still today the economical pressure to save power by improving the efficiency and to reduce the mass of space amplifiers. Two figures are best characterizing this environment: the savings in launch and system costs per satellite are for DC power saving 3.000 €/W and for mass reduction 20.000 €/kg. Therefore, it might be of interest to have a short look on the history of some of the most important space TWT parameters as reviewed by Kornfeld et al. [24].

Table 1.5 shows the performance characteristics of historic C-band space tubes and compares them with the first operational TWT built as TV relay tube by STC in 1952, D.C. Rogers [25]. Though the output power was increased from 2 to 70 W, the mass was reduced.

Figure 1.41 gives the efficiency improvements vs time of the leading space tube manufacturer. The significant improvements obtained in the first 30 years after the TWT invention led in the late 1970s to the impression that the TWT technology might be completely mature and will provide only little space for further improvements. In contrast to this, a steady and for the 1990s even accelerated efficiency

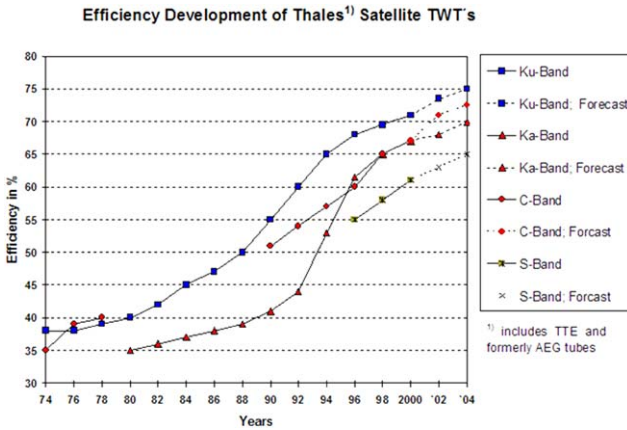


Fig. 1.41. Efficiency improvement of space TWTs (courtesy of TED)

improvement was found for the space TWTs of more or less all commercial manufacturers. The main reason for this performance explosion was the availability of codes to simulate the large signal beam to RF wave interaction in improved tapered helices. It is expected that efficiency might finally approach a level between 75% and 80%. Table 1.6 presents the frequency band, the output power, efficiency and future expected trends in the respective applications.

As seen from Table 1.6, there are many different applications for space TWTs ranging from standard telecommunication systems, TV- and digital radio broadcasting to modern digital internet and multimedia services. Also Earth observation with pulsed radar TWTs becomes increasingly important. New applications where the satellite TWT technology might be used are local multimedia services from small satellites or stratospheric balloons over big cities. Also, for the low Earth orbit satellite fleet of global positioning systems (GPS, Galileo) and their continuous upgrade, powerful and highly efficient TWTs might be used.

### Radar and ECM TWTs

Several types of microwave tubes are used for radars: magnetrons, crossed-field amplifiers (CFAs), klystrons and TWTs.

From a historical point of view, the magnetrons were the first microwave tubes to be used in radar transmitters, more than sixty years ago. But they are oscillators, and most of the radars, since several tens of years, require transmitters using a coherent amplification chain. Among the three types of amplifiers (CFAs, klystrons and TWTs), the TWTs are most widely used, thanks to their wide instantaneous bandwidth, high gain and noise free coherent operation.

#### Surface Radars

Surface radars are ground based or are used in naval systems (shipboard radars). The main types of surface radars are:

**Table 1.6.** Space TWT applications for communication and Earth observation

Application	Band frequency/GHz	Power efficiency	Future trend power efficiency
Direct Digital Radio Navigation/GPS & Galileo	L-band 1.1–1.5	50 to 150 W 55%	250 W 65%
Communication/TV-broadcast	S-band 2.3–2.6	70–90 W 59%	120 W 65%
Direct digital radio for automotive	S-band 2.3–2.6	200–240 W 61%	200–250 W 68%
Telecommunication & broadcasting	C-band 3.4–4.2	20–130 W 60–69%	150 W >73%
SAR, for Earth observation, Radar TWT, pulsed	C-band 5 to 6	5 kW 40%	>5 kW 45%
Scientific applications & deep space missions	X-band 7–8.5	25/120–170 W 60%	25/120–170 W 65%
Earth observation, radar TWT, pulsed	X-band 7–8	4 kW 40%	>4 kW 45%
Telecommunication and broadcasting Internet Multimedia services	Ku-band 10.7–12.75	25–200 W 62–68%	25–300 W 68–75%
Altimeter; radar application for Earth observation, pulsed	Ku-band 13–15 or 12–18	Up to 100 W 55%	150 W 60%
Telecommunication and multimedia Services	Ka-band 17–22	15–130 W 55–66%	15–220 W 55–70%
Deep Space & Scientific Mission	Ka-band 27–32	20–30 54%	20–100 58%
Multimedia Services for low orbit Satellites or Stratosphere Balloons	Q-band 40–45	40 W 40%	40–100 W 40–45%
Inter satellite links for multimedia Services	V-band 58–64	20 W 35%	20–100 W 35–40%

- long range surveillance radars for Air Traffic Control (ATC),
- air defence radars,
- tracking radars,
- fire control radars; those are most time integrated into weapon systems,
- trajectography radars.

Table 1.7 presents the relative bandwidth and the output power capability, as a function of frequency, for the TWTs (Ku- and Ka-band) and klystrons (up to and including X-band) made by TED for surface radars.



**Table 1.7.** Survey on surface radars

Frequency band	L	S	C	X	Ku	Ka
GHz	1.26–1.36	2.7–3.5	5.4–5.9	8.5–10.5	15–18	33–38
Relative bandwidth	3%	3 to 15%	5 to 10%	10%	10 to 20%	3 to 10%
Peak output power	4 MW	20 MW	1 MW	120 kW	2.5 kW	1 kW
Average	12 kW	20 kW	20 kW	5 kW	200 W	200 W

**Table 1.8.** Survey on missile radars

Frequency band	X	X	X	Ku	Ka	W
Type of tube	Helix TWT	CC TWT	Magnetron	TWT	TWT	TWT
Relative bandwidth (%)	2	3	Tunable in 600 MHz	20	3	1
Peak output power (kW)	20	120	220	2	1	0.15
Average output power (W)	800	1500	200	400	200	15

\* The Ka- and W-band TWT use interdigital delay lines; W\* under development

### *Airborne Radars*

Microwave tubes (magnetrons and TWTs) are used in airborne radar transmitters in two categories:

- multimode and multifunction radars; TWTs are widely used, either with coupled cavity slow wave structure or Helix;
- Terrain following radars; generally, TWTs are used.

### *Missile Seekers*

The requirements for microwave tubes (magnetrons, klystrons and TWTs) used in active RF missile seekers are small size and weight, high electrical efficiency, very short start-up time, capability to withstand very severe environmental conditions and high reliability after long storage periods.

Some examples are new generation MICA, ASTER and PAC3 missile seekers. The main performances are presented in Table 1.8. It shows the relative bandwidth and the output power capability for magnetrons and TWTs made by TED for airborne radars or missile seeker applications, as a function of frequency.

### *ECM Applications*

The requirements for microwave tubes used in ECM Systems are very wide instantaneous frequency bandwidth (more than one octave), small size and low weight and high electrical efficiency.

The only microwave tube which can meet a specification with more than one octave bandwidth is the Helix TWT. Table 1.9 presents TED's helix TWTs made for ECM systems.

**Table 1.9.** Survey on broadband ECM tubes

	Frequency band	6 to 18 GHz	18 to 40 GHz
Pulsed TWTs	Peak output power	2 kW	–
	Average output power	80 W	–
CW TWTs	CW output power	200 W	80 W

## 1.4 Extended Interaction Klystron EIK

### 1.4.1 Introduction

Similar to klystron and TWT, the extended interaction klystron (EIK) is a linear electron beam device which tries to combine the advantages of both, the ruggedness and high power capability of a klystron and the larger bandwidth of a TWT. Therefore, the EIK is especially similar to the rugged coupled cavity and interdigital line TWT.

Since the EIK can be considered as a refinement of both microwave devices, it is not easy to mention an inventor. The main work on EIKs seems to go back to Tore Wessel-Berg [26] and his “A General Theory of Klystrons with Arbitrary, Extended Interaction Fields” issued in 1957. He was working at SLAC where he improved efficiency and power capability of klystrons for the linear accelerators. Further pioneering work was done by Chodorow and Kulke [27] in the 1960s. It was recognised by those groups that the circuit impedance is enhanced proportional to the extended interaction region and that larger gain bandwidth product and higher efficiency could be obtained relative to the conventional klystron circuit, particularly in the submillimetres/millimetres region. These characteristics suit today requirements for Ka- to W-band air and space borne radars (see [28] and [29], respectively) and also ECM applications.

### 1.4.2 Extended Interaction Circuit Design

Figure 1.42 compares the principle cross-sections of a conventional two cavity klystron with an extended interaction klystron. The number of cavities and interaction gaps can differ depending on the required application. A 3-dimensional impression of a multicavity multigap design of an EIK is given in Fig. 1.43. This and the previous figure are taken from [28].

The extended interaction oscillator (EIO) is a single cavity device with interaction gaps (segmented drift tube) that function like a coupled cavity TWT structure with extremely strong cavity-to-cavity coupling. At sufficiently high beam currents, oscillations are sustained. Variation of the beam voltage allows 0.4% frequency tuning.

### 1.4.3 Typical Performance and Applications

The today leading manufacturer of EIKs, CPI-Canada, describes the typical frequency and power range as follows (Table 1.10) [30]. The instantaneous band-

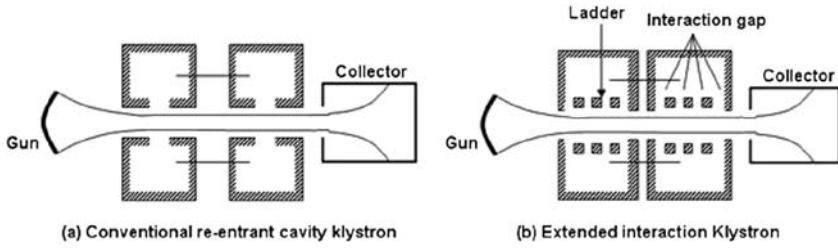


Fig. 1.42. Cross section of a conventional and extended interaction klystron

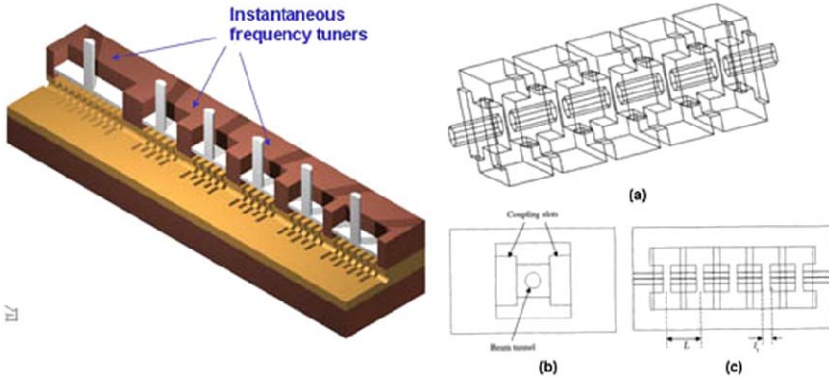


Fig. 1.43. Left: Rising sun type tunable EIK ladder circuit. Right: a 3-dimensional cross-section; b top-view; and c side-view of an EIK five gap structure in a cavity

Table 1.10. Typical power levels of pulsed and CW EIKs at various frequencies

Pulsed EIK		CW EIK	
3000 W	at 30 to 95 GHz	1500 W	at 30 GHz
400 W	at 140 GHz	100 W	at 95 GHz
50 W	at 220 GHz	30 W	at 140 GHz
5 W	at 280 GHz	1 W	at 220 GHz

width of those EIKs is about 1%. Because of these device characteristics, EIKs have been used for the following military, scientific and commercial applications:

- fire control radar
- seeker
- illuminator
- tracking radar
- low noise cw radar
- surveillance radar
- radio astronomy
- satellite communication
- cloud radar
- radar modelling
- fusion diagnostics
- plasma heating

## 1.5 Backward Wave Oscillator (BWO)

### 1.5.1 Introduction

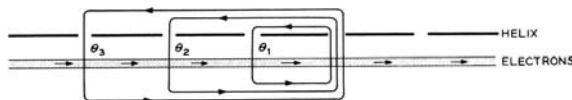
To find the roots of the backward wave oscillator (BWO), one has probably to go back to Rudolf Kompfner, one of the TWT inventors (see Sect. 1.3.1) and the period around 1950 to 1952. In 1951 S. Millmann [31] published on a *spatial harmonics amplifier for 6 mm wavelength* where the energy transport in backward direction with respect to the electron beam is clearly a device feature. Kompfner, working in this period intensely on microwave sources capable of electronic frequency tuning, mentions Millmanns work in his US patent filed in 1952 [32] on *Backward Wave Tubes*. How closely the work on the oscillator type of tubes was related to the amplifier devices is indicated by the patent filed by Kompfner and Williams [33] at the same date on *Backward Wave Amplifiers*. His work published together with N.T. Williams in 1953 [34] belongs also to this period of early investigations on *Backward Wave Tubes*. The investigated devices were based on linear electron beam/slow wave circuit interaction, using periodically disturbed wave guides but also helices. H. Heffner contributed in this period with his *Analysis on Backward Wave Traveling Wave Tubes* [35].

The application, these pioneers had in mind for the oscillator type of devices, was frequency modulated signal generation. Interesting information on this period can be found in J.R. Pierces review article on R. Kompfner and his work [36]. To avoid confusion, it should be mentioned that in some literature the BWO is also called the carcinotron.

### 1.5.2 BWO Operation Principle

The basic idea of the BWO is to use the space charge bunches of an electron beam interacting along their path with a periodic delay line structure (the first space harmonic). The delay line can be of all types (helices, periodically corrugated waveguides, folded waveguides, interdigital lines, etc.). The preferred type depends, as in TWTs, on the frequency range and power level of interest. When passing the periodic structure, the space charge bunch initiates a wave propagating in backward direction. If the phase velocity and the bunch velocity are such that the total phase delay in the loops is  $\theta_n = n \cdot 2\pi$ , a backward wave oscillation can start.

In Fig. 1.44 the situation is illustrated by an electron beam passing along a tape helix. The phase delay  $\theta_1$  in a closed loop between two adjacent gaps in the delay line is given by the sum of the phase lag  $\theta_e = \beta_e p$  during the time the electron bunch



**Fig. 1.44.** Electrons adjacent to a tape helix interacting with the fields in the helix gaps.  $\theta_1$ ,  $\theta_2$ , and  $\theta_3$  denote loop phase shifts for one, two and three periods, respectively

needs to travel with  $v_e$  to the next gap and the phase lag  $\theta_w = \beta_w p$  during the time the wave travels back with its phase velocity  $v_p$ . Here  $p$  is the pitch of the periodic structure,  $\beta_e$  and  $\beta_w$  are the propagation constants of the electron bunch and the wave, respectively. Thus, if  $\theta_1 = \beta_e p + \beta_w p = 2\pi$ , and according to Fig. 1.44  $\theta_2 = 2 \cdot 2\pi$ ,  $\theta_3 = 3 \cdot 2\pi$ , etc., one gets a feedback loop system with total gain eventually above 1 depending on the number of sub-loops or the length of the delay line, the coupling strength between electron bunch and electric field of the wave in the gap and the current in the electron beam.

Thus, the synchronism condition for BW oscillation is given by

$$\beta_e p = 2\pi - \beta_w p. \tag{1.68}$$

This compares simply to the quite different synchronism condition for the forward traveling wave amplification

$$\beta_e p = \beta_w p. \tag{1.69}$$

It is clear that in a delay line with large dispersion, the synchronism condition (1.68) is met optimally only by one frequency, which depends strongly on the propagation constant  $\beta_e$  and thus the beam voltage. To oscillate, the gain loop condition must also be met. Thus, a BWO oscillates only at a current higher than a certain start current  $I_{st}$ . Above this value, the summation of all gains in the loops yields  $>1$ . Within the framework of the small signal theory, the condition for the start current is given by

$$\beta L C_{st} = 2\pi(2^{-5/3}) = 1.97 \tag{1.70}$$

with  $C_{st}$  being the Pierce parameter (see Sect. 1.3),

$$C_{st} = (KI_{st}/4V)^{1/3}, \tag{1.71}$$

at the start current for oscillation. Below this current no oscillation can occur.  $I_{st}$  is of the order of a few mA for a voltage  $V$  of a few thousand volts for conventional O-type BWOs as sketched in Fig. 1.45.

To distinguish the O-type BWO where the magnetic field is parallel to the electron beam axis (used for focusing), in Fig. 1.46 a M-type BWO (see also Sect. 1.6.3)

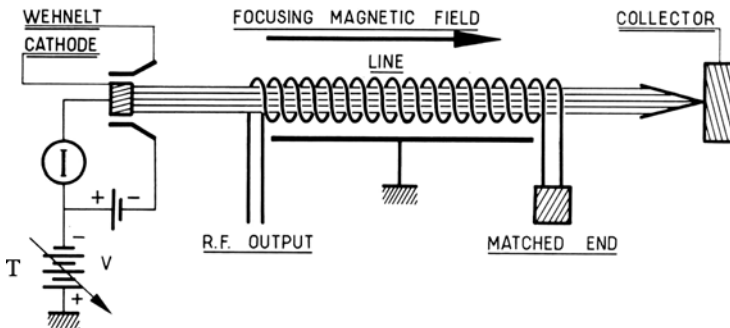


Fig. 1.45. O-type backward wave oscillator (O-carcinotron) with bifilar helix as delay line

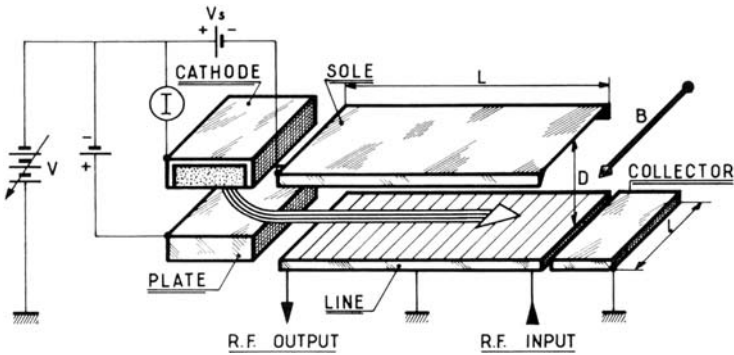


Fig. 1.46. M-type backward wave oscillator (M-carcinotron) with planar periodic delay line

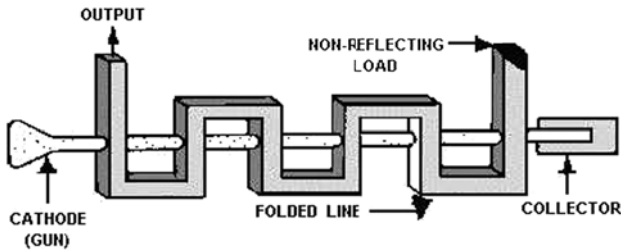


Fig. 1.47. Folded waveguide type of BWO

is sketched, which is an  $E \times B$  device. Though the basic interaction physics and synchronism condition is the same for O-type and M-type BWOs, the M-type BWO is an  $E \times B$  device with the magnetic field perpendicular to the beam axis and the electric field between delay line ground and sole.

A further example of an O-type BWO with a folded waveguide line is shown in Fig. 1.47. These types or interdigital lines are the most common BWOs. Further examples and a compact description of BWOs is, e.g. given by J. Arnaud in “The Encyclopedia of Electronics” issued by Charles Susskind [37].

### 1.5.3 BWO Applications

The typical applications for O-type BWOs are local oscillators and frequency tuneable microwave sources up to the THz range. There, 10 mW of CW power can be obtained in the frequency range from 0.1 to 1.5 THz with a tuning range of 200 GHz. The further development of THz BWO sources is a topic of increasing commercial interest.

## 1.6 Magnetrons and Cross-Field Amplifiers

### 1.6.1 Magnetrons

#### Introduction

Magnetrons are oscillators where all functions are grouped in one given volume between cathode and anode. Magnetron tubes are robust, compact and efficient. They are used as the final stage in ordinary transmitters (radars) but their main utilization is in industrial microwave heating applications (Table 1.11).

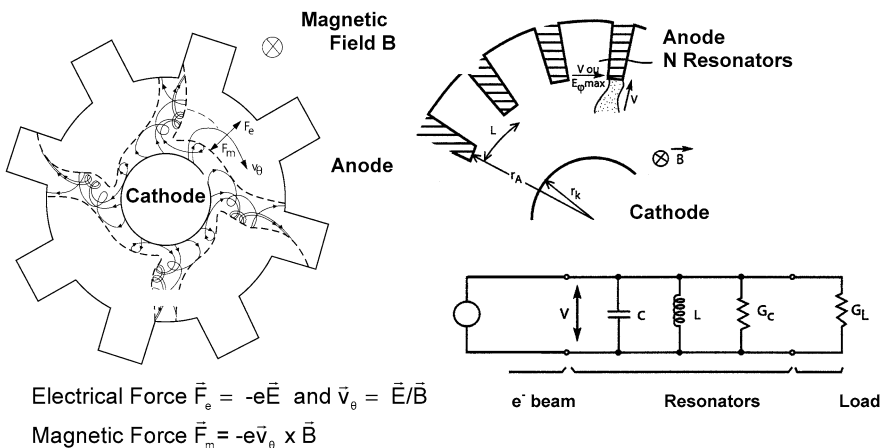
#### Microwave Circuit

Magnetrons consist of two coaxial electrodes: an inner cathode of radius  $r_K$  placed at the centre, and an outer anode of radius  $r_A$  (Figs. 1.48 and 1.49). A permanent magnet (at the origin of the designation of the magnetron) or an electromagnet is used to create a magnetic field  $B_Z$  parallel to the axis [9]. The anode is machined with an even number  $N$  of slots or resonating cavities which are coupled between themselves by their overflow or leakage field in the cathode/anode space. Consequently, we can distinguish  $N/2 + 1$  distinct resonance frequencies corresponding to phase differences  $\Delta\varphi = 0, 2\pi/N, 2\pi/(N/2), 2\pi/(N/3), \pi$  between two adjacent slots or cavities.

The modes are identified by the number  $n$  of times that the field pattern is repeated in going around the anode once [7]. In that way,  $\Delta\varphi$  becomes  $2\pi n/N$ . In

**Table 1.11.** Survey on industrial magnetrons

8.5–9.6 GHz	200 kW peak/200 W average	22 kV × 27.5 A	6.5 kg
2.45 GHz	5 kW CW	7.2 kV × 0.95 A	4.3 kg



**Fig. 1.48.** Magnetron (interaction)

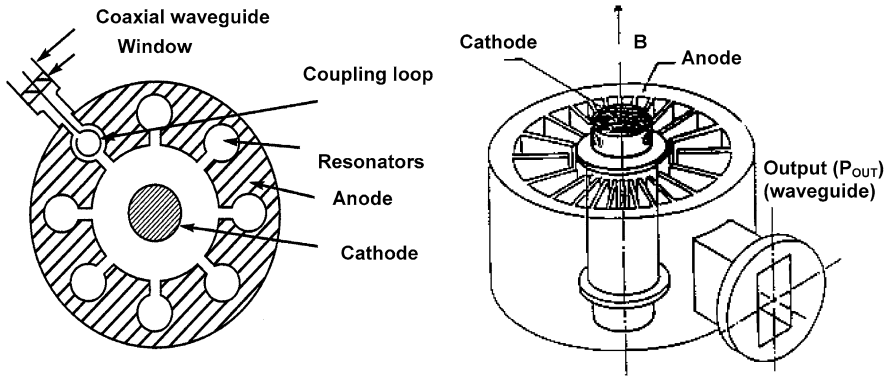


Fig. 1.49. Magnetron

practice, the most common mode is the “ $\pi$ ” mode, with  $n = N/2$ , that is, a phase difference of  $\pi$  between adjacent cavities. The distance between two adjacent cavities is  $l = \lambda n/N$ , which is equal to  $\lambda/2$  if  $\pi$  is the operating mode.

For a given resonance mode of frequency  $f = \omega/2\pi$ , the electromagnetic field and, for example, its  $E_\varphi$  component, varies along the anode (with a so-called abscissa  $s$ ) as described by the usual equation of a stationary wave:  $E_\varphi(s, t) = A \times \cos(2\pi s/\lambda) \cdot \cos \omega t$ . But, since a stationary wave can be considered as the sum of two progressive waves moving in opposite directions, each one with an amplitude equal to half of the original wave, the stationary wave equation can be rewritten as

$$E_\varphi = (A/2)[\cos(2\pi s/\lambda + \omega t) + \cos(2\pi s/\lambda - \omega t)] \tag{1.72}$$

or

$$E_\varphi = (A/2)[\cos \omega(t + s/v_\varphi) + \cos \omega(t - s/v_\varphi)], \tag{1.73}$$

where

$$v_\varphi = \lambda f = \lambda \omega / 2\pi. \tag{1.74}$$

Finally, an observer (or an electron, for example) moving along  $s$  at a velocity  $v_\theta = v_\varphi$  will be in phase with one of the two waves, for example  $A/2 \cdot \cos \omega(t - s/v_\varphi)$ , and will always see the same field.

Magnetrons are therefore multi-resonating microwave structures offering a number of resonance modes, each with the equivalent of two progressive waves, only one of which being taken into consideration for any given mode.

We will now consider the interaction process that takes place within magnetrons, i.e. the transformation of electron movement energy into electromagnetic energy.

### Interaction

The electrons emitted by the cathode would move radially towards the anode, but thanks to the magnetic field  $B_Z$ , their trajectories are curved and somewhere they



become concentric ( $v_r = 0$ ) to the cathode and the anode [3]. At that point, the electrons are subjected to an electrostatic force  $F_e = -eE_{\text{Anode}}$  and a magnetic force  $F_m = -e(v_\theta \times B_Z)$ , acting in opposing directions (Fig. 1.48). Then a radius  $r$  exists, between  $r_K$  and  $r_A$ , for which the amplitudes of these two fields are equal and characterized by  $v_r = 0$  and  $v_\theta = E_A/B_Z$ . Theoretically, the electron can rotate indefinitely around the magnetron axis at this radius.

The combined forces of  $F_e$  and  $F_m$  also apply – albeit very schematically – to all the electrons leaving the cathode at varying velocities. Also, all the electrons experience, to varying extents, the effects of the electromagnetic field and the space charge of the other electrons. In any case it can be said that most of the electrons rotate around in the space between cathode and anode about once, after which they terminate either on the anode or the cathode. Naturally, these electrons are replaced by those emitted non-stop by the cathode. The end result is a real cloud of electrons rotating between the anode and the cathode at a velocity approximately  $v_\theta$  [9].

$V_A$  (or  $E_A$ ) and  $B_Z$  are then adjusted so that  $v_\theta = v_\varphi$ , with  $v_\varphi = \omega(lN/n)/2\pi$  the phase velocity, deducted from the previous expressions of  $l$  and of  $v_\varphi$  (1.74). As explained above the rotating electrons always see the same microwave field  $E_\varphi$ . If  $E_\varphi$  is an accelerating field, they are continuously accelerated, and if  $E_\varphi$  is a decelerating field, they are continuously slowed down. This electron accelerating/decelerating is comparable to the TWT process, with the difference that, in the magnetron, the electrons follow a closed circular path and electron bunches are now replaced by  $n$  rotating electron arms or spokes, where  $n = N/2$  if the  $\pi$  mode is used, that is the most common case.

The energy transfer process in the magnetron is a little bit more complicated than that in the tubes examined in the previous sections. This takes place as follows: the electrons in the spokes are attracted to the anode but, at the same time, repulsed by the RF field. In other words, they are continuously transferring their potential energy, acquired via  $V_A$  (or  $E_A$ ) – to the RF field.

The whole microwave structure, including  $N$  resonators, can be regarded as a unique resonator, represented by an equivalent circuit similar to the one of the klystron cavity. In Fig. 1.48, we notice not only the 3 elements,  $L$ ,  $C$  and the loss conductance  $G_c$ , but also the load  $G_L$ . The load  $G_L$  is directly experienced by the electrons and converted from the final load – for example, the antenna or the microwaves oven – through the waveguides and the coupling loop or iris located in the bottom wall of one of the resonators. The beam loading is neglected. The voltage  $V$  in Fig. 1.48 is the microwave voltage between two anode vanes and is related to the electromagnetic field  $E_\varphi(r = r_A)$ . Almost all the electrons are supposed to arrive at the anode, that means on the top of the vanes, with a phase such that  $E_\varphi(r = r_A)$  is maximum. Therefore, their radial velocity is  $v_r = E_\varphi(r = r_A) \max / B_Z$ , while the azimuthal velocity is given by  $v_\theta = v_\varphi$ .

Moreover, we can write

$$E_\varphi(r = r_A) = MV/l, \quad (1.75)$$

where  $l$  is the distance between two vanes and  $M$  is the coupling factor between  $V$  and the electrons,  $M \approx \sin(\omega l / (2v_\theta)) / (\omega l / (2v_\theta))$ .

The kinetic power – which definitively is lost – of these electrons landing on the anode, is given by

$$P_A = I_0(m/2e)[v_r^2(r = r_A) + v_\theta^2] = I_0(m/2e) \left[ \frac{E_\varphi^2(r = r_A) \max}{B_Z^2} + v_\theta^2 \right]. \quad (1.76)$$

According to the equivalent circuit, the output power  $P_{OUT}$  delivered to the load  $G_L$  is

$$P_{OUT} = \frac{1}{2} N V^2 \cdot G_L = \frac{N}{2} \cdot \frac{\omega l^2 C}{M^2 Q_L} E_\varphi^2(\max) \quad (1.77)$$

with  $Q_L = \omega C / G_L = 1 / (R / Q) G_L$  and (1.75).

Thanks to the obvious expression  $P_{OUT} = V_0 I_0 - P_A$ , we get the approximate expression of the magnetron efficiency [9]

$$\eta = P_{OUT} / V_0 I_0 = (1 - m v_\theta^2 / 2e V_0) / (1 + I_0 m M^2 Q_L / B_Z^2 e N l^2 \omega C). \quad (1.78)$$

The efficiencies of magnetrons usually are quite large and very attractive, 30% up to 70% and even 80%.

A magnetron presents very few control or optimisation parameters: the high voltage  $V_A$  and the magnetic field  $B_Z$ . This is why an operating zone is defined in the plane ( $V_A$ ;  $B_Z$ ), where the magnetron correctly oscillates. Such a zone is located between two limits [3, 9]:

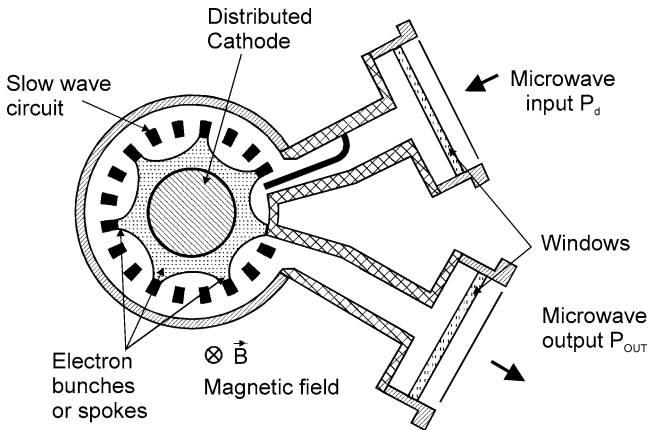
- the Hull parabola, below which (for  $B_Z$  increasing and/or  $V_A$  decreasing) the electrons are no more intercepted by the anode and begin to rotate around the cathode-anode space,
- the Hartree line that determines the synchronism condition (for a given mode). Typically, the operating point is quite close to the Hartree line.

From a technological and engineering point of view, the main parts and subassemblies look like the parts of the other microwave tubes, even if the geometries are notably different (Fig. 1.49).

However, let us notice the frequent use of cold cathodes without direct heating and based on the secondary emission. In this case, the primary electrons are the electrons, whose emission conditions are such that they are coming back and bombard the cathode (self-heating). Also quite all the magnetrons include straps, i.e. metallic wires that connect the vanes or the resonators, which must be at the same electromagnetic instantaneous potential. At the  $\pi$  mode, for instance, straps connect the vanes 0, 2, 4,  $N - 2$ ,  $N$ . Their objective is to minimize the risk of oscillation and the rise of unwanted oscillations or “parasitic” modes.

## 1.6.2 Cross-Field Amplifiers (CFA)

In the magnetrons and, generally speaking, in all the cross-field devices – also called “M-type” tubes – the electrons move under the influence of the perpendicular static electric field  $E \approx V_0 / (r_A - r_K)$  and magnetic field  $B_Z$  (Fig. 1.50). As a result, the



**Fig. 1.50.** Cross-field amplifier (CFA)

motion is perpendicular to both fields and, when the values of  $V_0$  and  $B_Z$  are carefully adjusted, the electron beam or clouds rotate in the narrow space KA between the cathode and the anode. If now the microwave circuit – at the same time the anode – is interrupted to provide input and output connections, we deal no more with a magnetron oscillator but with a cross-field amplifier (CFA).

In CFAs, resonators are preferably replaced by a specific slow wave structure, whose ends are terminated by the input and output couplers, which must be matched at least in the expected frequency bandwidth [3]. Between these two ends, a specific short circular drift space is located in order to minimize any coupling between input and output, but also to provide a necessary electron bunching debunching process (Fig. 1.50).

As soon as the drive power  $P_d$  is injected, the RF fields give rise to bunches or spokes which rotate in the KA space. This process is nearly the same as in the TWTs, where the beam is coupled to a growing forward or to a backward wave. At the same time, the energy transfer inside the spokes is the same as in the magnetrons [9].

In the case of a forward wave, the electrons and the microwave energy flow in the same direction, and the spokes travel in synchronism with the circuit wave, causing it to grow. In the case of a backward wave, the electrons and the microwave energy flow in opposite directions, and the amplification is obtained when  $P_d$  is injected at the circuit output. The slow forward wave circuits are often helix structures, when the backward circuits use strapped bar lines or interdigital structures.

It should be remembered that in CFAs and in magnetrons, the slow wave structure acts not only as the anode but also as the collector, and in spite of a usual high efficiency, a lot of power is dissipated in the structure, which must present excellent thermal capabilities.

The CFAs, also known as “amplitrons”, are characterized by impressive output powers (for example, 700 kW peak and 10 kW average), efficiencies around 70%

and instantaneous bandwidths in the order of 5 to 10%. The cathode voltages  $V_0$  are very acceptable ( $\leq 50$  kV) with perveances of  $P \approx 2 \times 10^{-6}$ . At the same time, the compactness and the lightness are other impressive advantages. The weak points remain not only the risk of oscillations and the possible noisy behaviour but also the low gains of  $\approx 11$  dB [3, 9].

As an important precaution, the RF drive pulse  $P_d$  must always be applied before  $V_0$ , for two main reasons. First, if the CFA employs a cold cathode – now the most frequent situation – the emission process may fail to build up. As a result, the modulator will be unloaded and so excessive voltage, arcing and damage. Secondly, the RF drive anterior to  $V_0$  and strictly present throughout the voltage pulse helps to control the space charge and prevents oscillations at band edge and the generation of broadband noise.

As for the ends of the slow wave circuit, the input VSWR must be very low ( $\leq 1.2:1$ ), not only in the frequency band but also outside, in order to avoid any starting of oscillation during the voltage pulse and during the rise and the fall of  $V_0$ . The resulting spurious output is referred to as “rabbit ears” because of the way they appear on a time display of  $P_{OUT}$ .

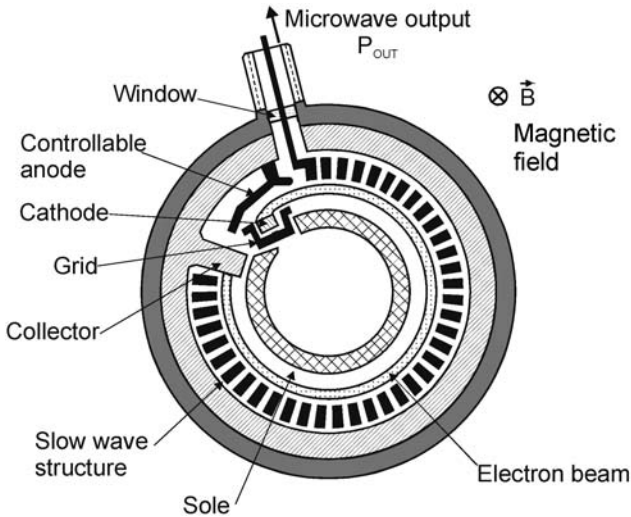
In addition, it should be pointed out that the transmission loss of the signal through the CFA in absence of beam current is very low. Then, the CFA can be considered transparent, and this advantageous characteristic is used in many system applications.

### 1.6.3 Cross-Field Backward Wave Oscillator (MBWO)

The M-type backward wave oscillators, sometimes called “carcinotrons”, are voltage tunable oscillators, mainly used as ECM (electronic counter measures) noise generators but also swept signal sources and drivers for high power transmitters. They are able to deliver, for example, 50 to 100 W with efficiencies of 50% from the L to the X band. They look like the former CFAs, but they use an injected thin beam, and the principle of their operation is close to the one of the backward oscillator (BWO) derived from the conventional TWTs [3].

The electron emission is not distributed over the total surface of the inner electrode, but uses a complete gun structure with a cathode of limited length, a “grid” and a controllable anode, this gun structure being at one end of the circular interaction space. The electrons are emitted approximately radially from the cathode towards the controllable anode but, because of the strong axial magnetic field  $B_Z$ , they are curved at  $90^\circ$  and enter the interaction region between the sole and the slow wave structure (Fig. 1.51). The sole voltage is a little bit lower than the anode potential in order to provide a radial electric field  $E_{r0}$ . Thanks to both  $E_{r0}$  and  $B_Z$ , the velocity of the electrons becomes  $E_{r0}/B_Z$  and is adjusted to get a thin electron beam following a circular path.

Usually the circuits are folded waveguides or interdigital delay lines, where the signal grows as it travels from the collector end to the electron gun end. The microwave output connector is located at this electron gun end. At the collector end,



**Fig. 1.51.** Cross-field backward wave oscillator (MBWO)

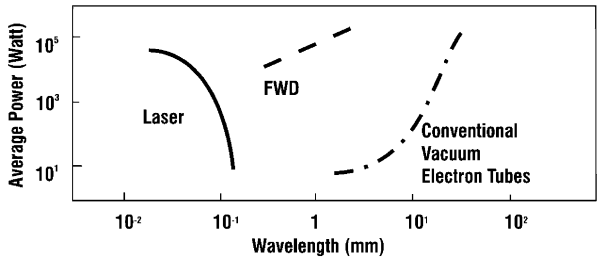
the MBWOs require a relatively large attenuator, well bonded to the heat sink of the tube, to absorb the unavoidable microwave reflections.

The electrons interact with a backward-wave space harmonic of the circuit, the energy on the circuit flowing opposite to the direction of the electron motion. This easily provides the feedback necessary for oscillation. The circuit is terminated at the collector end, but the microwave output is removed at the gun end.

Despite this short presentation, it is understandable that the design and the technology of MBWOs are critical, but the above mentioned performances remain very attractive.

## 1.7 Fast-Wave Devices

Conventional microwave tubes operate with longitudinal phase bunching of the interacting electrons and are commonly referred to as slow-wave devices, since in some way, the RF structure is configured so that the phase velocity of the electromagnetic (EM) field is slowed down to be a little bit lower than the electron beam velocity and is thus less than the velocity of light. This is most evident in the helix-type TWT and BWO where the transverse RF circuit dimensions are typically a fraction of the wavelength. The dimensions of the interaction circuits of klystrons, extended interaction tubes, magnetrons and cross-field amplifiers also have dimensions in the order of the wavelength or smaller. The inherent power limitation with these conventional microwave tubes is the tremendous decrease in the dimensions of the interaction structure with increasing frequency (that is, decreasing wavelength, see Fig. 1.52). Therefore, the possibility of extracting high average power in the millimeter (mm)



**Fig. 1.52.** Chart showing the limitation of conventional microwave tubes for the generation of higher power levels at elevated frequencies. Here, FWDs are fast-wave devices

wavelength range has been ruled out. In the case of two-level far-infrared LASERs, the possible average power, which can be generated, decreases with increasing wavelength since the energy between the interacting quantum levels ( $hf = 0.41$  meV at 100 GHz) becomes smaller than the thermal energy quantum at room temperature ( $kT = 25$  meV). To close the gap for the achievable average output power in the mm- and sub-mm wavelength range (Fig. 1.1), new interaction mechanisms had to be discovered, which operate in highly overmoded interaction circuits, i.e. in fast wave circuits where the electron beam is placed well away from the RF structure. With larger dimensions, the power-handling capability is enlarged. Since fast waves have a phase velocity larger than the velocity of light, the phase bunching mechanism in such fast-wave devices must be generated by a transverse interaction, e.g. (1) the electron-cyclotron interaction in a longitudinal magnetic field (“electron cyclotron maser”: ECM) or (2) the electron undulation in a wiggler field (“free-electron laser”: FEL).

The origin of the ECMs traces back to the late 1950s, when three investigators began to examine theoretically the generation of microwaves by the ECM interaction: R. Twiss in Australia [38], J. Schneider in the US [39] and A. Gaponov in Russia [40]. A short note on the possibility to use the rotational energy of a helical electron beam for microwave generation was published by German H. Kleinwächter in 1950 [41]. In early experiments with devices of this type, there was some debate about the generation mechanism and the relative roles of fast-wave interactions mainly producing azimuthal electron bunching and slow-wave interactions mainly producing axial bunching. The predominance of the fast-wave ECM resonance with its azimuthal bunching in producing microwaves was experimentally verified in the mid-1960s in the US [42] (where the term “electron cyclotron maser” was apparently coined) and in Russia [43] (where the term “gyrotron” was introduced).

FELs exploit relativistic electron beam technology to upshift the electron wiggler frequency. In this respect, perhaps a more descriptive name is that introduced by R.M. Phillips: UBITRON for an “undulated beam interaction electron tube”. Long wavelength FELs ( $\lambda \geq 0.5$  mm) are called free-electron masers (FEMs).

### 1.7.1 Interaction Principles

Fast-wave devices in which the phase velocity  $v_{\text{ph}}$  of the EM wave is greater than the speed of light  $c$ , generate or amplify coherent EM radiation by stimulated emission of bremsstrahlung from a beam of relativistic electrons. The electrons radiate because they undergo oscillations transverse to the direction of beam motion by the action of an external force (field). For such waves the electric field is mainly transverse to the propagation direction (TE or HE modes).

The condition for coherent radiation is that the contribution from the electrons reinforce the original emitted radiation in the oscillator or the incident EM wave in the amplifier. This condition is satisfied if a bunching mechanism exists to create electron density variations of a size comparable to the wavelength of the imposed EM wave. To achieve such a mechanism, a resonance condition must be satisfied between the periodic motion of the electrons and the EM wave in the interaction region [44–47]

$$\omega - k_z v_z \cong s \Omega, \quad s = 1, 2, \dots \quad (k_z v_z = \text{Doppler term}), \quad (1.79)$$

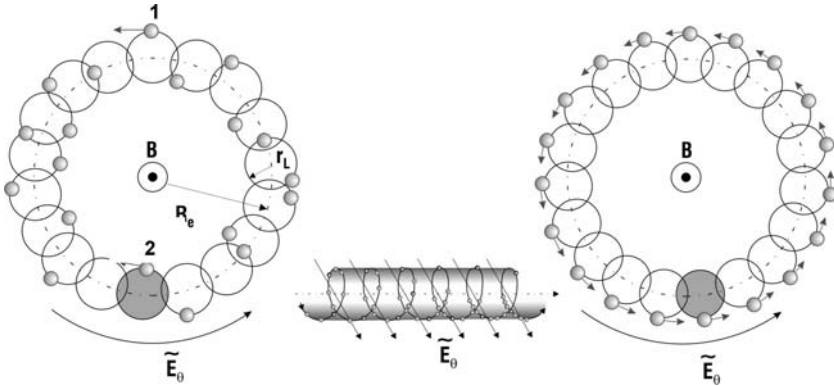
where  $\omega$  and  $k_z$  are the wave angular frequency and characteristic axial wavenumber, respectively,  $v_z$  is the translational electron drift velocity,  $\Omega$  is an effective frequency, which is associated with macroscopic oscillatory motion of the electrons, and  $s$  is the harmonic number.

1. In ECMs, the EM energy is radiated by relativistic electrons gyrating in an external longitudinal magnetic field. In this case, the effective frequency  $\Omega$  corresponds to the relativistic electron cyclotron frequency

$$\begin{aligned} \omega_c &= \Omega_{\text{co}}/\gamma \quad \text{with } \Omega_{\text{co}} = eB_0/m_0 \quad \text{and } \gamma = [1 - (v/c)^2]^{-1/2} \\ &= 1 + eV_0/m_0c^2, \end{aligned} \quad (1.80)$$

where  $-e$  and  $m_0$  are the charge and rest mass of an electron,  $\gamma$  is the relativistic factor,  $B_0$  is the magnitude of the guide magnetic field and  $V_0$  is the acceleration voltage. The nonrelativistic electron cyclotron frequency is  $f_0/\text{GHz} = 28B_0/\text{T}$ . A group of relativistic electrons gyrating in a strong magnetic field will radiate coherently due to bunching caused by the relativistic mass dependence of their gyration frequency. Bunching is achieved because, as an electron loses energy, its relativistic mass decreases and it thus gyrates faster. The consequence is that a small amplitude wave's electric field, while extracting energy from the particles, causes them to become bunched in gyration phase and reinforces the existing wave electric field. The strength of the magnetic field determines the radiation frequency.

The phase bunching process can be most easily understood in a reference frame in which the axial velocity vanishes. In Fig. 1.53 an annular electron beam with radius  $R_e$  is depicted in this frame. The electrons arranged around this annulus execute circular orbits with the Larmor radius  $r_L = v_{\perp}\gamma/\Omega_0$ . Typically  $r_L \ll R_e$ . Initially, the phase of the electrons in their cyclotron orbits is random, as shown in Fig. 1.53 (left).



**Fig. 1.53.** Principle of azimuthal phase bunching in an annular electron beam with initial random phasing of electrons in their cyclotron orbits (*left*) and with electron bunched in phase in their cyclotron orbits (*right*)

In the presence of a transverse RF electric field characteristic of a microwave cavity  $TE_{mn}$  mode, the electrons will be accelerated or decelerated. As a specific example, Fig. 1.53 depicts an electric field with only an azimuthal component, as is characteristic of  $TE_{0n}$  modes in circular waveguide. With random phasing, there is no net energy exchange. Electron 1 will be decelerated by the azimuthal electric field and thus lose energy, while electron 2 will be accelerated and hence gain an equal amount of energy.

Phase bunching and net transfer can occur if the wave frequency is slightly larger than the initial value of the cyclotron frequency

$$\omega' - \frac{eB_0}{m_e\gamma'_0} = (\delta\omega)' > 0, \tag{1.81}$$

where the subscript 0 denotes the initial value and the prime denotes the reference frame in which the electron axial velocity vanishes. Then, as electron 2 gains energy, its cyclotron frequency decreases; this electron falls farther from resonance gaining less energy on each successive cycle. On the other hand, electron 1, which initially loses energy, experiences an increasing value of  $\omega'_c$  and moves closer to exact resonance with the electric field, thereby using an increasing amount of energy on each successive cycle. An instability develops in which the wave energy grows in time and the electrons bunch in phase within their cyclotron orbits, as shown in Fig. 1.53 (right).

2. In the case of a spatially periodic magnetic or electric field (undulator/wiggler), the transverse oscillation frequency  $\Omega_b$  (bounce frequency) of the moving charges is proportional to the ratio of the electron beam velocity  $v_z$  to the wiggler field spatial period  $\lambda_w$ . Thus, the operating frequency of such devices, an example of which is the FEM [48–51], is determined by the condition that an electron in its rest frame “observes” both the radiation and the periodic external force at the same frequency. If the electron beam is highly relativistic ( $v_{ph} \cong v_z \cong c$ ),



the radiation will have a much shorter wavelength than the external force in the laboratory frame ( $\lambda \cong \lambda_w/2\gamma^2$  so that  $\omega \cong 2\gamma^2\Omega_b$ ). Therefore, FEMs are capable of generating EM radiation of very short wavelength determined by the relativistic Doppler effect. The bunching of the electrons in FEMs is due to the perturbation of the beam electrons by the ponderomotive potential well which is caused by “beating” of the EM wave with the spatially periodic wiggler field. It is this bunching that enforces the coherence of the emitted radiation

$$\Omega_b = k_w v_z, \quad k_w = 2\pi/\lambda_w. \quad (1.82)$$

In the case of the ECMs and FEMs, unlike most conventional microwave sources and lasers, the radiation wavelength is not determined by the characteristic size of the interaction region. Such fast-wave devices require no periodically rippled walls or dielectric loading and can instead use a simple hollow-pipe oversized waveguide as a circuit. These devices are capable of producing very high power radiation at cm-, mm-, and sub-mm wavelengths since the use of large waveguide or cavity cross sections reduces wall losses and breakdown restrictions, permitting the passage of larger, higher power electron beams. It also relaxes the constraint that the electron beam in a single cavity can only remain in a favourable RF phase for half of a RF period (as in klystrons and other devices employing transition radiation). In contrast with klystrons, the reference phase for the waves in fast-wave devices is the phase of the electron oscillations. Therefore, the departure from the synchronism condition, which is given by the transit angle  $\theta = (\omega - k_z v_z - s\Omega)L/v_z$ , can now be of order  $2\pi$  or less, even in cavities or waveguides that are many wavelengths long.


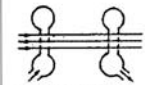


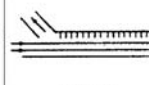
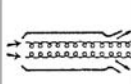
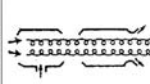
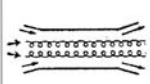
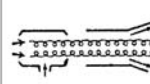
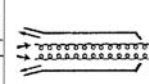
### 1.7.2 Dispersion Diagrams of Fast-Wave Interactions

Many configurations can be used to produce coherent radiation based on the ECM instability. The departure point for designs based on a particular concept is the wave-particle interaction. Dispersion diagrams, also called  $\omega-k_z$  plots or Brillouin diagrams [44–47], show the region of cyclotron interaction (maximum gain of the instability) between an EM mode and a fast electron cyclotron mode (fundamental or harmonic) as an intersection of the waveguide mode dispersion curve (hyperbola)

$$\omega^2 = k_z^2 c^2 + k_\perp^2 c^2 \quad (1.83)$$

with the beam-wave resonance line (straight) given by (1.79). In the case of a device with cylindrical resonator, the perpendicular wavenumber is given by  $k_\perp = X_{mn}/R_0$ , where  $X_{mn}$  is the  $n$ th root of the derivative of the corresponding Bessel function ( $TE_{mn}$  modes) and  $R_0$  is the waveguide radius. Phase velocity synchronism of the two waves is given in the intersection region. The interaction can result in a device that is either an oscillator or an amplifier. In the following subsections, different ECM devices and the FEM are classified according to their dispersion diagrams. Table 1.12 presents a review of ECM devices (also called gyro-devices) and a comparison with the corresponding conventional linear beam (O-type) devices.

**Table 1.12.** Review of the interaction circuits of gyro-devices and comparison with corresponding conventional linear-beam (O-type) devices

<p><b>"O" TYP DEVICES</b></p>	 <p><b>MONOTRON</b></p>	 <p><b>KLYSTRON</b></p>	 <p><b>TWT</b></p>	 <p><b>TWYSTRON</b></p>	 <p><b>BWO</b></p>
<p><b>TYPE OF GYRO-DEVICE</b></p>	 <p><b>GYRO-MONOTRON</b></p>	 <p><b>GYRO-KLYSTRON</b></p>	 <p><b>GYRO-TWT</b></p>	 <p><b>GYRO-TWYSTRON</b></p>	 <p><b>GYRO BWO</b></p>

### Gyrotron Oscillator and Gyro-Klystron Amplifier

Gyrotron oscillators and gyro-klystrons are devices which usually utilize only weakly relativistic electron beams ( $V_0 < 100\text{ kV}$ ,  $\gamma < 1.2$ ) with high transverse momentum (pitch angle  $\alpha = v_\perp/v_z > 1$ ) [46, 47]. The wavevector of the radiation in the cavity is almost transverse to the direction of the external magnetic field ( $k_\perp \gg k_z$ , and the Doppler shift is small) resulting, according to (1.79) and (1.80), in radiation near the electron cyclotron frequency or one of its harmonics

$$\omega \cong s\Omega_c, \quad s = 1, 2, \dots \tag{1.84}$$

In the case of cylindrical cavity tubes, the operating mode is close to cutoff ( $v_{ph} = \omega/k_z \gg c$ ), and the frequency mismatch  $\omega - s\Omega_c$  is small but positive in order to achieve correct phasing, i.e. keeping the electron bunches in the retarding phase. The Doppler term  $k_z v_z$  is of the order of the gain width and is small compared with the radiation frequency. The dispersion diagrams of fundamental and harmonic gyrotrons are illustrated in Figs. 1.54 and 1.55, respectively. The velocity of light line is determined by  $\omega = ck_z$ . For given values of  $\gamma$  and  $R_0$ , a mode represented by  $X_{mn}$  and oscillating at frequency  $\omega$  is only excited over a narrow range of  $B_0$ . Quasi-optical gyrotrons employ a Fabry–Perot mirror resonator perpendicular to the electron beam, also providing  $k_\perp \gg k_z$  [46].

Cyclotron harmonic operation reduces the required magnetic field for a given frequency by the factor  $s$ . At low voltages, the number of electron orbits required for efficient bunching and deceleration of electrons can be large, which means that the resonant interaction has a narrow bandwidth and that the RF field may have moderate amplitudes. In contrast with this, at high voltages, electrons should execute only about one orbit. This requires correspondingly strong RF fields, possibly leading to RF breakdown, and greatly broadens the cyclotron resonance band, thus making possible an interaction with many parasitic modes.

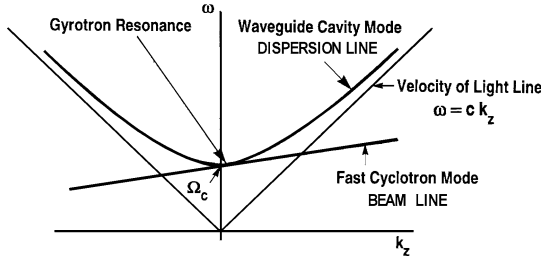


Fig. 1.54. Dispersion diagram of gyrotron oscillator (fundamental resonance)

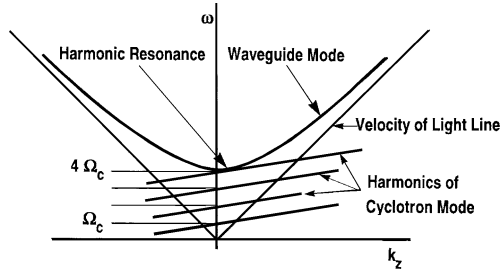


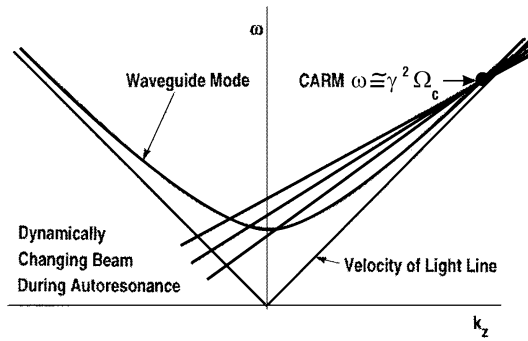
Fig. 1.55. Dispersion diagram of harmonic frequency gyrotron oscillator

### Cyclotron Autoresonance Maser (CARM)

In a gyrotron with a highly relativistic beam ( $\geq 1$  MeV), an efficient interaction will lead to an average energy loss in the order of the initial electron energy. As a result, the change in the gyrofrequency is much greater than in the mildly relativistic case. It is therefore desirable to identify the condition under which such a highly relativistic electron beam remains in synchronism with the RF field. A possibility for achieving synchronism is to utilize the interaction of electrons with EM waves propagating with a phase velocity close to the speed of light in the direction of the magnetic field. In this case, the Doppler shift term  $k_z v_z$  is large, and the appropriate resonance condition is

$$\omega \cong k_z v_z + s \Omega_c. \tag{1.85}$$

If  $v_{ph} \cong c$ , the increase in cyclotron frequency due to extraction of beam energy (decrease of  $\gamma$ ) nearly compensates the decrease in the Doppler shifted term. Therefore, if the resonance condition is initially fulfilled, it will continue to be satisfied during the interaction. This phenomenon is called autoresonance, and the cyclotron maser devices operating in the relativistic Doppler-shifted regime are called cyclotron autoresonance masers [52]. Figure 1.56 shows how the Brillouin diagram of the fast cyclotron wave changes during the autoresonance interaction such that the working frequency  $\omega$  remains constant even though both  $\Omega_c$  and  $v_z$  are based on the same instability mechanism as that of the gyrotron but changing. The CARM interaction corresponds to the upper intersection and is operated far above cutoff. The instability is convective, so a feedback, e.g. by a Bragg resonator [52], is required



**Fig. 1.56.** Dispersion diagram of the cyclotron autoresonance maser (CARM)

for an oscillator; and it is necessary to carefully discriminate against the other interactions corresponding to the lower frequency intersection in the dispersion diagram (Fig. 1.56). The problem can be alleviated by employing the fundamental  $TE_{11}$  or ( $HE_{11}$  hybrid mode) and properly choosing system parameters to be within the stability limit. Compared to a gyrotron, there is a large Doppler frequency upshift of the output ( $\omega \cong \gamma^2 \Omega_c$ ) permitting a considerably reduced magnetic field  $B_0$ . Since the axial bunching mechanism can substantially offset the azimuthal bunching, the total energy of the beam and not only the transverse component is available for RF conversion.

In contrast to the gyrotron, the CARM has an electron beam with low to moderate pitch angle ( $\alpha < 0.7$ ). The efficiency of CARMs is extremely sensitive to spread in the parallel beam velocity. The velocity spread  $\Delta v_z/v_z$  must be lower than 1% to achieve the full theoretically expected efficiency of 40% [52].

### Gyro-Travelling Wave Tube (Gyro-TWT)

From the theoretical point of view, the gyro-TWT differs from the CARM only in regimes of operation. The gyro-TWT utilizes a moderately relativistic electron beam to interact with a fast waveguide mode in an oversized structure near the grazing intersection of the frequency versus wavenumber plot (see Fig. 1.57) where the resonance line is tangent to the EM mode. This produces high gain and efficiency because the phase velocities of the two modes are nearly matched and the group velocity of the waveguide mode is nearly equal to  $v_z$ . In the gyro-TWT regime ( $\omega/k_z \gg c$ ), the axial bunching mechanism is too weak to be of any significance. To benefit from autoresonance, the cutoff frequency should be reduced relative to the cyclotron frequency.

### Gyro-Backward Wave Oscillator (Gyro-BWO)

If the electron beam and/or magnetic field is adjusted so that the straight fast-wave beam line crosses the negative  $k_z$ -branch of the waveguide mode hyperbola (see

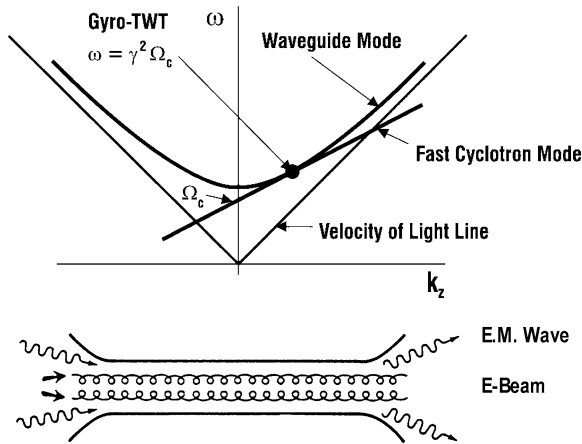


Fig. 1.57. Dispersion diagram and scheme of interaction circuit of gyro-TWT amplifier

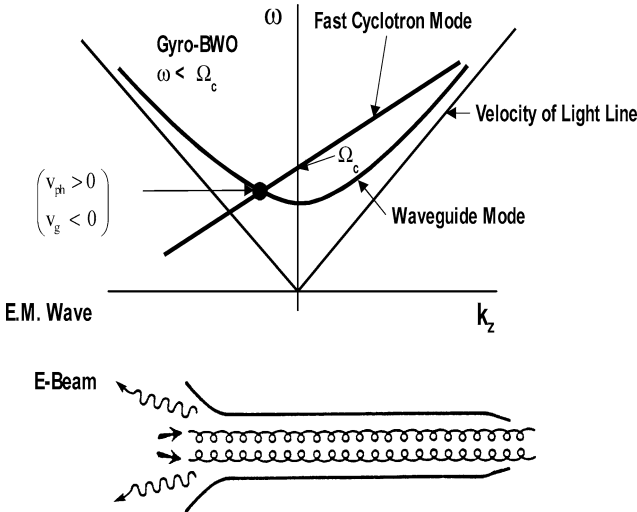


Fig. 1.58. Dispersion diagram and scheme of interaction circuit of gyro-BWO

Fig. 1.58), then an absolute instability (internal feedback) with a “backward wave” occurs. In the gyro-BWO the frequency of operation is now governed by the slope of the line, which is a function of  $v_z$ , and thus of the beam acceleration voltage  $V_0$ . Consequently, just as in the case of other BWOs (e.g. carcinotron), the frequency of oscillations can be continuously changed very fast over a broad range, using  $V_0$  in place of  $B_0$ . However, there is a Doppler down shift in frequency ( $\Omega_c/2 < \omega < \Omega_c$ ), so that very high magnetic fields are required for high frequency operation.

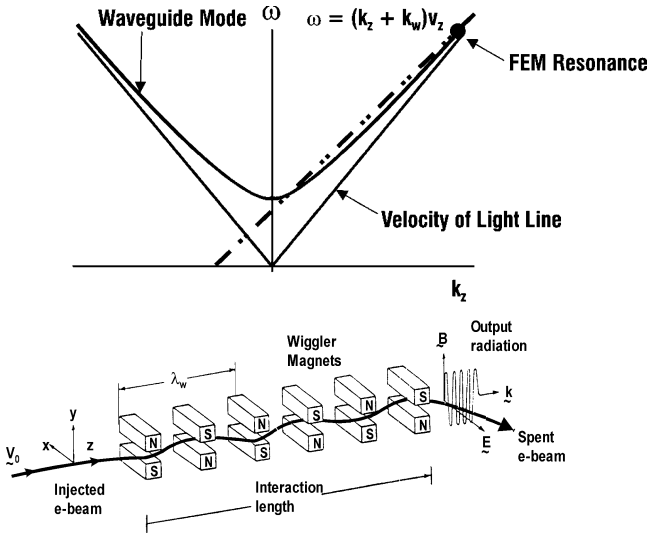


Fig. 1.59. Dispersion diagram and scheme of interaction of FEM

### Free-Electron Maser (FEM)

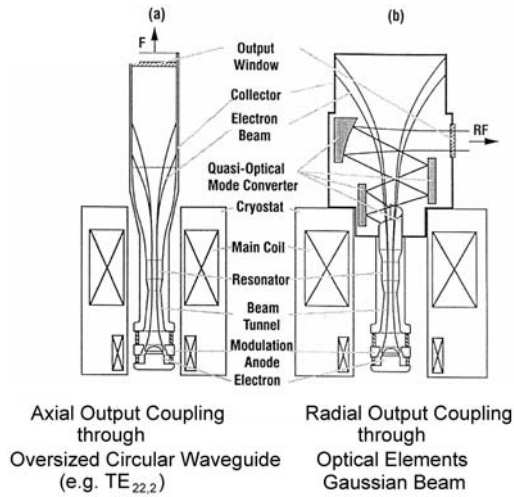
The resonance condition in FEMs is given by

$$\omega - k_z v_z = k_w v_z \quad \text{with } k_w = 2\pi/\lambda_w, \tag{1.86}$$

where  $\lambda_w$  is the spatial period of the wiggler. The generated radiation has a much shorter wavelength than the external force in the laboratory frame:  $\lambda \cong \lambda_w/2\gamma^2$ . The basis FEM configuration and the corresponding dispersion diagram is shown in Fig. 1.59. Electrons in the injected electron beam undulate in the periodic magnetic field  $B_w$  of the wiggler.

### 1.7.3 Gyrotron Oscillator

Gyrotron oscillators (gyromonotrons or simply gyrotrons) were the first ECMs to undergo major development. Increases in device power were the result of Russian developments from the early 1970s in magnetron injection guns, which produce electron beams with the necessary transverse energy (while minimizing the spread in transverse energies) and in tapered, open-ended waveguide cavities that maximize efficiency by tailoring the electric field distribution in the resonator [46]. Typical conventional gyrotrons are built as shown schematically in Fig. 1.60. A gyrotron can be described as follows. The magnetron injection gun produces an annular electron beam with the desired beam parameters. The beam is transported to the interaction region, where the interaction cavity converts a fraction of the beam power to RF power. In case of axial output coupling, the spent beam will be collected on the uniform output waveguide section after the uptaper, and the RF power in the  $TE_{mn}$  mode



**Fig. 1.60.** Schematic of gyrotron with solenoids, magnetron injection gun with annular emitter ring, beam tunnel, cylindrical interaction cavity with cutoff section and output taper, cylindrical output waveguide and RF window: **a** with axial output coupling; **b** with radial output coupling [47]

is coupled through the axial output vacuum window. In the case of radial output coupling, a quasi-optical mode converter is connected to the output waveguide and it transforms the rotating  $TE_{mn}$  mode with an axial power flow to a Gaussian mode with a radial power flow. The power is then transmitted through a radially located vacuum window, and the spent beam is dissipated on the collector.

A strong externally applied magnetic field in the interaction region is chosen such that the cyclotron frequency or one of its harmonics is close to the frequency of the RF field in the beam frame of reference. The interaction region consists of an open-ended waveguide cavity, usually with a circular transverse cross-section. The electrons in the beam must have a substantial transverse velocity  $v_{\perp}$  and the usual longitudinal velocity  $v_z$ . Most of this transverse velocity comes as a result of adiabatic compression resulting from the increasing magnetic field leading to the interaction region. The final ratio of transverse to longitudinal velocity  $\alpha = v_{\perp}/v_z$  in the interaction region is typically between 1 and 2 for gyrotrons that use magnetron injection guns with thermionic cathodes, mostly in temperature limited operation. The electrons follow helical paths around the lines of force of the external field. At high frequencies the use of superconductive magnets is mandatory. By variation of the magnetic field, a sequence of discrete modes can be excited. The frequency scaling is determined by the value of  $B_0/\gamma$ . Modern high power high order volume mode gyrotron oscillators for fusion plasma applications employ an internal quasi-optical mode converter with lateral microwave output, a single-stage depressed collectors (SDC) for energy recovery and a chemical vapour deposition (CVD) diamond window.

## Gyrotrons for Fusion Plasma Heating

At present, gyrotron oscillators are mainly used as high power mm-wave sources for electron cyclotron heating (ECH) applications and for diagnostics of magnetically confined plasmas in controlled thermonuclear fusion research [53]. Long-pulse (a few sec) gyrotrons utilizing open-ended cylindrical resonators which generate output powers of 100–500 kW per unit, at frequencies in the range 28–160 GHz, have been used very successfully for plasma formation, ECH and local current density profile control by noninductive electron cyclotron current drive (ECCD) in tokamaks and stellarators. Gyrotron complexes with total power of up to 4.5 MW have been installed. As experimental devices become larger and operate at higher magnetic fields ( $B_0 = 6$  T) and higher plasma densities ( $n_{e0} = 1\text{--}2 \times 10^{20}/\text{m}^3$ ) in steady state, present and forthcoming ECRH requirements call for gyrotron output powers of at least 1 MW, CW at frequencies ranging from 100–170 GHz. Since efficient ECH&CD need axisymmetric, narrow, pencil-like mm-wave beams with well defined polarization, single-mode emission is necessary in order to generate a TEM<sub>00</sub> Gaussian beam mode at the plasma torus launching antenna. Single-mode mm-wave gyrotron oscillators capable of high average power, 0.5–1 MW per tube, in long-pulse or CW operation, are currently under development in several scientific and industrial laboratories [46, 47, 53, 54].

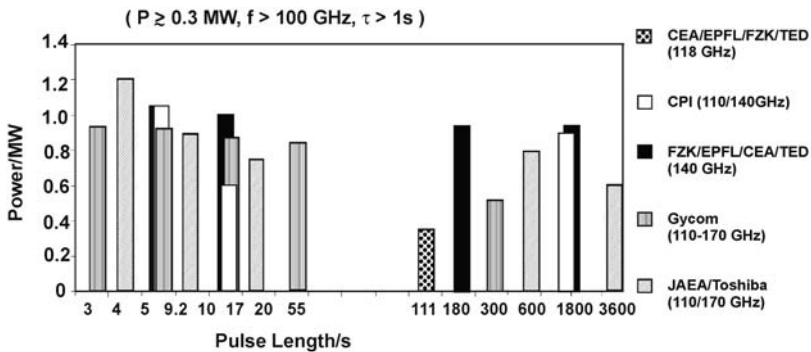
Table 1.13 and Fig. 1.61 summarize the present status of long-pulse gyrotrons for EC H&CD applications at 110–170 GHz [54]. The maximum pulse length of commercially available 140 GHz megawatt-class gyrotrons employing synthetic diamond output windows is 30 minutes (CPI and European FZK-CRPP-CEA-TED collaboration). The world record parameters of the European 140 GHz gyrotron are: 0.92 MW output power at 30 min pulse duration, 97.5% Gaussian mode purity and 44% efficiency, employing a single-stage depressed collector for energy recovery. A maximum output power of 1.2 MW in 4.1 s pulses was generated with the JAEA-TOSHIBA 110 GHz gyrotron. The Japan 170 GHz ITER gyrotron holds the energy world record of 2.16 GJ (0.6 MW, 60 min) for tubes with an output power of more than 0.5 MW. The Russian 170 GHz ITER gyrotron achieved 0.5 MW with a pulse duration of 300 s. Figure 1.62 shows the 118 GHz and 140 GHz long-pulse gyrotrons developed by the EU team.

To achieve output powers in excess of 2 MW at frequencies around 170 GHz and long pulses, it is necessary to employ a coaxial-cavity geometry. A maximum output power of 2.2 MW (1 ms pulse length) was obtained at FZK with an efficiency of 28%. At the nominal output power of 1.5 MW the efficiency increases from 30% to 48% in operation with an SDC [47]. Two MW synthetic diamond windows are feasible. At power levels around 1 MW the coaxial-cavity gyrotron can probably operate at frequencies  $>300$  GHz. This means that the gyrotron oscillator is the dominant mm-wave source for high power ECH and ECCD. Even in the case of local non-inductive current drive for suppression of plasma instabilities in future tokamak fusion reactors, the gyrotron is a good option, since ultra broadband Brewster windows and specific magnets allow stepwise frequency tuning in the seconds time-scale in the full D-band (110–170 GHz) [47]. Diagnostic gyrotrons deliver  $P_{\text{OUT}} = 40$  kW



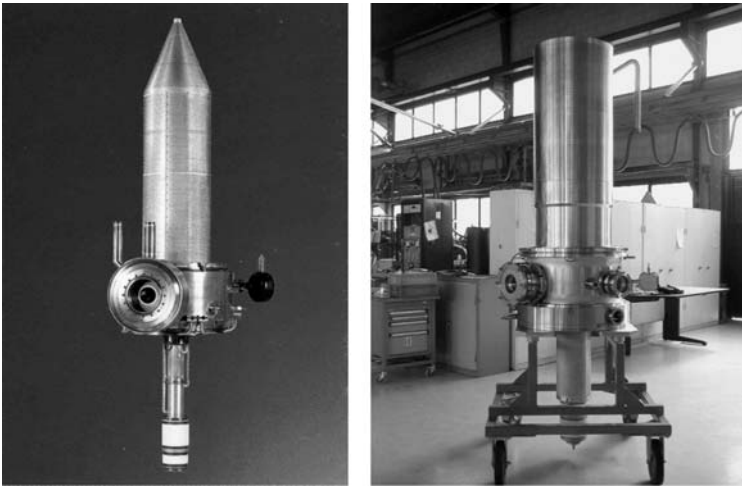
**Table 1.13.** Development status of long pulse gyrotron oscillators for fusion plasma applications at 110–170 GHz [54]

Institution	Frequency (GHz)	Cavity mode	Output mode	Power (MW)	Efficiency (%)	Pulse length(s)	Fusion device
CPI, Palo Alto	110	TE <sub>22,6</sub>	TEM <sub>00</sub>	1.05	31	5.0	D III-D
				0.6	31	10.0	D III-D
	140	TE <sub>28,7</sub>	TEM <sub>00</sub>	0.9	33 (SDC)	1800	W7-X
GYCOM-M (TORIY, IAP), Moscow,	110	TE <sub>19,5</sub>	TEM <sub>00</sub>	0.93	36	2.0	D III-D
				0.5	35	5.0	D III-D
				0.35	33	10.0	D III-D
Nizhny Novgorod	140	TE <sub>22,6</sub>	TEM <sub>00</sub>	0.96	36	1.2	ASDEX-U
				0.54	36	3.0	W7-AS
				0.9	44 (SDC)	21	ITER
	170	TE <sub>25,10</sub>	TEM <sub>00</sub>	0.5	40 (SDC)	300	ITER
GYCOM-N (SALUT, IAP), N. Novgorod	140	TE <sub>22,6</sub>	TEM <sub>00</sub>	0.8	32	0.8	W7-AS
				0.88	50.5 (SDC)	1.0	W7-AS
				0.5	30	0.7	T 10
JAEA, TOSHIBA, Naka,	110	TE <sub>22,6</sub>	TEM <sub>00</sub>	1.2	38 (SDC)	4.1	JT 60-U
				1.0	36 (SDC)	5.0	JT 60-U
				0.5	34 (SDC)	16.0	JT 60-U
Otawara	170	TE <sub>31,8</sub>	TEM <sub>00</sub>	1.0	43.4 (SDC)	800	ITER
				0.6	45.5 (SDC)	3600	ITER
THALES, CEA, CRPP,	118	TE <sub>22,6</sub>	TEM <sub>00</sub>	0.53	32	5.0	TORE SUPRA
				0.35	23	111	TORE SUPRA
FZK, EUROPE	140	TE <sub>28,8</sub>	TEM <sub>00</sub>	1.0	49 (SDC)	12	W7-X
				0.92	44 (SDC)	1800	W7-X



**Fig. 1.61.** State-of-the-art of long-pulse gyrotrons for EC H&CD applications at 110–170 GHz

with  $\tau = 40 \mu\text{s}$  at frequencies up to 650 GHz ( $\eta \geq 4\%$ ) [53]. Operating at the fundamental or the second harmonic of the electron cyclotron frequency enables the gyrotron to act as such a medium power step tunable, mm-wave, sub-mm wave and



**Fig. 1.62.** CEA/CRPP/FZK/TED-gyrotrons. *Left:* 118 GHz, 0.35 MW, 11 s with liquid nitrogen Cryo-Window. *Right:* 140 GHz, 0.92 MW, 1900 s with CVD-diamond window and SDC

THz source in the frequency range from 38 GHz (fundamental) to 1005 GHz (TE<sub>6,11</sub> mode, second harmonic) [54].

### Gyrotrons for Industrial Applications in Materials Processing

Recently, CW gyrotrons have also been successfully utilized in materials processing (e.g. sintering of advanced nanocrystalline- and piezo-ceramics, surface hardening, joining or dielectric coating of metals and alloys) and in plasma chemistry [53]. Such technological applications require sources with the following parameters:  $f \geq 24$  GHz,  $P_{OUT} = 10\text{--}30$  kW,  $\eta \geq 30\%$ . The present state-of-the-art of industrial CW gyrotrons for technological applications is summarized in Table 1.14 [54].

The use of gyrotrons appears to be of great interest if one can realize a relatively simple, low cost device which is easy to use (such as a magnetron). Gyrotrons with low magnetic field (operating at the second harmonic of the electron cyclotron frequency) which can be provided by a permanent magnet system, low anode voltage, high efficiency and long lifetime are under development (see Table 1.14).

#### 1.7.4 Gyro-Amplifiers

Bunching of electrons in gyro-devices has much in common with that in conventional linear electron beam devices, namely, klystron, TWT, twystron and BWO. In both cases the primary energy modulation of electrons gives rise to bunching (azimuthal or longitudinal) which is inertial. The bunching continues even after the primary modulation field is switched off (at the drift sections of klystron-type and twystron-type devices). This analogy suggests the correspondence between linear-beam (O-type) devices and various types of gyro-devices (Table 1.12).

**Table 1.14.** Performance parameters of industrial CW gyrotron oscillators for technological applications [54]

Institution	Frequency (GHz)	Cavity mode	Output mode	Power (kW)	Efficiency (%)	$V_0$ (kV)	Magnet
CPI,	28	TE <sub>02</sub>	TE <sub>02</sub>	15	38	40	room temp.
Palo Alto	28(2 $\Omega_c$ )	TE <sub>02</sub>	TE <sub>02</sub>	10.8	33.6	30	room temp.
	60	TE <sub>02</sub>	TE <sub>02</sub>	30	38	40	cryo. mag.
CPI, NIFS	84	TE <sub>15,3</sub>	TEM <sub>00</sub>	50	14	80	cryo. mag.
GYCOM/	24.15(2 $\Omega_c$ )	TE <sub>11</sub>	TE <sub>11</sub>	3.5	23	12	room temp. PM, 116 kg
IAP,	24.15	TE <sub>32</sub>	TE <sub>32</sub>	36	50	33	room temp.
Nizhny	23(2 $\Omega_c$ )	TE <sub>12</sub>	TE <sub>12</sub>	13	50	25	room temp.
Novgorod				28	32	25	room temp.
	28.3(2 $\Omega_c$ )	TE <sub>12</sub>	TE <sub>12</sub>	12	20	25	PM, 68 kg
	30(2 $\Omega_c$ )	TE <sub>02</sub>	TE <sub>02</sub>	10	42	26	room temp.
				30	35	26	room temp.
	37.5	TE <sub>62</sub>	TEM <sub>00</sub>	20	35	30	cryo. mag.
	83	TE <sub>93</sub>	TEM <sub>00</sub>	10–40	30–40	25–30	cryo. mag.
MITSUBISHI,	28(2 $\Omega_c$ )	TE <sub>02</sub>	TE <sub>02</sub>	15	38.7	21	PM, 600 kg tapered B
Amagasaki							
UNIV. Fukui	300	TE <sub>22,8</sub>	TEM <sub>00</sub>	2.0	11	15	cryo. mag.

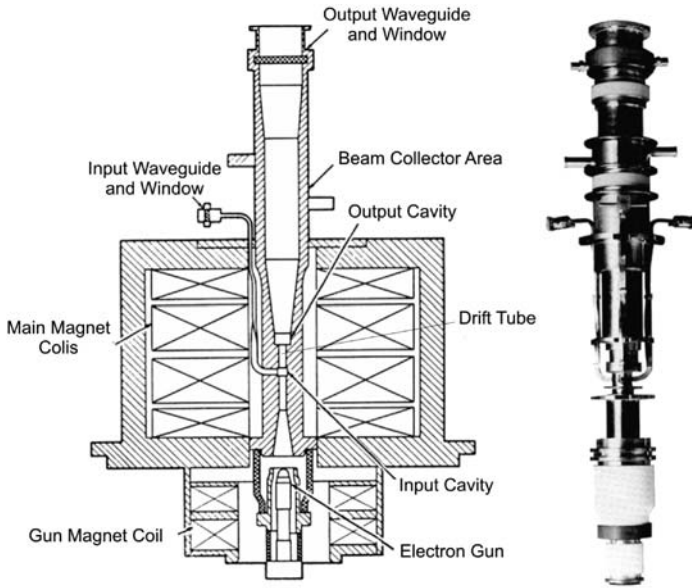
Figure 1.63 shows the cross-section and the photograph of a two cavity gyro-klystron amplifier. Advanced devices use several staggered cavities (up to 5) and optimized shape of magnetic field. The state-of-the-art of weakly relativistic gyro-klystrons is given in Table 1.15 [54].

Table 1.16 summarizes the status of the high-power relativistic gyro-klystron development at the University of Maryland [54]. For comparison, the experimental results of the SLAC periodic permanent magnet 11.4 GHz klystron are: 75 MW output power with 48% efficiency and 55 dB gain at a pulse duration of 1.5  $\mu$ s.

The circuit employed in a gyro-TWT consists simply of a modestly oversized waveguide. Since no resonant structures are present, the gyro-TWT is potentially capable of much larger bandwidth than a gyro-klystron. Recent devices employ tapered magnetic field, interaction circuit and two partially loaded stages in order to optimize the beam-wave interaction along the waveguide [55].

The sensitivity to velocity spread can be strongly reduced by coupling between the second harmonic cyclotron mode of a gyrating electron beam and the radiation field in the region of near infinite phase velocity over a broad bandwidth by using a cylindrical waveguide with a helical corrugation on its inner surface [56]. The state-of-the-art of weakly relativistic pulse gyro-TWTs is given in Table 1.17.

The gyro-twystron, a hybrid device, is derived from the gyro-klystron by extending the length of the drift section and replacing the output cavity with a slightly tapered waveguide section like in a gyro-TWT. The output waveguide section is excited



**Fig. 1.63.** Schematic cross-section and photograph of a pulsed gyro-klystron amplifier (CPI, formerly Varian)

**Table 1.15.** Weakly relativistic gyro-klystron experimental results

Institution	Frequency (GHz)	Mode	No. of cavities	Power (kW)	Efficiency (%)	Gain (dB)	BW (%)
CPI, Palo Alto	10 ( $2\Omega_c$ )	TE <sub>01</sub>	3	20	8.2	10	0.2
	28	TE <sub>01/02</sub>	2	76	9	30	0.2
CPI, Litton, NRL, UNIV. MARYLAND	93.8	TE <sub>01</sub>	4	118 (10 av.)	29.5	24.7	0.64
			5	130 (10 av.)	33	39.5	0.75
GYCOM- M (TORIY), Moscow	35.0	TE <sub>02</sub>	2	750 (5 av.)	24	20	0.6
			2	350	32	19	0.9
IAP, Nizhny Novgorod	35.1 ( $2\Omega_c$ )	TE <sub>02</sub>	3	250 (1.2 av)	35	40	1.4
			3	160	40	30	0.5
			3	300	22	22	0.1 PM, 350 kg
			2	258	18	17	0.3
IAP, ISTOK	93.5	TE <sub>02</sub>	2	207	30	21	0.2
			3	340	24.5	23	0.3
			4	2.5 (CW)	25	31	0.36
NRL, Washington, D.C.	34.9	TE <sub>01</sub>	3	54	30	30	0.4
			3	225	31	30	0.82
			4	60	25	27	0.69
			5	84	34	42	0.37
			4	72	27	48	0.44

**Table 1.16.** Relativistic pulse gyro-klystron experimental results [54]

Institution	Frequency (GHz)	Mode	No. of cavities	Power (MW)	Efficiency (%)	Gain (dB)	Type
IAP, Nizhny Novgorod	30	TE <sub>5,3</sub>	2	5	25	27	TE <sub>5,2</sub> /TE <sub>5,3</sub>
UNIV. MARYLAND	8.57	TE <sub>01</sub>	3	75	32	30	coaxial
	9.87		2	24	30	33	max. power
	9.87	TE <sub>01</sub>	3	27	32	36	max. efficiency
			3	16	37	33	max. gain
			3	20	28	50	coaxial
	17.14 (2Ω <sub>c</sub> )	TE <sub>02</sub>	3	27	13	25	coaxial
			4	18.5	7.0	23.3	
	19.76 (2Ω <sub>c</sub> )	TE <sub>02</sub>	2	32	29	27	
29.57 (3Ω <sub>c</sub> )	TE <sub>03</sub>	2	1.8	2.0	14		

**Table 1.17.** Development status of weakly relativistic gyro-TWTs (short pulse) [54]

Institution	Frequency (GHz)	Mode	Power (kW)	Efficiency (%)	Gain (dB)	Bandwidth (%)
CPI, Palo Alto	5.18	TE <sub>11</sub>	120	26	20	7.3
	93.7	TE <sub>11</sub>	28	7.8	31	2
NRL, Washington, D.C.	32.3	TE <sub>10</sub>	50	28	25	11
	34.0	TE <sub>01</sub>	137	17	47	3.3
	35.6	TE <sub>11</sub>	70	17	60	17
IAP, Nizhny Novgorod	36.3	TE <sub>21</sub> /TE <sub>11</sub>	180	27	27	10
MIT, Cambridge	140	HE <sub>061</sub> <sup>0</sup>	30	12	29	1.6
UNIV. HSINCHU	34.2	TE <sub>11</sub>	62	21	33	12
	33.6	TE <sub>11</sub>	93	26.5	70	8.6
UC LOS ANGELES	9.3	TE <sub>10</sub>	55	11	27	11
	15.7 (2Ω <sub>c</sub> )	TE <sub>21</sub>	207	12.9	16	2.1
	93.4	TE <sub>01</sub>	75	22	60	4.5

by the beam of electrons that are bunched because of modulation in the input cavity. The gyro-twystron configuration can mitigate the problem of microwave breakdown at high power levels, since the microwave energy density in the output waveguide can be much smaller than in an output cavity.

The development of high-power gyro-amplifiers has opened up a number of possible applications to advanced mm-wave radars for high resolution ranging and imaging in atmospheric and planetary science (e.g. cloud and space-debris monitoring) as well as for deep-space and specialized satellite communications.

A 120-element phased-array 34 GHz radar system (4' beam width) using two 0.5 MW gyro-klystrons with 50 MHz bandwidth, 100 μs pulse duration and 0.01 duty factor is operating in Russia. In the USA, a W-band radar system employing

a 92 kW, 94 GHz gyro-klystron with 420 MHz bandwidth and a duty factor of 0.11 (10 kW average power) is operating.

The cost of a future linear electron–positron collider with centre of mass energy in the TeV range will depend both on the number of microwave phase-coherent amplifiers required to drive the collider and on the cost of each amplifier. In the past, the microwave amplifier of choice for driving the highest energy linear electron accelerators has been the klystron (e.g. S-band). In considering microwave amplifier requirements for future supercolliders there has been a widespread perception that higher frequency and higher peak power will be required. Because of inherent limitations when simultaneously handling high power and high frequencies in klystron circuits, other types of amplifiers as relativistic gyro-klystrons and gyro-twystrons have been explored.

The klystron development programs will probably result in producing microwave amplifiers that are suitable for linear colliders in the energy range up to 1 TeV. However, for multi-TeV supercolliders, 34 GHz gyro-klystrons producing about 100 MW of peak power in 1  $\mu$ s are needed [53].

Due to their larger bandwidth, gyro-TWTs can be used as output amplifiers in mm-wave communication systems.

### 1.7.5 Gyro-BWO

Gyro-BWOs are being developed as fast and continuously frequency tunable drivers of FEMs and for materials processing applicators with extremely homogeneous EM-field distribution (by frequency sweeping). The status of weakly relativistic devices is summarized in Table 1.18.

### 1.7.6 Free-Electron Maser (FEM)

Free-electron lasers (FELs) differ from the other high-power microwave sources considered in this chapter in that they have demonstrated output over a range of frequencies extending far beyond the microwave spectrum, well into the visible and ultraviolet range [48–51]. To achieve this spectral versatility, FELs exploit relativistic beam technology to upshift the electron “wiggle” frequency by an amount roughly proportional to  $\gamma^2$ . The magnetostatic wiggler is the most common, but not the sole means, for providing electron undulation. An electrostatic wiggler or the oscillatory field of a strong electromagnetic wave can also play this role. The distinction between long wavelength free-electron maser (FEM) ( $\lambda \geq 0.5$  mm) and short wavelength FELs is natural because higher current and lower energy beams are typically employed in this regime and space-charge effects are more important. In particular, the dominant interaction mechanism is often coherent Raman scattering. Also, while short wavelength FELs excite optical modes, dispersion due to the beam dielectric effects and finite transverse dimensions in the drift tubes and cavities are important effects at longer wavelengths. A low power (3 W, 2 ms pulses) FEL operating at radio frequencies (FER) employing a 420 V, 0.2 A electron beam holds the world record for long

**Table 1.18.** Development status of weakly relativistic pulse gyro-BWOs [54]. Only the 24.7 GHz device is operating in CW

Institution	Frequency (GHz)	Mode	Power (kW)	Efficiency (%)	Bandwidth (%)
IAP, Nizhny Novgorod, FZK, Karlsruhe	24.7	TE <sub>21</sub> /TE <sub>11</sub>	7	15 23 (SDC)	5
IAP, Nizhny Novgorod	35–38	TE <sub>21</sub> /TE <sub>11</sub>	34	7	15
MIT, Cambridge, LLNL, Livermore	140	TE <sub>12</sub> <sup>c</sup>	2	2	9
NRL, Washington, D.C.	27.8 29.2	TE <sub>10</sub> <sup>r</sup> TE <sub>10</sub> <sup>r</sup>	2 6	9 15	3 13
UNIV. Hsinchu	33.5	TE <sub>11</sub> <sup>c</sup>	20–67 100 164	6.5–21.7 25 41	5 8.5 1
UNIV. Strathclyde	8.5	TE <sub>21</sub> /TE <sub>11</sub>	60	16	17
UNIV. Utah	10	TE <sub>10</sub> <sup>r</sup>	0.72	10	8

r: rectangular waveguide; c: circular waveguide

wavelength ( $f = 266$  MHz,  $\lambda = 1.1$  m,  $\lambda_w = 0.04$  m,  $B_w = 0.04$  T). The highest CW power generated by a FEM is 36 W (15 GHz) whereas the IR (3.1  $\mu$ m)-FEL at Thomas Jefferson National Accelerator Facility obtained a record average power of 2.13 kW at 3.5% efficiency employing beam energy recovery ([54], and references therein).

The FEM appears to be potentially capable of fulfilling all the requirements for a frequency tunable high-power mm-wave source. Coverage of the entire frequency range of 130–260 GHz presents no severe problem, and even higher frequencies are quite feasible. Rapid tunability over more than  $\pm 5\%$  could be obtained by variation of the beam energy. The interaction occurs in a cavity operating in low-order modes, which have very good coupling to a Gaussian beam output. The relatively low RF wall loading and the use of high electron beam energy ( $>0.5$  MeV) and a multi-stage depressed collector are compatible with a high unit power at high efficiencies if the electron beam interception could be maintained at an acceptable level. A survey of the development status of short pulse FEM oscillators and amplifiers is presented in Table 1.19 [54]. Electrostatic, pulseline/modulation and induction linac accelerators are employed.

The induction-linac based 140 GHz, 2 GW short-pulse (20–30 ns) LLNL-FEM was successfully employed in high-power microwave transmission measurements in fusion plasmas where the nonlinear absorption (higher transmission) at ECH frequencies was observed which is only possible at such high power levels. The UCSB-FEL was used to study nonlinear dynamics in semiconductor nanostructures and devices.

**Table 1.19.** Development status of pulse free-electron masers

Institution	Frequency (GHz)	Mode	Power (MW)	Efficiency (%)	Voltage (MV)	Current (kA)	Type
FOM, Nieuwegein	206	HE <sub>11</sub> <sup>r</sup>	0.73(0.5)	5.7(3.9)	1.77	0.0072	oscillator
	167	HE <sub>11</sub> <sup>r</sup>	0.36(0.26)	3.1(2.3)	1.61	0.0071	oscillator
	169	HE <sub>11</sub> <sup>r</sup>	0.1	0.9	1.60	0.007	oscillator
				(14 with MDC)			
IAP/INP Novosibirsk	75	TEM	100	4.2	0.8	3.0	oscillator
JINR Dubna/IAP	30.74	TM <sub>11</sub> <sup>c</sup> /TE <sub>11</sub> <sup>c</sup>	48	35(30)	0.8	0.17(0.02)	oscillator
	38.2	TM <sub>12</sub> <sup>c</sup> /TE <sub>11</sub> <sup>c</sup>	3	3(3)	0.8	0.15(0.2)	oscillator
Nizhny Novgorod	35	TE <sub>11</sub> <sup>c</sup>	30	10	1.5	0.2	amplifier
LLNL, Livermore	34.6	TE <sub>01</sub> <sup>r</sup>	1000	34(7.2)	3.5	0.85(4.0)	amplifier
	140	TE <sub>11</sub> <sup>c</sup>	2000	13.3(10)	6.0	2.5(3.0)	amplifier
			500–1000 in up to 50				
MIT, Cambridge	27.5	TE <sub>11</sub> <sup>c</sup>	1	10.3(6.3)	0.32	0.03(0.05)	oscillator
	35.2	TE <sub>11</sub> <sup>c</sup>	0.8	8.6(5.2)	0.31	0.03(0.05)	amplifier
NRL, Washington, D.C.	13.2–16.6	TE <sub>11</sub> <sup>c</sup>	4.2	18	0.245	0.094	amplifier
RI, Moscow	6–25	TE <sub>11</sub> <sup>c</sup> /TM <sub>01</sub> <sup>c</sup>	10	1.7	0.6	1	spont. emiss.
TRW, Redondo Beach	35	TE <sub>01</sub> <sup>r</sup>	0.1	9.2	0.3	0.004	oscillator
	35	TE <sub>01</sub> <sup>r</sup>	0.002	6.9	0.29	0.0001	amplifier
UC Santa Barbara	120–880		0.027	0.5	2.6	0.002	oscillator

r: rectangular waveguide; c: circular waveguide

## 1.8 Future Trends and Applications

After the structural reorganization of most of the microwave tube manufacturers, as explained in Sect. 1.1.2, the market is still performing evolution and the needs of the customers change [1]. Certainly the three main applications listed in Sect. 1.1.1 will be always with us, but in different ways.

The use of TWTs in space and especially on communication satellites is important and still increases, probably because of the robustness and reliability of these tubes, long lifetime, high efficiency, and low weight of the whole associated transmitter. Also they are able to provide the large required power, 200 W/tube and several kW in total. As a matter of fact, on powerful transmitters, tubes are preferred compared to solid state devices, because the size and the cost of a tube do not at



all increase proportionally to its RF output power. On the contrary, this is also why the tubes are not seen in our everyday life, where the small power transistors are prevalent (mobile phones, computers).

The extraordinary success of microwave ovens using cheap magnetrons is also keeping with this presentation: magnetrons are robust, compact, reliable in a domestic and hostile industrial environment and capable of delivering approximately 800 W, in the S-band.

According to Fig. 1.1, we point out that the tubes become more attractive than the solid state devices when the operating frequency increases, what is the general tendency. Except some conventional ones, most of the modern radars use phased array antennas, working with a great number of low power modules and therefore solid state devices. However, in military aircrafts and especially missiles, tubes are still used (50 to 100 W, X-band, 2 to 3 octaves instantaneous bandwidths) again, because of their compactness and robustness with respect to vibrations, shocks and temperature variations.

As for the ISM applications, developments and improvements are foreseen in several directions: lower costs, fewer risks of arcing and parasitic oscillations, higher frequencies, better linearity, larger bandwidths, capabilities to deliver custom designed specific components, such as windows, waveguides and safety devices. Developments of new tubes may be extrapolated from the IOTs or the MBKs. In medical applications new low cost and compact MW magnetrons or klystrons will be requested. In the future there will be the possibility to provide a whole equipment including not only the microwave tube, the supplies and the cooling system, but also the electron linear accelerator. In that way the interface problems will disappear and the maintenance time, the overall cost, the number of failures will be reduced.

At higher frequencies, the impressive development of the present gyrotron oscillators is being followed by the one of gyroamplifiers, capable to be amplitude and frequency modulated, with the intention to be used not only on plasma fusion reactors but also for deep space communications, in some specific radars or in power transmission systems. Therefore, provided that theoretical developments, breakthroughs, and technological progress should come available on time, microwave tubes still have a confident future.

The R&D activity on microwave tubes, which requires a deep knowledge of many scientific areas and the mastery of many technologies, induces and encourages the tube physicists and technicians to be interested in the development of other electron vacuum devices, for instance:

- specific high efficiency multistage plasma (HEMP<sup>®</sup>) thrusters, whose design is based on the TWT principle and, more precisely, on PPM focusing and depressed collectors;
- Cs atomic clock, where the RF cavity design and machining, the control of RF leakages, the screening of the magnetic fields, the quality of the vacuum and the reliability are familiar to microwave tube experts.

The presently rising micro- and nanotechnologies will also be important, especially regarding the combination of solid state and vacuum devices. For instance, 1  $\mu\text{m}$  long needles (tips) with a diameter of 20 to 50 nm can be not only manufactured but also arranged in arrays of one or several  $\text{mm}^2$ , giving rise to very small cold cathodes. Associated to a grid for beam modulation at the cathode and to RF cavities, they can be the master parts of very compact microwave triodes, TWTs or IOTs, which can be used to boost the solid state amplifiers. The state-of-the-art of such vacuum microelectronic TWTs employing so-called Spindt cathodes is  $P = 55\text{ W}$  at  $f = 4.5\text{ GHz}$  (NEC Corporation: 50 000 tips giving 90 mA) and  $P = 28\text{ W}$  at  $f = 11.5\text{ GHz}$  (Northrop Grumman: 540 000 tips giving 56 mA).

In conclusion, microwave tubes are currently progressing and will progress in the future in the two main directions:

- the improvements of their basic principles and technologies;
- the evolution towards totally new devices using, at least partly, their concepts and these technologies.

Therefore, the future of microwave tubes is really encouraging and the microwave tube community is engaged in a long term program.

## References

- [1] R.H. Abrams, B. Levush, et al., Vacuum electronics in the 21st centuries, *IEEE Microwave Mag.* **2**, 61 (Sept.) (2001)
- [2] M. Sedlacek, *Electron Physics of Vacuum Gaseous Devices* (Wiley, Hoboken, 1996)
- [3] A.S. Gilmour, *Microwave Tubes* (Artech House, London, 1986)
- [4] J.F. Gittins, *Power Travelling Wave Tube* (The English Universities Press, Ltd., 1964)
- [5] A. Septier, *Focusing of Charged Particles*, vol. 1 & 2 (Academic, 1967)
- [6] P.T. Kirstein, G.S. Kino, *Waters WE: Space Charge Flow* (McGraw-Hill, New York, 1967)
- [7] S. Ramo, J.R. Whinnery, T. Van Duzer, *Fields and Waves in Communications Electronics* (Wiley, New York, 1984)
- [8] R. Warnecke, P. Guenard, *Les Tubes Électroniques à Commande par Modulation de Vitesse* (Gauthier-Villars, 1951)
- [9] J.W.ewartowski, H.A. Watson, *Principles of Electron Tubes* (Van Nostrand, Princeton, 1965)
- [10] A.H.W. Beck, *Space Charge Waves & Slow Electromagnetic Waves* (Pergamon Press, 1958)
- [11] A. Leblond, *Les Tubes Hyperfréquences* (Masson, 1972)
- [12] N.E. Lindenblad, U.S. Patent 2,300,052, filed May 4, 1940, issued October 27, 1942
- [13] R. Kompfner, The traveling wave valve, *Wirel. World* **53**, 369 (Nov.) (1946)
- [14] H.-T. Schmidt, Homepage. [www.hts-homepage.de/WesternElectric/WesternElectric700.html](http://www.hts-homepage.de/WesternElectric/WesternElectric700.html)
- [15] <http://accelconf.web.cern.ch/accelconf/p95/ARTICLES/RPA17.PDF>
- [16] J.R. Pierce, *Traveling Wave Tubes* (D. Van Nostrand, Princeton, 1950)
- [17] H.J. Wolkstein, Effect of collector potential depression on the efficiency of traveling wave tubes, *RCA Rev.* **19**, 259 (June) (1958)

- [18] W. Neugebauer, T.G. Mihran, A ten stage electrostatic depressed collector for improving klystron efficiency, *IEEE Trans. Electron Devices* **ED-19**(1) (Jan.) (1972)
- [19] A.S. Gilmour Jr., *Principles of Traveling Wave Tubes* (Artech House, London, 1994 & 1999)
- [20] J.R. Pierce, *Theory and Design of Electron Guns* (D. Van Nostrand, Princeton, 1954)
- [21] I.L. Langmuir, K. Blodgett, Currents limited by space charge between concentric spheres, *Phys. Rev.* **24**, 53 (July) (1924)
- [22] C.C. Cutler, The nature of power saturation in traveling wave tubes, *Bell Sys. Tech. J.* **35**, 841 (1956)
- [23] J.E. Rowe, *Nonlinear Electron Wave Interaction Phenomena* (Academic, New York, 1965)
- [24] G. Kornfeld, E. Bosch, From History to Future of Satellite TWT Amplifiers, *Frequenz Zeitschrift für Telekommunikation*, Band 55, 9-10/2001
- [25] D.C. Rogers, *Proc. IEE* **100**(Pt. III), 151 (May) (1953)
- [26] Tore Wessel-Berg, A General Theory of Klystrons with Arbitrary, Extended Interaction Fields, M.L. Report No. 376 (1957)
- [27] M. Chodorow, B. Kulke, *IEEE Trans. Electron Devices* **ED-13**, 439 (1966)
- [28] Y.M. Shin, G.S. Park, G.P. Scheitrum, G. Caryotakis, Circuit analysis of an extended interaction klystron, *J. Korean Phys. Soc.* **44**(5), 1239 (May) (2004)
- [29] B. Steer, State of the art W-band EIK for Cloudsat, in *International Vacuum Electronics Conference, IVEC 2004*, Monterey, 2004
- [30] B. Steer, Wide bandwidth, high average power eiks drive new radar concepts, in *International Vacuum Electronics Conference, IVEC 2000*, Monterey, 2000
- [31] S. Millmann, A spatial harmonics amplifier for 6 mm wavelength, *Proc. IRE* **39**, 1035 (Sept.) (1951)
- [32] R. Kompfner, The backward wave tube, U.S. Patent 2,985,790, filed 17 May 1952
- [33] R. Kompfner, N.T. Williams, Backward-wave amplifier, U.S. Patent 2,916,657, filed 17 May 1952
- [34] R. Kompfner, N.T. Williams, Backward-wave tubes, *Proc. IRE* **41**, 1602 (November) (1953)
- [35] H. Heffner, Analysis of the backward-wave traveling-wave tube, *Proc. IRE* **42**, 930 (June) (1954)
- [36] J.R. Pierce, R. Kompfner, Nat'l Academies Press, Biographical Memoirs, pp. 156–181 (1983). Use also: <http://books.nap.edu/books/0309033918/html/156.html>
- [37] J. Arnaud, Backward wave tubes, in *The Encyclopedia of Electronics*, ed. by C. Susskind (Reinhold Publishing Corporation, New York, 1962)
- [38] R.Q. Twiss, Radiation transfer and the possibility of negative absorption in radio astronomy, *Aust. J. Phys.* **11**, 424, 564 (1958)
- [39] J. Schneider, Stimulated emission of radiation by relativistic electrons in a magnetic field, *Phys. Rev. Lett.* **2**, 504 (1959)
- [40] A.V. Gaponov, *Izv. VUZ Radiofiz.* **2**, 450, 837 (1959)
- [41] H. Kleinwächter, Zur Wanderfeldröhre, *Elektrotechnik* **4**, 245 (1950) (in German)
- [42] J.L. Hirshfield, J.M. Wachtel, Electron cyclotron masses, *Phys. Rev. Lett.* **12**, 533 (1964)
- [43] A.V. Gaponov, M.I. Petelin, V.K. Yulpatov, The induced radiation of excited classical oscillators and its use in high frequency electronics, *Izv. VUZ Radiofiz.* **10**, 1414 (1967)
- [44] V.L. Granatstein, I. Alexeff, et al., *High-power Microwave Sources* (Artech House, Boston, London, 1987)
- [45] J. Benford, J. Swegle, *High-power Microwave Sources* (Artech House, Boston, London, 1992)

- [46] C.J. Edcombe (ed.), *Gyrotron Oscillators – their Principles and Practice* (Taylor & Francis, London, 1993)
- [47] M.V. Kartikeyan, E. Borie, M.K.A. Thumm, *Gyrotrons – High Power Microwave and Millimeter Wave Technology* (Springer, Berlin, 2003)
- [48] T.C. Marshall, *Free Electron Lasers* (MacMillan, New York, 1985)
- [49] P. Sprangle, T. Coffey, New high power coherent radiation sources, *Infrared Millim. Waves* **13**, 19 (1985)
- [50] H.P. Freund, T.M. Antonsen Jr., *Principles of Free-electron Lasers*, 2d edn. (Chapman & Hall, London, 1996)
- [51] H.P. Freund, G.R. Neil, Free-electron lasers: Vacuum electronic generators of coherent radiation, *Proc. IEEE* **87**, 782 (1999)
- [52] M.I. Petelin, One century of cyclotron radiation, *IEEE Trans. Plasma Sci.* **PS-27**, 294 (1999)
- [53] A.V. Gaponov-Grekhov, V.L. Granatstein, *Application of High-Power microwaves* (Artech House, Boston, London, 1994)
- [54] M. Thumm, State-of-the-art of high power gyro-devices and free electron masers, Update 2006, FZKA 7289 (2007)
- [55] K.R. Chu, Overview of research on the gyrotron traveling-wave amplifier, *IEEE Trans. Plasma Sci.* **PS-30**, 903 (2002)
- [56] G.G. Denisov, V.L. Bratman, A.D.R. Phelps, S.V. Samsonov, Gyro-TWT with a helical operating waveguide: new possibilities to enhance efficiency and frequency bandwidth, *IEEE Trans. Plasma Sci.* **PS-26**, 508 (1998)